Rep. Prog. Phys. **72** (2009) 126001 (40pp) doi:10.1088/0034-4885/72/12/126001

Nearly perfect fluidity: from cold atomic gases to hot quark gluon plasmas

Thomas Schäfer[1] **and Derek Teaney**[2,3]

[1] Department of Physics, North Carolina State University, Raleigh, NC 27695, USA
[2] Department of Physics, State University of New York at Stony Brook, Stony Brook, NY 11794, USA
[3] RIKEN-BNL Research Center, Brookhaven National Laboratory, Upton, NY 11973, USA

Received 21 April 2009, in final form 17 July 2009
Published 12 November 2009
Online at stacks.iop.org/RoPP/72/126001

Abstract
Shear viscosity is a measure of the amount of dissipation in a simple fluid. In kinetic theory shear viscosity is related to the rate of momentum transport by quasi-particles, and the uncertainty relation suggests that the ratio of shear viscosity η to entropy density s in units of $\hbar/k_B$ is bounded by a constant. Here, $\hbar$ is Planck's constant and k_B is Boltzmann's constant. A specific bound has been proposed on the basis of string theory where, for a large class of theories, one can show that $\eta/s \geqslant \hbar/(4\pi k_B)$. We will refer to a fluid that saturates the string theory bound as a perfect fluid. In this review we summarize theoretical and experimental information on the properties of the three main classes of quantum fluids that are known to have values of η/s that are smaller than $\hbar/k_B$. These fluids are strongly coupled Bose fluids, in particular liquid helium, strongly correlated ultracold Fermi gases and the quark gluon plasma. We discuss the main theoretical approaches to transport properties of these fluids: kinetic theory, numerical simulations based on linear response theory and holographic dualities. We also summarize the experimental situation, in particular with regard to the observation of hydrodynamic behavior in ultracold Fermi gases and the quark gluon plasma.

(Some figures in this article are in colour only in the electronic version)

This article was invited by G Baym.

Contents

1. Introduction

A fluid is a material that can be described by the laws of fluid dynamics. These laws imply that the response of a fluid to slowly varying external perturbations is completely governed by conservation laws. In the case of simple fluids, such as water, the conserved quantities are mass, energy and momentum.

The study of fluids is one of the oldest problems in physics [1]. Understanding why certain materials make good fluids, and others do not, has nevertheless remained a very difficult question. The quality of a fluid can be characterized by its shear viscosity η. Shear viscosity is defined in terms of the friction force F per unit area A created by a shear flow with transverse flow gradient $\nabla_y v_x$:

$$\frac{F}{A} = \eta\, \nabla_y v_x. \tag{1}$$

Viscosity causes dissipation which converts part of the kinetic energy of the flow to heat. A good fluid is therefore characterized by a small shear viscosity. Indeed, the inverse of shear viscosity, $\varphi = 1/\eta$, is sometimes called fluidity.

The molecular theory of transport phenomena in dilute gases goes back to Maxwell. Maxwell realized that shear viscosity is related to momentum transport by individual molecules. A simple estimate of the shear viscosity of a dilute gas is

$$\eta = \tfrac{1}{3}\, npl_{\rm mfp}, \tag{2}$$

where n is the density, p is the average momentum of the molecules and $l_{\rm mfp}$ is the mean free path. The mean free path can be written as $l_{\rm mfp} = 1/(n\sigma)$ where σ is a suitable transport cross section. This implies that the shear viscosity of a dilute gas grows with temperature (as $p \sim T^{1/2}$) but is approximately independent of density. This counterintuitive result is confirmed by experiment, going back to experiments carried out by Maxwell himself [2]. Equation (2) also shows that the viscosity of an ideal gas is infinite, not zero. In order to achieve thermal equilibrium we have to view the ideal gas as the limit of an interacting system in which the scattering cross section σ is taken to zero. In this limit the mean free path, and with it the viscosity, goes to infinity.

At low temperatures gases condense into the liquid (or solid) state. In a liquid transport is no longer governed by the motion of individual molecules. A simple picture, due to Frenkel, Eyring and others, is that momentum transport is due to processes that involve the motion of vacancies [3]. These processes can be viewed as thermally activated transitions in which a molecule or a cluster moves from one local energy minimum to another. The viscosity scales as [4, 5]

$$\eta \simeq hn{\rm e}^{E/(k_{\rm B}T)}, \tag{3}$$

where E is the activation energy and h is Planck's constant. We note that the viscosity of a liquid has a very strong dependence on temperature. We also observe that the overall scale involves Planck's constant. The appearance of h is related to Eyring's assumption that the collision time of the molecules is $h/(k_{\rm B}T)$, the shortest timescale in a liquid. We will come back to this assumption below. Equation (3) shows that the viscosity of a liquid grows as the temperature is lowered. Together with equation (2) this result implies that the viscosity of a typical fluid has a minimum as a function of temperature, and that the minimum is likely to occur in the vicinity of the liquid–gas phase transition.

Experimental results show that the minimum value of the viscosity of good fluids, like water, liquid helium and liquid nitrogen, differs by many orders of magnitude, see the data in table 1. The SI unit for viscosity is pascal second (Pa s), the CGS unit is poise (P). Note that $1\,{\rm Pa\,s} = 10\,{\rm P}$. Clearly, it is desirable to normalize the viscosity to a suitable thermodynamic quantity in order to make more useful comparisons. Equations (2) and (3) indicate that a suitable ratio is provided by η/n. We note that the ratio of viscosity over mass density $\rho = mn$ is known as the kinematic viscosity $\nu = \eta/\rho$. The behavior of solutions of the Navier–Stokes equation is governed by the Reynolds number

$$Re = \left(\frac{\rho}{\eta}\right) vL, \tag{4}$$

which is the ratio of a property of the flow, its characteristic velocity v multiplied by its characteristic length scale L, over a property of the fluid, its kinematic viscosity. Good fluids attain larger Reynolds numbers, and are more likely to exhibit turbulent flow. Data for the ratio η/n are tabulated in table 1. We observe that the ratios η/n for good fluids are indeed similar in magnitude.

A disadvantage of considering the ratio η/n is that it is not possible to include relativistic fluids in the comparison. In the case of a relativistic fluid the number of particles is not conserved. As a consequence the quantity n is not well defined in an interacting system. In a quark gluon plasma (QGP), for example, only the net number of quarks (the number of quarks minus the number of anti-quarks) is well defined, but the number of quarks or the number of gluons is not. In section 3.1 we will show that the Reynolds number of a relativistic fluid is defined in terms of the ratio $\eta/(sT)$, where s is the entropy density and T is the temperature. This indicates that we should consider the ratio η/s instead of η/n. We note that this ratio is well defined in both the relativistic and non-relativistic limit, and that $s \sim nk_{\rm B}$ for many fluids. For example, in a non-interacting relativistic Bose gas $s/n \simeq 3.6\,k_{\rm B}$, and for non-interacting fermions $s/n \simeq 4.2\,k_{\rm B}$. In a weakly interacting non-relativistic gas $s/n \simeq k_{\rm B}$ up to logarithms of $gn/(mT)^{3/2}$, where g is the degeneracy factor. Data for η/s in units of $\hbar/k_{\rm B}$ are also given in table 1.

We observe that good fluids are characterized by $\eta/s \sim \hbar/k_{\rm B}$. This value is consistent with simple theoretical estimates. Consider the kinetic theory estimate in equation (2). In the strong coupling limit the mean free path becomes very small, but the uncertainty relation suggests that $pl_{\rm mfp} \gtrsim \hbar$ [9]. For a rough estimate we may use the relation $s \simeq 3.6 k_{\rm B} n$ and conclude that $\eta/s \gtrsim \hbar/(10.8\,k_{\rm B})$. A bound on η/s is also indicated by the high temperature limit of Eyring's formula, equation (3). We note, however, that kinetic theory is not reliable in the regime $\eta/s \sim \hbar/k_{\rm B}$, and other methods are needed to determine the minimum value of η/s.

Table 1. Viscosity η, viscosity over density and viscosity over entropy density ratio for several fluids. Data for water and helium taken from [6, 7] and [8], data for Li and the quark gluon plasma (QGP) will be explained in section 5. For water and helium we show data at atmospheric pressure and temperatures just below the boiling point and the λ transition, respectively. These data points roughly correspond to the minimum of η/n at atmospheric pressure. We also show data near the tri-critical point which roughly corresponds to the global minimum of η/s. Note that the QGP does not have a well-defined density.

Fluid	P (Pa)	T (K)	η (Pa s)	η/n ($\hbar$)	η/s ($\hbar/k_B$)
H_2O	0.1×10^6	370	2.9×10^{-4}	85	8.2
^{4}He	0.1×10^6	2.0	1.2×10^{-6}	0.5	1.9
H_2O	22.6×10^6	650	6.0×10^{-5}	32	2.0
^{4}He	0.22×10^6	5.1	1.7×10^{-6}	1.7	0.7
^{6}Li ($a = \infty$)	12×10^{-9}	23×10^{-6}	$\leqslant 1.7 \times 10^{-15}$	$\leqslant 1$	$\leqslant 0.5$
QGP	88×10^{33}	2×10^{12}	$\leqslant 5 \times 10^{11}$		$\leqslant 0.4$

A precise value of the viscosity bound was proposed based on results from string theory. Kovtun *et al* conjectured that [10]

$$\frac{\eta}{s} \geqslant \frac{\hbar}{4\pi k_B}, \tag{5}$$

for all fluids. We will call a fluid that saturates the bound (5) a 'perfect fluid'. A perfect fluid dissipates the smallest possible amount of energy, and satisfies the laws of fluid dynamics in the largest possible domain. In a typical fluid, hydrodynamics is an effective description of long wavelength fluctuations, but in a perfect fluid hydrodynamics is reliable at distances as short as the inter-particle spacing.

The viscosity bound conjecture raises a number of interesting questions:

- Is the conjecture in equation (5) correct? Does this bound, or some other bound on η/s, follow from the general principles of quantum mechanics and statistical mechanics?
- Is there a 'perfect fluid' in nature, i.e. can we observe a fluid that attains the value $\eta/s = \hbar/(4\pi k_B)$? If yes, what are the characteristics of such a fluid? Is it possible to describe the fluid in terms of quasi-particles?
- How is η/s correlated with other transport properties, such as bulk viscosity, diffusion constants and conductivities? Are there bounds on other transport properties?

We will not be able to provide definitive answers to these questions in this review. There are, however, a number of recent results, from both theory and experiment, that shed light on these issues:

- The experimental realization of new classes of quantum fluids. Prior to 1995 the only bulk quantum fluids that could be studied in the laboratory were the two isotopes of liquid helium, ^{4}He and ^{3}He. In 1995 several groups achieved quantum degeneracy in dilute atomic Bose gases. In 1999 experimentalists also succeeded in producing degenerate atomic Fermi gases [11, 12]. Using Feshbach resonances it is possible to experimentally control the interaction between the atoms, and to study equilibrium and transport properties as a function of the interaction strength.
- The experimental discovery of almost ideal hydrodynamic flow in a completely different physical system, the QGP created in heavy ion collisions at the Relativistic Heavy Ion Collider (RHIC) at Brookhaven National Laboratory [13–15]. The QGP also exhibits a large energy loss for high energy colored particles, and a very small heavy quark diffusion constant.
- Progress in non-equilibrium field theory culminated in the calculation of transport coefficients of weakly coupled gauge theory plasmas [16–18]. These results complete the program of using kinetic theory to calculate the transport properties of the three main classes of quantum liquids: Bose gases, Fermi gases and gauge theory plasmas.
- The theoretical discovery of a completely new method for computing the transport properties of very strongly coupled fluids [19]. This method is based on the holographic duality between certain strongly coupled field theories in $d = 4$ space–time dimensions and weakly coupled string theory in $d = 10$ [20]. For gauge theories that have a weakly coupled string dual the shear viscosity to entropy density ratio at infinite coupling is $\eta/s = \hbar/(4\pi k_B)$. It was also shown that the first correction to this result at finite but large coupling increases η/s [21], and it was conjectured that $\eta/s = \hbar/(4\pi k_B)$ is a universal lower bound [10].

It is the goal of this review to summarize these recent developments. For this purpose we shall concentrate on three representative fluids: ^{4}He, a strongly coupled Bose fluid; atomic Fermi gases near a Feshbach resonance, which are the most strongly coupled Fermi liquids; and the QGP near the critical temperature for condensation into hadron gas, which is a very strongly coupled plasma. The review is structured as follows: in section 2 we discuss the thermodynamics of these quantum fluids. In section 3 we review theoretical approaches to transport properties. We briefly summarize the hydrodynamic description of relativistic and non-relativistic fluids, as well as superfluids in sections 3.1–3.3. A general connection between transport coefficients and the underlying field theory is provided by Kubo relations, which we introduce in section 3.4. In section 3.5 we concentrate on fluids that can be described in terms of weakly coupled quasi-particles. In this case transport properties can be computed using kinetic theory. In section 4 we summarize results for transport coefficients that have been obtained using holographic dualities. Finally, in section 5 we discuss experimental results for the viscosity and other transport properties of strongly coupled quantum fluids.

Needless to say, a review of this size cannot adequately summarize all the work that has been done on the transport

properties of quantum fluids. A standard reference on the properties of liquid helium is [8], recent reviews on strongly coupled Fermi gases are [22, 23] and the physics of the strongly coupled QGP is discussed in [24]. The kinetic theory of dilute Bose and Fermi gases is covered in textbooks, see [25, 26], and the kinetic theory of gauge fields was reviewed in [27]. Reviews of the AdS/CFT correspondence with an emphasis on transport theory are [28, 29], and reviews of relativistic hydrodynamics can be found in [30–32].

2. Strongly coupled quantum fluids

In this section we will discuss equilibrium properties of strongly interacting quantum fluids. We will specify the effective action for bosonic, fermionic and gauge theory fluids, identify the relevant physical scales and discuss the nature of low energy excitations.

2.1. Bose fluids: dilute Bose gases

A gas of atoms satisfying Bose statistics can be described in terms of a scalar field $\psi(\boldsymbol{x}, t)$ governed by the Hamiltonian

$$H = \int \mathrm{d}^3x\ \psi^*(\boldsymbol{x}, t)\left(-\frac{\hbar^2\boldsymbol{\nabla}^2}{2m}\right)\psi(\boldsymbol{x}, t) + \frac{1}{2}\int \mathrm{d}^3x_1 \int \mathrm{d}^3x_2\ \psi^*(\boldsymbol{x}_1, t)\psi(\boldsymbol{x}_1, t)V(\boldsymbol{x}_1 - \boldsymbol{x}_2) \times\psi^*(\boldsymbol{x}_2, t)\psi(\boldsymbol{x}_2, t), \tag{6}$$

where m is the mass of the boson and $V(\boldsymbol{x})$ is a potential. The Hamiltonian is invariant with respect to translations and rotations, as well as under the $U(1)$ symmetry $\psi \to \exp(\mathrm{i}\alpha)\psi$. Symmetries correspond to conservation laws. Translations and rotations correspond to the conservation of linear and angular momentum, and the $U(1)$ symmetry is associated with the conservation of the number of atoms. The Schrödinger equation is also invariant under Galilean transformations $\boldsymbol{x} \to \boldsymbol{x} - \boldsymbol{v}t$ which act on the field as $\psi(\boldsymbol{x}, t) \to \exp(\mathrm{i}m\boldsymbol{v}\cdot\boldsymbol{x} - \frac{\mathrm{i}}{2}m\boldsymbol{v}^2t)\psi(\boldsymbol{x} - \boldsymbol{v}t, t)$. This symmetry will play a role when we consider the motion of fluids.

If the typical momenta are small compared with $1/r_0$, where r_0 is the range of the potential, we can approximate the interaction by a contact term. For very small momenta the leading contribution is an s-wave interaction:

$$V(\boldsymbol{x}_1 - \boldsymbol{x}_2) = C_0\delta(\boldsymbol{x}_1 - \boldsymbol{x}_2), \tag{7}$$

where C_0 can be related to the scattering length a, $C_0 = 4\pi\hbar^2a)/m$. In order to make connections with the physics of relativistic fluids it is also useful to introduce the lagrangian $\mathcal{L} = \mathrm{i}\hbar\psi\partial_0\psi - \mathcal{H}$, where $\mathcal{H}$ is the Hamiltonian density. The lagrangian is

$$\mathcal{L} = \psi^\dagger\left(\mathrm{i}\hbar\partial_0 + \frac{\hbar^2\boldsymbol{\nabla}^2}{2m}\right)\psi - \frac{C_0}{2}\left(\psi^\dagger\psi\right)^2. \tag{8}$$

In the following we shall consider many-body systems described by this lagrangian. We first study the relevant scales in a weakly interacting Bose gas governed by the s-wave scattering length. At high temperatures the Bose gas is a classical Boltzmann gas. The average energy of the atoms is $\frac{3}{2}k_\mathrm{B}T$ and the average momenta are of order $(mk_\mathrm{B}T)^{1/2}$. The importance of quantum statistics is governed by the parameter nv_Q, where n is the density, $v_\mathrm{Q} = \lambda^3$ is the quantum volume and

$$\lambda = \frac{2\pi\hbar}{\sqrt{2\pi mk_\mathrm{B}T}} \tag{9}$$

is the thermal wave length. Quantum statistics becomes important for $nv_\mathrm{Q} \sim 1$, and Bose condensation in an ideal gas occurs at $nv_\mathrm{Q} = 2.61$, corresponding to a critical temperature

$$T_\mathrm{c} = \frac{2\pi\hbar^2}{mk_\mathrm{B}}\left(\frac{n}{\zeta(3/2)}\right)^{2/3}. \tag{10}$$

The effects of a non-zero scattering length can be taken into account order by order in an expansion in $an^{1/3}$. At high temperatures this is the standard virial expansion:

$$P = nk_\mathrm{B}T\left\{1 + b_2n + O(n^2)\right\}, \tag{11}$$

where P is the pressure and b_2 is the second virial coefficient. In the limit of small a the second virial coefficient of a single component Bose gas is given by [33]

$$b_2 = -\frac{1}{4\sqrt{2}}\lambda^3 + 2a\lambda^2, \tag{12}$$

where the first term is due to quantum statistics and the second term is related to the interaction. The second virial coefficient is finite in the limit of a large scattering length. As $a \to \infty$ the interaction part approaches $-\sqrt{2}\lambda^3$, and the role of interactions is governed by the same parameter that controls the effects of quantum statistics.

The interaction also shifts the critical temperature for Bose condensation. The calculation of this shift is a non-perturbative problem, even if the scattering length is small. This is related to the fact that fluctuations become large in the vicinity of a second order phase transition, and perturbation theory breaks down. One can show that $\delta T_\mathrm{c} \sim an^{1/3}T_\mathrm{c}$, and there is a physical argument that a repulsive scattering length ($a > 0$) increases the value of T_c [34]. A numerical calculation using the Landau–Ginzburg effective lagrangian gives [35]

$$\Delta T_\mathrm{c} = (1.32 \pm 0.02)an^{1/3}T_\mathrm{c}. \tag{13}$$

Dilute Bose gases in which the scattering length is attractive are not stable, but it is possible to create metastable systems confined by external fields. Weak repulsive interactions increase the transition temperature but suppress the condensate fraction. If $an^{1/3}$ is large then the Bose fluid will typically solidify, but the phase structure and critical density depend on details of the interaction. A hard sphere gas freezes at $an^{1/3} \simeq 0.24$ [36].

An issue which is very important for transport properties is the nature of the quasi-particle excitations. At high temperatures the cross section for binary scattering between the atoms decreases with the thermal wavelength, $\sigma \sim \lambda^2 \sim 1/(mT)$, and the mean free path $l_\mathrm{mfp} \sim 1/(n\sigma)$ is large.

As a consequence the atoms are good quasi-particles. At very low temperatures the system is superfluid and there is a Goldstone boson, the phonon, related to the breaking of the $U(1)$ phase symmetry. Phonons are derivatively coupled and the interaction at low energy is weak. This implies that the mean free path at low temperatures, $T \ll T_c$, is also large. The phonon dispersion relation in a weakly non-ideal ($na^3 < 1$) Bose gas was first computed by Bogoliubov. The result is

$$\epsilon_p = \frac{1}{2m}\sqrt{\left(p^2 + 8\pi an\right)^2 - (8\pi an)^2}. \qquad (14)$$

For small momenta the dispersion relation is linear, $\epsilon_p \simeq c_s p$, and the phonon velocity is given by $c_s = \sqrt{4\pi an}/m$.

2.2. Bose fluids: liquid helium

A simple s-wave interaction is sufficient for understanding the properties of trapped atomic Bose gases, but more accurate potentials are required for even a qualitative description of liquid ^{4}He. Accurate ^{4}He potentials can be written as the sum of a short range term and a long range van der Waals potential:

$$V(r) = V_{sr}(r) - \frac{C_6}{r^6}. \qquad (15)$$

The coefficient C_6 defines the van der Waals length scale $l_{vdW} = (mC_6/\hbar^2)^{1/4}$. Accurate parametrizations of V_{sr} can be found [37, 38]. These potentials have a van der Waals length $l_{vdW} \simeq 10.2a_0$, an effective range $r \simeq 14a_0$ and a very large scattering length $a \simeq 189a_0$, where $a_0 = 0.529$ Å is the Bohr radius. The large s-wave scattering length is related to the existence of a very weakly bound ^{4}He dimer. The binding energy of the dimer is $B = -1.1 \times 10^{-7}$ eV. There are many interesting universal effects governed by the large scattering length [39]. The density of liquid ^{4}He is too large for these phenomena to be important, but universal effects have been observed in dilute atomic gases in which the scattering length is large.

In the case of ^{4}He the interaction between the atoms is not weak, and it cannot be characterized in terms of the scattering length only. In the high temperature limit ^{4}He is a classical gas, and corrections to the ideal gas behavior are described by the virial expansion. The virial expansion provides a very accurate description of the equation of state at normal pressure for temperatures above 10 K. At temperatures below 10 K one has to rely on quantum Monte Carlo (QMC) methods or variational many-body wave functions [40]. At atmospheric pressure ^{4}He liquefies at 4.22 K, and it becomes superfluid at $T_c = 2.17$ K. This temperature can be compared to the critical temperature for Bose condensation of an ideal gas with the density of liquid helium, $n = 1/(3.6\,\text{Å})^3$, which is $T_c^0 = 3.1$ K. The dependence of T_c on the density in the case of a hard sphere gas was studied by Grüter *et al* [41]. Helium is well described by an effective hard sphere parameter $a = 2.20$ Å. Grüter *et al* show that for $na^3 \lesssim 0.1$ the critical temperature is larger than that of a non-interacting gas, in agreement with equation (13). The increase in T_c is small, reaching about 6%. For larger values of na^3 the critical temperature drops rapidly, until freezing occurs at $na^3 \sim 0.25$.

The presence of strong interactions also manifests itself in a small condensate fraction. Glyde *et al* measured the number of condensed atoms $N_0(T)$ using neutron scattering on liquid ^{4}He at saturated vapor pressure [42]. They find $N_0(T)/N = f(1 - (T/T_c)^\gamma$ with $f \simeq (7.25 \pm 0.75) \times 10^{-2}$ and $\gamma = 5.5 \pm 1$. The superfluid transition is in the universality class of the three-dimensional $O(2)$ model. Renormalization group arguments predict a mild non-analyticity in the specific heat, $c_v \sim t^{-\alpha}$ with $t = (T - T_c)/T_c$ and $\alpha = -0.0151(3)$ [43]. This prediction agrees reasonably well with micro gravity experiments which find $\alpha = -0.01285(4)$ [44].

The excitation spectrum of superfluid ^{4}He shows important differences as compared with the spectrum of a dilute Bose condensed gas. As expected, at small momenta the excitations are phonons with a linear dispersion relation $\epsilon(p) = c_s p$, where the speed of sound at normal pressure is $c_s = 238\,\text{m s}^{-1}$. At larger momenta the dispersion relation has a second minimum, called the roton minimum. The dispersion relation in the vicinity of the minimum is

$$\epsilon(p) = \Delta + \frac{(p - p_0)^2}{2m^*}, \qquad (16)$$

where $\Delta/k_B = 8.7$ K, $m^* = 0.14\,m$ and $p_0/\hbar = 1.9$ Å^{-1}. The roton plays a significant role in determining the specific heat and transport properties near the critical temperature. The existence of the roton is closely related to strong short range correlations in liquid helium. These correlations can be quantified in terms of the static structure factor $S(q)$, which is the Fourier transform of the density correlation function

$$S(q) = \frac{1}{\rho}\int d^3x\, e^{-iq\cdot x}\left[\langle\rho(0)\rho(x)\rangle - \langle\rho(0)\rangle^2\right]. \qquad (17)$$

The static structure factor vanishes linearly in q for small momenta, and approaches a constant value for large q. $S(q)$ has a sharp maximum at intermediate values of q, which reflects the presence of correlations at the scale of the typical inter-atomic distance. Feynman proposed a variational wave function for excitations in liquid helium which gives $\epsilon(q) = q^2/(2mS(q))$ [45]. This relation can also be derived from an effective hydrodynamic Hamiltonian, see [25]. Feynman's result reproduces both the phonon dispersion relation at low momentum, and the roton minimum at larger momentum. In order to study the kinetics of liquid helium one has to understand the scattering of phonons and rotons. The phonon–phonon and phonon–roton interaction is determined by the equation of state and by constraints from Galilean invariance and $U(1)$ symmetry [25]. We will discuss these constraints in more detail in the next section, in connection with superfluid Fermi gases.

2.3. Fermi liquids: the dilute Fermi gas at unitarity

In this section we consider non-relativistic Fermi liquids. Fermionic systems are interesting because it is possible to make strongly correlated liquids with only zero range interactions. The Fermi liquid is described by the same lagrangian as in equation (8)

$$\mathcal{L} = \psi^\dagger\left(i\partial_0 + \frac{\nabla^2}{2m}\right)\psi - \frac{C_0}{2}\left(\psi^\dagger\psi\right)^2, \qquad (18)$$

where ψ is now a two-component fermion field with mass m. The coupling constants C_0 is related to the scattering length by the same relation as in the bosonic case, $C_0 = (4\pi\hbar^2 a)/m$.

Over the last 10 years there has been truly remarkable progress in the study of cold, dilute gases of fermionic atoms in which the scattering length a of the atoms can be controlled experimentally. These systems can be realized in the laboratory using Feshbach resonances, see [46] for a review. A small negative scattering length corresponds to a weak attractive interaction between the atoms. This regime is known as the Bardeen–Cooper–Schrieffer (BCS) limit. As the strength of the attractive interaction increases the scattering length becomes larger. It diverges at the point where a two-body bound state is formed. The point $a = \infty$ is called the unitarity limit, because the scattering cross section saturates the s-wave unitarity bound $\sigma = 4\pi/k^2$. On the other side of the resonance the scattering length is positive. For large positive values of a the two-body binding energy is related to the scattering length by $B = \hbar^2/(ma^2)$. The regime in which the binding energy becomes large is called the Bose–Einstein condensation (BEC) limit.

We now consider properties of the many-body system as a function of the s-wave scattering lengths. In the high temperature limit the equation of state is again that of an ideal gas, and the leading correction is described by the virial expansion. For small a the second virial coefficient is

$$b_2 = \frac{1}{8\sqrt{2}}\lambda^3 + \frac{1}{2}a\lambda^2. \tag{19}$$

In the limit $a \to \infty$ the interaction term goes to $-\lambda^3/(2\sqrt{2})$. The Fermi gas becomes degenerate as $n\lambda^3 \sim 1$. In the limit in which the scattering length is large the Fermi gas becomes strongly interacting at the same temperature at which quantum effects become important.

At low temperatures and in the BCS limit, $a < 0$ and $n^{1/3}|a| < 1$, the Fermi gas can be described as a Landau–Fermi liquid. The excitations are weakly interacting particles and holes which carry the quantum numbers of the elementary fermions. At very low temperatures the particle–particle interaction near the Fermi surface becomes large, and the Fermi liquid undergoes a phase transition to a BCS superfluid. The transition temperature is [47]

$$T_c = \frac{8e^\gamma E_F}{(4e)^{1/3}e^2\pi}\exp\left(-\frac{\pi}{2k_F|a|}\right), \tag{20}$$

where γ is the Euler constant. The Fermi momentum k_F is defined by the relation

$$n = \frac{k_F^3}{3\pi^2}, \tag{21}$$

and $E_F = k_F^2/(2m)$ is the Fermi energy. This relation defines a 'Fermi momentum' even in the case that no sharp Fermi surface exists. Note that $T_F \equiv E_F$ is the degeneracy temperature (we have set $k_B = 1$). Also note that $n^{1/3}|a| < 1$ implies $T_c \ll T_F$.

In the Bose–Einstein limit the fermions form tightly bound molecules. The residual interaction between the molecules is repulsive, and the many-body system behaves as a weakly non-ideal Bose gas. The Bose gas condenses at the critical temperature given in equation (10). Using the fact that the mass of molecules is $2m$, and that their density is $n/2$, we get

$$T_c = 0.21 E_F. \tag{22}$$

Variational calculations suggest that at zero temperature the evolution from weak to strong coupling is smooth [48]. The system is a pair condensate for all values of the coupling, but the size of the pairs evolves from being much smaller than the inter-particle spacing in the BEC limit to being much larger in the BCS limit. This idea is confirmed by QMC calculations [49] and experimental observations [50].

Of particular interest is the crossover ('unitarity') regime where $a \to \infty$. The Fermi gas at unitarity possesses a number of interesting properties. First of all, the system is scale invariant [51, 52]. This implies, for example, that all energy scales in the many-body system, such as the critical temperature, the gap and the chemical potential, are proportional to the Fermi energy:

$$T_c = \alpha E_F, \qquad \Delta = \beta E_F, \qquad \mu = \xi E_F. \tag{23}$$

Similarly, all length scales are given by numerical constants times the inverse Fermi momentum. The values of the universal constants $\alpha, \beta, \xi, \ldots$ can be determined using QMC calculations, or from experiments on harmonically trapped fermions. QMC calculations performed by Burovski *et al* give $T_c = 0.152(7)E_F$ [53], and Carlson *et al* obtained $\Delta = 0.50(3)E_F$ [54] and $\mu = 0.44(1)E_F$ [55]. A summary of experimental results was recently given by Luo and Thomas [56].

Second, the unitarity regime is the most strongly correlated simple many-body system. The crossover regime is continuously connected to both the non-interacting Fermi gas and the non-interacting Bose gas, but neither limit provides a quantitatively accurate description. Very important for the purpose of this review is the observation of hydrodynamic behavior and low viscosity in very dilute Fermi gases in the unitarity limit.

In order to study the kinetic description of a dilute Fermi gas at unitarity we have to determine the nature of the quasi-particles and their interaction. In the high temperature limit the excitations are elementary fermions, even in the limit $a \to \infty$. This is related to the fact that the average cross section is of order λ^2, where $\lambda \sim T^{-1/2}$ is the thermal wave length. In the low temperature superfluid phase the dominant excitation is the phonon. The dispersion relation is

$$\epsilon_p = c_s p, \qquad c_s = \sqrt{\frac{\xi}{3}}\, v_F, \tag{24}$$

where $v_F = k_F/m$ is the Fermi velocity and ξ is the universal parameter defined in equation (23). Corrections to equation (24) are of the order $p^2/(m\mu)$ [57], and become large when $p \sim k_F$. The dispersion relation for momenta near k_F is not well constrained. The static structure factor has been measured in QMC simulations, and it does not show a liquid-like peak [58]. This suggests that the dispersion relation does not have a roton minimum.

The three- and four-phonon interaction is completely fixed by the equation of state and symmetry constraints. These constraints are most easily derived from an effective lagrangian for the phonon field. The phonon field is defined as the phase of the order parameter

$$\langle\psi\psi\rangle = |\langle\psi\psi\rangle| e^{2i\varphi}. \tag{25}$$

We now construct the most general lagrangian for the field φ which is consistent with Galilei invariance and $U(1)$ symmetry. A $U(1)$ transformation changes the phase of the wave function and acts as a shift on the phonon field, $\varphi \to \varphi + \alpha$. Invariance under the $U(1)$ symmetry requires that the lagrangian only contains derivatives of φ. The phase symmetry can be extended to time-dependent transformations $\psi \to \exp(i\alpha(t))\psi$ if the chemical potential transforms as $\mu \to \mu + \hbar\partial_0\alpha$. This is a symmetry of the effective lagrangian if the chemical potential always appears in the combination $\mu + \hbar\partial_0\varphi$. Finally, under a Galilei transformation with velocity $\boldsymbol{v}$ the phonon transforms as $\varphi(\boldsymbol{x}, t) \to \varphi(\boldsymbol{x} - \boldsymbol{v}t) - m\boldsymbol{v}\cdot\boldsymbol{x} + O(\boldsymbol{v}^2)$. This implies that time derivatives of φ have to be accompanied by spatial derivatives of φ. At leading order in derivatives of φ we can incorporate these symmetries by constructing a lagrangian that only depends on the variable

$$X = \mu - \hbar\partial_0\varphi - \frac{(\hbar\boldsymbol{\nabla}\varphi)^2}{2m}. \tag{26}$$

The functional form of the lagrangian $\mathcal{L}(X)$ is fixed by the observation that for a constant phonon field the lagrangian reduces to a function of μ. Since differentiating the lagrangian with respect to the chemical potential gives the density this function must be the pressure $P(\mu)$. We conclude that

$$\mathcal{L} = P(X) = \frac{2^{5/2}m^{3/2}}{15\pi^2\xi^{3/2}}\left(\mu - \hbar\partial_0\varphi - \frac{(\hbar\boldsymbol{\nabla}\varphi)^2}{2m}\right)^{5/2}, \tag{27}$$

where we have used the fact that, up to a numerical factor, the pressure of the interacting system is equal to that of a free gas. We have also used the fact that this factor can be related to the ratio $\xi = \mu/E_{\rm F}$. Phonons are low energy excitations and we can expand equation (27) in powers of $\partial_0\varphi$ and $\nabla_i\varphi$. We find

$$\begin{aligned}\mathcal{L} = {} & \tfrac{1}{2}(\partial_0\phi)^2 - \tfrac{1}{2}c_{\rm s}^2(\boldsymbol{\nabla}\phi)^2 - \alpha\left[(\partial_0\phi)^3 - 9c_{\rm s}^2\partial_0\phi(\boldsymbol{\nabla}\phi)^2\right] \\ & - \tfrac{3}{2}\alpha^2\left[(\partial_0\phi)^4 + 18c_{\rm s}^2(\partial_0\phi)^2(\boldsymbol{\nabla}\phi)^2 - 27c_{\rm s}^4(\boldsymbol{\nabla}\phi)^4\right] + \cdots,\end{aligned} \tag{28}$$

where we have rescaled the field $\varphi = \text{const} \times \phi$ to make it canonically normalized. We have also defined $\alpha = \pi c_{\rm s}^{3/2}\xi^{3/4}/(3^{1/4}8\mu^2)$. We observe that the three- and four-phonon vertices are completely fixed by the speed of sound $c_{\rm s}$. This implies that there are no free parameters that enter into the kinetic theory of phonons. We also note that equation (27) generates phonon self-interactions to arbitrary order in the phonon field, but to leading order in the number of derivatives. Terms involving higher derivatives of φ were constructed in [52]. These terms involve non-trivial constraints from not just scale invariance, but from the full conformal symmetry of the Fermi gas at unitarity.

About units. Up to this point, we have explicitly displayed factors of $\hbar$, c and $k_{\rm B}$. From now on we will work in natural units and set $\hbar = k_{\rm B} = c = 1$.

2.4. Gauge theories: Quantumchromodynamics (QCD)

QCD is governed by the lagrangian

$$\mathcal{L} = -\frac{1}{4}G^a_{\mu\nu}G^a_{\mu\nu} + \sum_f^{N_{\rm f}}\bar{\psi}_f(i\not{D} - m_f)\psi_f, \tag{29}$$

where ψ_f is a Dirac fermion with flavor index f and m_f is the quark mass. We have suppressed the color ($A = 1, \ldots, N_{\rm c}$) and spinor ($\alpha = 1, \ldots, 4$) indices of the fermion fields. The covariant derivative acting on the quark fields is

$$i\not{D}\psi = \gamma^\mu\left(i\partial_\mu + gA^a_\mu\frac{\lambda^a}{2}\right)\psi, \tag{30}$$

where A^a_μ is a gauge potential and λ^a ($a = 1, \ldots, N_{\rm c}^2 - 1$) are the Gell–Mann matrices. The field strength tensor is defined by

$$G^a_{\mu\nu} = \partial_\mu A^a_\nu - \partial_\nu A^a_\mu + gf^{abc}A^b_\mu A^c_\nu, \tag{31}$$

where f^{abc} are the $SU(N_{\rm c})$ structure constants and g is a coupling constant. In the standard model $N_{\rm c} = 3$ and $N_{\rm f} = 6$, but three out of the six flavors are too heavy to play much of a role in the dynamics of QCD, and we shall mostly concentrate on $N_{\rm f} = 3$ flavors. The total quark density

$$\rho_{\rm q} = \sum_f \psi_f^\dagger\psi_f \tag{32}$$

is conserved and we can introduce a chemical potential μ coupled to $\rho_{\rm q}$. The phase structure and transport properties of QCD at finite μ are an interesting subject [59], but in this review we will concentrate on QCD at non-zero temperatures and zero or very small chemical potentials. It is interesting to note that at low quark densities the relevant degrees of freedom are protons and neutrons. In the low energy limit the interaction between neutrons and protons is governed by an effective lagrangian of the type given in equation (18). The scattering length is a function of the quark masses, and it is theoretically possible to tune the light quark masses to a point where the neutron–neutron scattering length diverges. The real world is close to this point, as the experimental value of the scattering is $a_{nn} \simeq -17\,\text{fm}$ is much larger than typical QCD scales. This implies that there is a point in the QCD phase diagram where the long distance physics is equivalent to that of a dilute atomic Fermi gas at unitarity.

For many purposes we can consider the first three flavors (up, down and strange) to be approximately massless. In this limit the QCD lagrangian contains a single dimensionless parameter, the coupling constant g. If quantum effects are taken into account the coupling becomes scale dependent. At leading order the running coupling constant is

$$g^2(q) = \frac{16\pi^2}{b_0\log(q^2/\Lambda^2_{\rm QCD})}, \qquad b_0 = \frac{11}{3}N_{\rm c} - \frac{2}{3}N_{\rm f}. \tag{33}$$

This result implies that as a quantum theory, QCD is not characterized by a dimensionless coupling, but by a dimensionful scale, the QCD scale parameter $\Lambda_{\rm QCD}$. This phenomenon is called dimensional transmutation. We also observe that the coupling decreases with increasing momentum. This is the phenomenon of asymptotic freedom.

At high temperatures the dominant momenta are on the order of T, and for $T \gg \Lambda_{\rm QCD}$ asymptotic freedom implies that bulk thermodynamics is governed by weak coupling. The weak coupling expansion of the equation of state is

$$P = T^4 \left\{ c_0 + c_2 g^2 + c_3 g^3 + (c_4' \log(g) + c_4) g^4 + \cdots \right\}, \quad (34)$$

where the first term is the Stefan–Boltzmann law and

$$c_0 = \frac{\pi^2}{90} \left(2\left(N_{\rm c}^2 - 1\right) + 4 N_{\rm c} N_{\rm f} \frac{7}{8} \right) \quad (35)$$

depends on the number of degrees of freedom ($2(N_{\rm c}^2 - 1)$ gluons and $4N_{\rm c}N_{\rm f}$ quarks). We note that in a theory of massless particles the equation of state is always sensitive to quantum statistics, even if the temperature is high. The first correction is [60]

$$c_2 = -\frac{N_{\rm c}^2 - 1}{144} \left(N_{\rm c} + \frac{5}{4} N_{\rm f} \right). \quad (36)$$

The perturbative expansion in equation (34) is evaluated with g taken to be the running coupling constant evaluated at a scale $q \sim T$. The precise scale is not uniquely determined—changing the scale corresponds to reshuffling higher order corrections in the perturbative expansion. The scale is usually chosen to improve the apparent rate of convergence. This criterion gives a value close to $2\pi T$.

We note that the perturbative expansion is not a power series in the fine structure constant $\alpha_{\rm s} = g^2/(4\pi)$. The expansion contains square roots and logarithms of $\alpha_{\rm s}$. Non-analytic terms in the expansion are related to infrared sensitive diagrams. For example, the g^3 term in equation (34) is due to ring diagrams (also called the plasmon term). Ring diagrams are one-loop gluon diagrams in which the leading order gluon self-energy has been summed to all orders. We also note that the weak coupling expansion cannot be extended to arbitrarily high powers in g. At $O(g^6)$ one encounters infrared divergent diagrams which can only be summed non-perturbatively, by computing the partition function of three-dimensional QCD at zero temperature.

In order to analyze the relevant scales in high temperature QCD in more detail we consider the current–current interaction

$$\mathcal{M} = j_\mu^a \Pi_{\mu\nu}^{ab} j_\nu^b, \quad (37)$$

where j_μ^a is a color current and $\Pi_{\mu_\nu}^{ab}$ is the gluon polarization function. The tensor structure of the gluon polarization function can be decomposed into a transverse and a longitudinal part:

$$\Pi_{\mu\nu}(q) = \Pi^{\rm T}(q) P_{\mu\nu}^{\rm T} + \Pi^{\rm L}(q) P_{\mu\nu}^{\rm L}$$
$$P_{ij}^{\rm T} = \delta_{ij} - \hat{q}_i \hat{q}_j, \qquad P_{00}^{\rm T} = P_{0i}^{\rm T} = 0, \quad (38)$$
$$P_{\mu\nu}^{\rm L} = -g_{\mu\nu} + \frac{q_\mu q_\nu}{q^2} - P_{\mu\nu}^{\rm T}.$$

We will consider the polarization function in the limit of weak coupling ($g < 1$), and for $\omega \ll q \ll T$, where ω, q are the energy and momentum transfer. We find

$$\Pi^{ab\,{\rm L}}(q) = \frac{\delta^{ab}}{\boldsymbol{q}^2 + m_{\rm D}^2}, \quad (39)$$

$$\Pi^{ab\,{\rm T}}(q) = \frac{\delta^{ab}}{\boldsymbol{q}^2 - {\rm i}\frac{\pi}{4} m_{\rm D}^2 \frac{\omega}{|q|}}, \quad (40)$$

where

$$m_{\rm D}^2 = g^2 T^2 \left(1 + \frac{N_{\rm f}}{6} \right) \quad (41)$$

is called the Debye mass. The longitudinal term governs the color-Coulomb interaction between static charges. We observe that the Coulomb interaction is screened at distances $r \sim m_{\rm D}^{-1} \sim 1/(gT)$. In perturbation theory the static magnetic interaction is unscreened [16], but non-static magnetic interactions are dynamically screened at a distance $r \sim (m_{\rm D}^2 \omega)^{-1/3}$. This phenomenon, known as Landau damping, is due to the coupling of gluons to particle–hole (or particle–antiparticle) pairs, and also play a role in electromagnetic plasmas. Unlike classical plasmas the QCD plasma has a non-perturbative static magnetic screening mass $m_{\rm M} \sim g^2 T$. This is the scale that determines the non-perturbative g^6 term in the pressure. Modes below the magnetic screening scale contribute

$$P \sim T \int^{m_{\rm M}} {\rm d}^3 k \sim g^6 T^4. \quad (42)$$

The gluon polarization tensor also determines the propagation of gluonic modes. For this purpose we need the full energy and momentum dependence of $\Pi^{\rm T,L}$, see [61]. For momenta $q \gg gT$ there are two transverse modes with dispersion relation $\omega \simeq q$. For momenta $q < gT$ there are two transverse and one longitudinal mode. The longitudinal mode is sometimes called the plasmon. The energy of all three modes approaches $\omega = \omega_{\rm p} = m_{\rm D}/\sqrt{3}$ as $q \to 0$. The quantity $\omega_{\rm p}$ is known as the plasma frequency. The gluon (and plasmon) decay constant in the limit $q \to 0$ is [62]

$$\gamma = 6.64 \frac{g^2 N_{\rm c} T}{24\pi}. \quad (43)$$

An important issue is how small the coupling has to be in order for the perturbative estimates to be applicable. The convergence properties of the weak coupling expansion for the pressure are extremely poor. The series shows no signs of converging unless the coupling is taken to be much smaller than one, $g \ll 1$, corresponding to completely unrealistic temperatures on the order of 1 TeV. The problem is mostly due to the non-analytic terms in the expansion, and convergence can be improved significantly by considering resummation schemes or self-consistent quasi-particle expansions [63]. Convergence can also be improved by using a hierarchy of effective field theories for the hard ($p \sim T$), electric ($p \sim gT$) and magnetic ($p \sim g^2 T$) sectors of the QCD plasma [64]. Ordinary perturbation theory corresponds to treating the hard and the electric sector perturbatively, but convergence can be

improved by treating both the electric and the magnetic sector non-perturbatively [65].

Despite these advances accurate results at temperatures that can be reached in heavy ion collisions at RHIC have to rely on numerical simulations of the QCD partition function on a space–time lattice, see [66] for a review. Lattice simulations with realistic quark masses find a phase transition at the critical temperature $T_c = 192(8)\,\mathrm{MeV}$ [67]. The transition is a rapid (but smooth) crossover from a low temperature phase that exhibits chiral symmetry breaking and confinement to a chirally restored and deconfined high temperature phase[4]. The energy density reaches about 85% of the ideal gas value at $T \simeq 2T_c$ and then evolves very slowly toward the non-interacting limit.

Below the critical temperature the degrees of freedom are hadrons. The lightest hadrons are pions, which are the Goldstone bosons associated with the spontaneous breaking of the chiral symmetry of the QCD lagrangian. We can view pions as a spin–isospin sound wave that propagates in the QCD vacuum. Because quarks are not massless the chiral symmetry is not exact, and pions have non-zero masses. The masses of the charged and neutral pions are $m_{\pi^\pm} = 139\,\mathrm{MeV}$ and $m_{\pi^0} = 135\,\mathrm{MeV}$. The lightest particle which is not a type of sound wave is the rho meson, with a mass of 770 MeV. The chiral symmetry constrains the pion scattering amplitudes. As in the case of phonons, these constraints are obtained most easily from the low energy effective chiral lagrangian. At leading order we have

$$\mathcal{L} = \frac{f_\pi^2}{4}\mathrm{Tr}\left[\partial_\mu \Sigma \partial^\mu \Sigma^\dagger\right] + \left[B\,\mathrm{Tr}(M\Sigma^\dagger) + \mathrm{h.c.}\right] + \cdots, \quad (44)$$

where $\Sigma = \exp(\mathrm{i}\phi^a\lambda^a/f_\pi)$ $(a = 1, \ldots, 8)$ is the chiral field, $f_\pi = 93\,\mathrm{MeV}$ is the pion decay constant, B is proportional to the quark condensate, and $M = \mathrm{diag}(m_u, m_d, m_s)$ is the mass matrix. We note that f_π can be viewed as the stiffness of the QCD vacuum:

$$f_\pi^2 = \frac{2m_q}{m_\pi^2}\frac{\partial P_{\mathrm{vac}}}{\partial m_q}, \quad (45)$$

where $P_{\mathrm{vac}} \simeq 0.5\,\mathrm{GeV\,fm^{-3}}$ is the vacuum pressure and $m_q = (m_u + m_d)/2$. This result follows from the Gell–Mann–Oakes–Renner relation $m_\pi^2 f_\pi^2 = (m_u + m_d)\langle\bar\psi\psi\rangle$ together with $(\partial P_{\mathrm{vac}})/(\partial m) = \langle\bar\psi\psi\rangle$. An expansion of Σ in powers of the field ϕ^a determines the interaction between pions. Restricting ourselves to the $SU(2)$ flavor sector (pions only) we get

$$\mathcal{L} = \frac{1}{2}(\partial_\mu\phi^a)^2 - \frac{1}{2}m_\pi^2(\phi^a)^2 + \frac{1}{6f_\pi^2}\left[(\phi^a\partial_\mu\phi^a)^2 - (\phi^a)^2(\partial_\mu\phi^b)^2\right] + \cdots, \quad (46)$$

where ϕ^a $(a = 1, 2, 3)$ is the pion field. This result is clearly analogous to the phonon interaction in equation (28). There are, however, some minor differences. Because of parity and isospin symmetry there are no vertices with an odd number of pions. We also note that the leading four-pion interaction has two derivatives, while the four-phonon term involves four derivatives.

[4] This issue is not completely settled. Aoki *et al* find distinct crossover transitions at significantly lower temperatures, $T_\chi = 151\,\mathrm{MeV}$ for chiral symmetry restoration, and $T_{\mathrm{dec}} = 175\,\mathrm{MeV}$ for deconfinement [68].

2.5. Gauge theories: super-conformal QCD

QCD is a complicated theory, and a significant amount of effort has been devoted to the study of generalizations of QCD that possess a larger amount of symmetry, in particular supersymmetry. Supersymmetry is a symmetry that relates bosonic and fermionic fields. The simplest supersymmetric cousin of QCD is SUSY gluodynamics, a theory of gluons and massless fermions in the adjoint representation of the color group called gluinos. Theories with more supersymmetry involve extra fermions and colored scalar fields. The most supersymmetric extension of QCD is a theory with four supersymmetries, called $\mathcal{N} = 4$ SUSY QCD. Theories with even more supersymmetry contain fields with spin 3/2 and 2, and therefore involve gravitational interactions. These theories are known as supergravity.

The lagrangian of $\mathcal{N} = 4$ SUSY QCD is

$$\mathcal{L} = -\tfrac{1}{4}G^a_{\mu\nu}G^a_{\mu\nu} - \mathrm{i}\bar\lambda^a_i\sigma^\mu D_\mu\lambda^a_i + D^\mu\phi^{\dagger a}_{ij}D_\mu\phi^a_{ij} + \mathcal{L}_{\lambda\lambda\phi} + \mathcal{L}_{\phi^4}, \quad (47)$$

where $G^a_{\mu\nu}$ is the usual field strength tensor, λ^a_i is the gluino field and ϕ^a_{ij} is a colored Higgs field. The gluino is a two-component (Weyl) fermion in the adjoint representation of the color group. The index i $(i = 1, \ldots, 4)$ transforms in the fundamental representation of a global $SU(4)_R$ 'R-symmetry'. This symmetry interchanges the bosons and fermions that are related by the four supersymmetries, and is analogous to the flavor symmetry of QCD. The Higgs is a scalar field in the adjoint representation of color, and in an anti-symmetric tensor (six dimensional) of $SU(4)_R$. Note that the total number of fermionic fields, $8(N_c^2 - 1)$, is indeed equal to the number of bosonic fields. We have not explicitly displayed the Yukawa couplings $\mathcal{L}_{\lambda\lambda\phi}$ and Higgs self-couplings $\mathcal{L}_{\phi^4}$, see [69]. Both interaction terms only involve the dimensionless gauge coupling g.

$\mathcal{N} = 4$ SUSY QCD has a vanishing beta function and is believed to be a conformal field theory (CFT). As a consequence there is no dimensional transmutation, no confinement or spontaneous symmetry breaking and no phase transition. The theory is a Coulomb phase for all values of the coupling g and the temperature T. However, if g is not small then there is no obvious way to compute thermodynamic or transport properties of the plasma.

An interesting new approach is provided by the duality between strongly coupled large N_c gauge theory and weakly coupled string theory on $\mathrm{AdS}_5 \times \mathrm{S}_5$ discovered by Maldacena [20]. We will have more to say about this approach in section 4. For now we observe that the correspondence can be extended to a finite temperature. In this case the relevant configuration is an $\mathrm{AdS}_5 \times \mathrm{S}_5$ black hole. The temperature of the gauge theory is given by the Hawking temperature of the black hole, and the entropy is given by the Hawking–Beckenstein formula $S = A/(4G)$, where A is the surface area of the event horizon and G is Newton's constant.

The AdS/CFT correspondence makes predictions for the thermodynamics of the gauge theory in the limit of a large number of colors, $N_c \to \infty$. The perturbative expansion of a $SU(N_c)$ Yang–Mills theory involves the 't Hooft coupling $\lambda = g^2N_c$. In the weak coupling limit we take $N_c \to \infty$ with

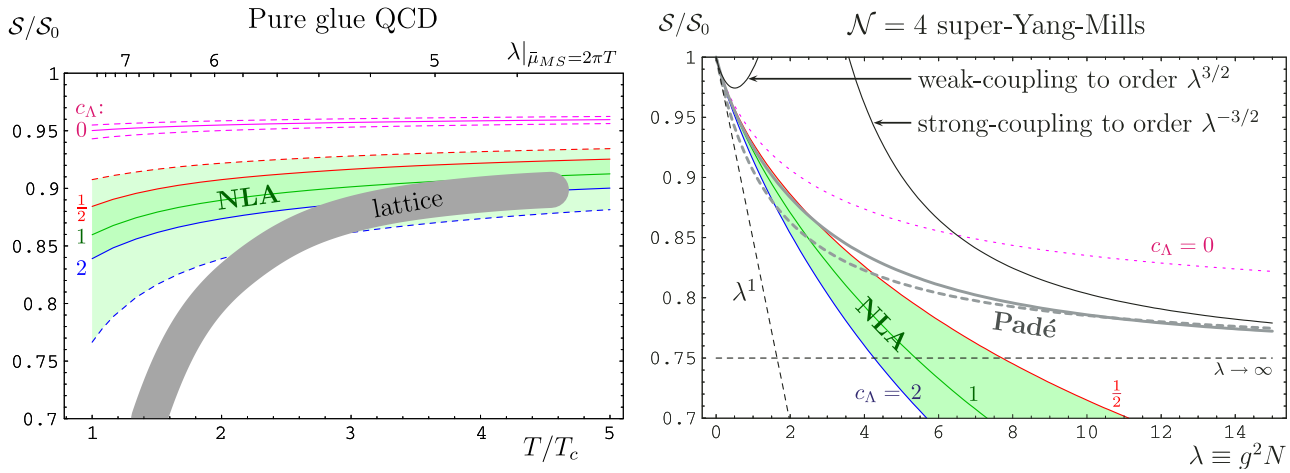

Figure 1. Entropy density in units of the Stefan–Boltzmann value for pure gauge QCD and $\mathcal{N}=4$ supersymmetric QCD. The left panel shows the entropy density of pure gauge QCD as a function of T/T_c. The gray band is the lattice result. The solid lines show a resummed QCD calculation [63]. The different lines correspond to different choices for a non-perturbative parameter c_Λ. The dashed lines mark an error band determined by variations in the QCD renormalization scale. The right panel shows the entropy density of SUSY QCD as a function of the 't Hooft coupling λ. The curves are labeled as in the left panel.

$\lambda = \text{const}$ and $\lambda \ll 1$. Using the AdS/CFT correspondence we can also study the strong coupling limit $N_c \to \infty$ with $\lambda \gg 1$. $\mathcal{N}=4$ SUSY QCD is a conformal theory and scale invariance implies that $\epsilon = 3P$ as well as $s = 4P/T$, where ϵ is the energy density and s is the entropy density. By dimensional analysis the entropy density of the interacting system must be proportional to the entropy density s_0 of the free system. The weak and strong coupling expansions for s/s_0 are [70–72]

$$\frac{s}{s_0} = \begin{cases} \frac{3}{4} + \frac{45\zeta(3)}{32}\lambda^{-3/2} + \cdots & \lambda \gg 1, \\ 1 - \frac{3}{2\pi^2}\lambda + \frac{\sqrt{2}+3}{\pi^3}\lambda^{3/2} + \cdots & \lambda \ll 1. \end{cases} \tag{48}$$

This result has a number of remarkable features. First we observe that the entropy density at infinite coupling only differs by a factor 3/4 from the result in the free theory. We also note that the first non-trivial corrections in the strong and weak coupling limit are consistent with the idea that the evolution from weak to strong coupling is smooth. Equation (48) was compared with resummed perturbation theory and Pade approximants in [73], see figure 1. The authors argue that at the 'QCD-like' point $s/s_0 = 0.85$ neither the strong nor the weak coupling expansion are quantitatively reliable, but that resummed perturbation theory is useful in this regime.

3. Transport theory

In this section we summarize theoretical approaches to transport phenomena in strongly coupled quantum fluids. The most general of these approaches is hydrodynamics. Hydrodynamics is based on the observation that correlation functions at low energy and small momentum are governed by the evolution of conserved charges. Conservation laws imply that the densities of conserved charges cannot relax locally, but have to propagate or diffuse out to large distance. This corresponds to hydrodynamic excitations with dispersion laws of the form $\omega \sim q$ (sound) or $\omega \sim iq^2$ (diffusion).

Hydrodynamics can be developed as an expansion in derivatives of the fluid velocity and the thermodynamic variables. The leading order theory, called ideal hydrodynamics, only depends on the equation of state, and is exactly time reversible. The next order theory, (first order) viscous hydrodynamics, involves a new set of parameters called transport coefficients, and describes dissipative, time-irreversible phenomena. The validity of hydrodynamics is controlled by the relative size of the next-to-leading order terms. If dissipation is dominated by shear viscosity[5] then the expansion parameter is $1/Re$, where Re is the Reynolds number defined in equation (4).

The values of the transport coefficients can be extracted from experiment, or computed from an underlying field theory. The connection between transport coefficients and correlation functions in a (quantum) field theory is provided by linear response theory. Using linear response theory one can relate transport coefficients to the zero energy and zero momentum limit of a retarded correlation function. These relations are known as Kubo formulae, see section 3.4.

Calculations based on the Kubo formula are difficult, in particular if the interaction is not weak. The situation simplifies if the system allows a microscopic description in terms of quasi-particles. In that case we can use an intermediate effective theory, known as kinetic theory, to relate the microscopic lagrangian to the hydrodynamic description. Kinetic theory also provides a more microscopic criterion for the applicability of hydrodynamics. Using the kinetic estimate for the shear viscosity in equation (2) we get $1/Re \sim (c_s/v)(l_{mfp}/L)$ where c_s is the speed of sound and the ratio

$$Kn = \frac{l_{mfp}}{L} \tag{49}$$

is called the Knudsen number. Hydrodynamics is valid if the mean free path is much smaller than the characteristic size, and the Knudsen number is small.

[5] If dissipation is dominated by heat transport, then the expansion parameter is $1/(Re \cdot Pr)$, where Pr is the Prandtl number defined in equation (140).

The calculation of transport coefficients in kinetic theory is reviewed in section 3.5. If the interaction between quasi-particles is strong then the kinetic description breaks down. A new approach to extracting transport properties from a strongly coupled field theory is the holographic method which we will discuss in the next section. Using holography the calculation of the retarded correlator can be reduced to a classical computation in a suitable dual theory.

3.1. Hydrodynamics

3.1.1. Non-relativistic fluids. The hydrodynamics of a one-component non-relativistic fluid is governed by the conservation laws of energy, mass (particle number) and momentum:

$$\frac{\partial \epsilon}{\partial t} + \boldsymbol{\nabla} \cdot \boldsymbol{j}^{\epsilon} = 0, \tag{50}$$

$$\frac{\partial \rho}{\partial t} + \boldsymbol{\nabla} \cdot \boldsymbol{g} = 0, \tag{51}$$

$$\frac{\partial g_i}{\partial t} + \nabla_j \Pi_{ij} = 0. \tag{52}$$

Here, ϵ is the energy density, ρ is the mass density, $\boldsymbol{g}$ is the momentum density and Π_{ij} is the stress tensor. The relations between the conserved currents and the hydrodynamic variables are called constitutive relations. These relations can be determined order by order in an expansion in derivatives of the flow velocity and the thermodynamic variables. The leading order result is called 'ideal hydrodynamics'. At this order the constitutive relations are completely fixed by Galilean invariance, rotational invariance and conservation of entropy. The result is

$$\boldsymbol{j}^{\epsilon} = \boldsymbol{v}(\epsilon + P), \tag{53}$$

$$\boldsymbol{g} = \rho \boldsymbol{v}, \tag{54}$$

$$\Pi_{ij} = P\delta_{ij} + \rho v_i v_j, \tag{55}$$

where $\epsilon = \epsilon_0 + \frac{1}{2}\rho v^2$ and ϵ_0 is the energy density in the rest frame of the fluid. There are six hydrodynamic variables, $\boldsymbol{v}$, ρ, ϵ and P, which are determined by the five conservation laws (50)–(51). In order for the equations to close we need to supply an equation of state $P = P(\epsilon, \rho)$. Since hydrodynamic variables evolve slowly, the equation of state is the one in thermal equilibrium.

In ideal hydrodynamics the equations of continuity and momentum conservation are

$$\frac{\partial \rho}{\partial t} + \boldsymbol{\nabla} \cdot (\rho \boldsymbol{v}) = 0, \tag{56}$$

$$\frac{\partial \boldsymbol{v}}{\partial t} + (\boldsymbol{v} \cdot \boldsymbol{\nabla})\, \boldsymbol{v} = -\frac{1}{\rho} \boldsymbol{\nabla} P. \tag{57}$$

The equation of momentum conservation is known as the Euler equation. In the case of ideal hydrodynamics the equation of energy conservation can be rewritten as conservation of entropy:

$$\frac{\partial s}{\partial t} + \boldsymbol{\nabla} \cdot (\boldsymbol{v} s) = 0. \tag{58}$$

At next order in the derivative expansion dissipative terms appear. The size of these terms is controlled by new parameters called transport coefficients. The relation $\boldsymbol{g} = \rho \boldsymbol{v}$ is not modified (it follows from Galilean invariance), but two new coefficients appear in the stress tensor. We can write $\Pi_{ij} = P\delta_{ij} + \rho v_i v_j + \delta\Pi_{ij}$ with

$$\delta\Pi_{ij} = -\eta \left(\nabla_i v_j - \nabla_j v_i - \tfrac{2}{3}\delta_{ij} \boldsymbol{\nabla} \cdot \boldsymbol{v}\right) - \zeta \delta_{ij} \left(\boldsymbol{\nabla} \cdot \boldsymbol{v}\right). \tag{59}$$

Here, η is the shear viscosity and ζ is the bulk viscosity. The correction to the energy current has the form $j_i^{\epsilon} = v_i(\epsilon + P) + v_j \delta\Pi_{ij} + Q_i$ with

$$\boldsymbol{Q} = -\kappa \boldsymbol{\nabla} T, \tag{60}$$

where T is the temperature and κ is the thermal conductivity. The second law of thermodynamics implies that $\eta, \zeta, \kappa \geqslant 0$. The equation of momentum conservation with the viscous stresses (59) included is known as the Navier–Stokes equation.

The linearized hydrodynamic equations describe the propagation of sound and diffusive modes. In the case of a non-relativistic fluid there is a pair of sound modes that couple to the pressure/density and the longitudinal velocity, a pair of diffusive shear modes that couple to the transverse velocity and a diffusive heat mode. The longitudinal and transverse components of the velocity are defined by $\boldsymbol{v} = \boldsymbol{v}^{\mathrm{L}} + \boldsymbol{v}^{\mathrm{T}}$ with $\boldsymbol{\nabla} \times \boldsymbol{v}^{\mathrm{L}} = 0$ and $\boldsymbol{\nabla} \cdot \boldsymbol{v}^{\mathrm{T}} = 0$. The hydrodynamic modes govern the hydrodynamic correlation functions. The transverse velocity correlation function is defined by

$$\begin{aligned} S_{ij}^{vv}(\omega, \boldsymbol{k}) &= \langle \delta v_i^{\mathrm{T}} \delta v_j^{\mathrm{T}} \rangle_{\omega, \boldsymbol{k}} \\ &= \int \mathrm{d}^3x\, \mathrm{d}t\; \mathrm{e}^{\mathrm{i}(\omega t - \boldsymbol{k}\cdot\boldsymbol{x})} \langle \delta v_i^{\mathrm{T}}(\boldsymbol{x}, t) \delta v_j^{\mathrm{T}}(0, 0) \rangle, \end{aligned} \tag{61}$$

where $\delta v_i^{\mathrm{T}}(\boldsymbol{x}, t) = v_i^{\mathrm{T}}(\boldsymbol{x}, t) - \langle v_i^{\mathrm{T}}(\boldsymbol{x}, t) \rangle$ is a fluctuation of the velocity. Linearized hydrodynamics gives

$$S_{ij}^{vv}(\omega, \boldsymbol{k}) = \frac{2T}{\rho} \left(\delta_{ij} - \hat{k}_i \hat{k}_j\right) \frac{\nu \boldsymbol{k}^2}{\omega^2 + \nu^2 \boldsymbol{k}^4}, \tag{62}$$

where $\nu = \eta/\rho$ is the kinetic viscosity. The dependence of the correlation function on ω and $\boldsymbol{k}$ is determined by the laws of hydrodynamics, equations (50–51), and the overall normalization is fixed by the thermodynamic relation

$$\langle \delta v_i(\boldsymbol{x}, t) \delta v_j(\boldsymbol{x}', t) \rangle = \frac{T}{\rho} \delta_{ij} \delta(\boldsymbol{x} - \boldsymbol{x}'). \tag{63}$$

We observe that the transverse velocity correlation function has a diffusive pole, where the diffusion constant is given by the kinematic viscosity. The entropy correlation function has a diffusive pole governed by the thermal diffusion constant $\chi = \kappa/(c_p \rho)$, where c_p is the specific heat at constant pressure. The correlation function is

$$S^{ss}(\omega, \boldsymbol{k}) = \langle \delta s \delta s \rangle_{\omega, \boldsymbol{k}} = \frac{2c_p}{\rho} \frac{\chi \boldsymbol{k}^2}{\omega^2 + \chi^2 \boldsymbol{k}^4}. \tag{64}$$

The pressure correlation function contains the sound pole and is given by

$$S^{pp}(\omega, \boldsymbol{k}) = \langle \delta p \delta p \rangle_{\omega, \boldsymbol{k}} = 4\rho T c_{\mathrm{s}}^3 \, \frac{\gamma c_{\mathrm{s}}^2 \boldsymbol{k}^2 + \gamma_{\mathrm{T}}(\omega^2 - c_{\mathrm{s}}^2 \boldsymbol{k}^2)}{(\omega^2 - c_{\mathrm{s}}^2 \boldsymbol{k}^2)^2 + 4\gamma^2 c_{\mathrm{s}}^2 \omega^2}, \tag{65}$$

where $c_s = [(\partial P)/(\partial \rho)|_s]^{1/2}$ is the speed of sound and $\gamma = \gamma_{\eta,\zeta} + \gamma_T$ is the coefficient of sound absorption (the inverse sound attenuation length). The contributions to γ from viscosity and thermal conductivity are given by

$$\gamma_{\eta,\zeta} = \frac{\boldsymbol{k}^2}{2\rho c_s}\left(\zeta + \frac{4}{3}\eta\right), \qquad \gamma_T = \frac{\boldsymbol{k}^2 c_s \rho}{2T}\chi\left(\frac{\partial T}{\partial P}\right)_s. \quad (66)$$

These results illustrate the criterion for the validity of hydrodynamics given above. Hydrodynamics is based on a small momentum expansion. Applied to equation (65) this implies that $\omega \sim c_s k \gg k^2\eta/\rho$. Taking the characteristic size to be $L \sim 1/k$ this is equivalent to $\eta/(c_s\rho L) \ll 1$. A more microscopic criterion follows from the kinetic estimate of the shear viscosity given in equation (2): hydrodynamics describes sound waves with a wave length that is large compared with the mean free path, $L \gg l_{\rm mfp}$.

3.1.2. Superfluid hydrodynamics. Superfluidity is characterized by the spontaneous breakdown of the $U(1)$ symmetry associated with the conserved particle number. By Goldstone's theorem the spontaneous breaking of a continuous symmetry leads to the appearance of a gapless mode. This mode has to be included in the hydrodynamic description of the system. We introduced the Goldstone boson field φ in equation (25). The quantity $\boldsymbol{v}_s = \boldsymbol{\nabla}\varphi/m$ can be interpreted as the superfluid velocity. Since $\boldsymbol{v}_s$ is the gradient of a phase the superfluid velocity is irrotational, $\boldsymbol{\nabla} \times \boldsymbol{v}_s = 0$.

We have to generalize the constitutive equations to include both the normal fluid velocity $\boldsymbol{v}_n$ and the superfluid velocity $\boldsymbol{v}_s$. In the ideal fluid case (no dissipation) the result is completely fixed by Galilean invariance and thermodynamic relations. The constitutive equations are

$$\boldsymbol{g} = \rho_n \boldsymbol{v}_n + \rho_s \boldsymbol{v}_s, \quad (67)$$

$$\Pi_{ij} = P\delta_{ij} + \rho_n v_{n,i} v_{n,j} + \rho_s v_{s,i} v_{s,j}, \quad (68)$$

$$\boldsymbol{j}^\epsilon = \rho s T \boldsymbol{v}_n + (\mu + \tfrac{1}{2}\boldsymbol{v}_s^2)(\rho_n \boldsymbol{v}_n + \rho_s \boldsymbol{v}_s) + \rho_n \boldsymbol{v}_n \boldsymbol{v}_n \cdot (\boldsymbol{v}_n - \boldsymbol{v}_s), \quad (69)$$

where ρ_n and ρ_s are the normal and superfluid density of the system. The total density $\rho = \rho_n + \rho_s$ is the sum of the normal and superfluid contributions. The ratio ρ_s/ρ is a function of the temperature, the chemical potential and the relative velocity $|\boldsymbol{v}_n - \boldsymbol{v}_s|$. This function, like the equation of state $P(\mu, T, |\boldsymbol{v}_n - \boldsymbol{v}_s|)$, depends on microscopic details. The conservation laws are given by equations (50)–(51). These equations have to be supplemented by an equation of motion for the superfluid velocity. Landau showed that Euler's equation for the superfluid velocity is given by [74]

$$\frac{\partial \boldsymbol{v}_s}{\partial t} + (\boldsymbol{v}_s \cdot \boldsymbol{\nabla})\boldsymbol{v}_s = -\boldsymbol{\nabla}\mu. \quad (70)$$

Because $\boldsymbol{v}_s$ is irrotational we can rewrite the convective derivative on the lhs of equation (70) as a total derivative, $\boldsymbol{v}_s \cdot \boldsymbol{\nabla}\boldsymbol{v}_s = \frac{1}{2}\boldsymbol{\nabla}(\boldsymbol{v}_s^2)$.

As in the case of a normal fluid we may consider dissipative corrections to the constitutive equations. The form of these terms is constrained by rotational and Galilean invariance, and by the second law of thermodynamics. The viscous corrections to the energy momentum tensor are

$$\delta\Pi_{ij} = -\eta\left(\nabla_i v_{n,j} + \nabla_j v_{n,i} - \tfrac{2}{3}\delta_{ij}\boldsymbol{\nabla}\cdot\boldsymbol{v}_n\right) - \delta_{ij}\Big(\zeta_1 \boldsymbol{\nabla}\cdot(\rho_s(\boldsymbol{v}_s - \boldsymbol{v}_n)) + \zeta_2(\boldsymbol{\nabla}\cdot\boldsymbol{v}_n)\Big). \quad (71)$$

We observe that viscous shear stresses only arise from the normal component of the flow. In addition to the normal bulk viscosity term proportional to ζ_2 there is a second contribution that involves the relative motion of the normal and superfluid components. Two additional bulk viscosities appear in the dissipative correction to the rhs of equation (70). We replace $\boldsymbol{\nabla}\mu$ by $\boldsymbol{\nabla}(\mu + H)$ with

$$H = -\zeta_3 \boldsymbol{\nabla}\cdot(\rho_s(\boldsymbol{v}_s - \boldsymbol{v}_n)) - \zeta_4 \boldsymbol{\nabla}\cdot\boldsymbol{v}_n. \quad (72)$$

Onsager's symmetry principle requires that $\zeta_4 = \zeta_1$. The dissipative correction to the energy current is $\delta j_i^\epsilon = v_{n,j}\delta\Pi_{ij} + \rho_s(v_{s,i} - v_{n,i})H + Q_i$ where $Q_i = -\kappa\nabla_i T$ as in the case of a normal fluid.

Superfluid hydrodynamics contains two velocity fields, the normal flow velocity $\boldsymbol{v}_n$ and the superfluid (irrotational) flow velocity $\boldsymbol{v}_s$. This extra degree of freedom leads to an additional sound mode called second sound. The velocity of second sound depends strongly on temperature and vanishes at the critical temperature where $\rho_s/\rho \to 0$. If thermal expansion can be neglected second sound is an oscillatory motion of the superfluid against the normal fluid which does not lead to any mass transport and can be viewed as a pure entropy wave.

3.1.3. Relativistic fluids. In a relativistic fluid the equations of energy and momentum conservation can be written as a single equation

$$\partial_\mu T^{\mu\nu} = 0, \quad (73)$$

where $T^{\mu\nu}$ is the energy momentum tensor. In ideal fluid dynamics the form of $T_{\mu\nu}$ is completely fixed by Lorentz invariance,

$$T^{\mu\nu} = (\epsilon + P)u^\mu u^\nu + P\eta^{\mu\nu}, \quad (74)$$

where u^μ is the fluid velocity ($u^2 = -1$) and $\eta^{\mu\nu} = \mathrm{diag}(-1, 1, 1, 1)$ is the metric tensor. In a relativistic theory there need not be a conserved particle number. If a conserved particle number, for example baryon number, exists then there is a second hydrodynamic equation that expresses particle number conservation:

$$\partial_\mu(n u^\mu) = 0, \quad (75)$$

where n is the particle density. As in the non-relativistic case the hydrodynamic equations have to be supplemented by an equation of state $P = P(\epsilon)$ or $P = P(\epsilon, n)$. The four equations given in equation (73) can be split into two sets using the longitudinal and transverse projectors:

$$\Delta^{||}_{\mu\nu} = -u_\mu u_\nu, \qquad \Delta_{\mu\nu} = \eta_{\mu\nu} + u_\mu u_\nu. \quad (76)$$

With the help of the thermodynamic relations $\mathrm{d}\epsilon = T\,\mathrm{d}s$ and $\epsilon + P = sT$ the longitudinal equation is equivalent to entropy conservation

$$\partial_\mu(s u^\mu) = 0, \quad (77)$$

and the transverse equation is the relativistic Euler equation

$$Du_\mu = -\frac{1}{\epsilon + P}\nabla_\mu^\perp P\,, \tag{78}$$

where $D = u\cdot\partial$ and $\nabla_\mu^\perp = \Delta_{\mu\nu}\partial^\nu$. Comparison with equation (57) shows that the inertia of a relativistic fluid is governed by $\epsilon + P$.

The form of the dissipative terms depends on the precise definition of the fluid velocity. A useful choice is to define u^μ by the requirement that in the local rest frame $T^{00} = \epsilon$ and $T^{0i} = 0$. This definition is called the Landau frame [74]. In this frame the dissipative correction to the energy momentum tensor in the rest frame has the same form as in the non-relativistic case, see equation (59). We write the stress tensor as $T^{\mu\nu} = T_0^{\mu\nu} + \delta^{(1)}T^{\mu\nu} + \delta^{(2)}T^{\mu\nu} + \cdots$, where $T_0^{\mu\nu}$ is the stress tensor of the ideal fluid given in equation (74), $\delta^{(1)}T^{\mu\nu}$ is the first order viscous correction, etc. A covariant expression for $\delta^{(1)}T^{\mu\nu}$ is

$$\delta^{(1)}T^{\mu\nu} = -\eta\sigma^{\mu\nu} - \zeta\Delta^{\mu\nu}\partial\cdot u, \tag{79}$$

where we have defined

$$\sigma^{\mu\nu} = \Delta^{\mu\alpha}\Delta^{\nu\beta}\left(\partial_\alpha u_\beta + \partial_\beta u_\alpha - \tfrac{2}{3}\eta_{\alpha\beta}\partial\cdot u\right). \tag{80}$$

The dissipative correction to the conserved particle current is $j_\mu = nu_\mu + \delta j_\mu$ with

$$\delta^{(1)}j_\mu = -\kappa\left(\frac{nT}{\epsilon+P}\right)^2\Delta_\mu^\perp\left(\frac{\mu}{T}\right), \tag{81}$$

where κ is the thermal conductivity and μ is the chemical potential associated with the conserved density n. Alternatively, one can define the velocity via the conserved particle current (Eckart frame). In that case there is no dissipative contribution to j_μ and the thermal conductivity appears in the stress tensor.

The hydrodynamic equations determine the propagation of sound and diffusive modes. We consider the case without a conserved particle number. In this case all the modes can be found by considering correlation functions of the energy–momentum current $g^i = T^{0i}$. The longitudinal and transverse correlation functions are

$$S_{gg}^{\rm L}(\omega,\boldsymbol{k}) = 2sT\,\frac{\Gamma_{\rm s}\omega^2\boldsymbol{k}^2}{(\omega^2 - c_{\rm s}^2\boldsymbol{k}^2)^2 + (\Gamma_{\rm s}\omega\boldsymbol{k}^2)^2}, \tag{82}$$

$$S_{gg}^{\rm T}(\omega,\boldsymbol{k}) = \frac{2\eta\boldsymbol{k}^2}{\omega^2 + (\frac{\eta}{sT}\boldsymbol{k}^2)^2}. \tag{83}$$

As in the non-relativistic fluid we find a pair of sound waves and a pair of diffusive shear modes. The sound attenuation length is given by

$$\Gamma_{\rm s} = \frac{\frac{4}{3}\eta + \zeta}{sT}\,, \tag{84}$$

and the analog of the kinematic viscosity is the ratio $\eta/(sT)$.

A new issue that arises in viscous relativistic hydrodynamics is the apparent lack of causality of the equations of motion. The problem can be seen by inspecting the linearized equation for the diffusive shear mode. The equation is first order in time, but second order in spatial gradients. As a result discontinuities in the initial conditions can propagate with infinite speed. This is not really a problem of the hydrodynamic description—the relevant modes are outside the domain of validity of hydrodynamics—but the acausal modes cause difficulties in numerical implementations. To overcome these difficulties one can include second order gradient corrections in the stress tensor. The resulting theory is called second order viscous hydrodynamics. One can show that for physically reasonable ranges of the second order coefficients the theory is causal [31]. In general, there are a large number of second order terms. A complete classification of the second order terms in a relativistic conformal fluid was recently given in [75]. Conformal symmetry implies that $\zeta = 0$ and $\delta^{(1)}T_{\mu\nu} = -\eta\sigma_{\mu\nu}$. The second order correction is

$$\begin{aligned}\delta^{(2)}T^{\mu\nu} = {}&\eta\tau_{\rm II}\left[{}^{\langle}D\sigma^{\mu\nu\rangle} + \tfrac{1}{3}\sigma^{\mu\nu}(\partial\cdot u)\right]\\ &+\lambda_1\sigma^{\langle\mu}{}_\lambda\sigma^{\nu\rangle\lambda} + \lambda_2\sigma^{\langle\mu}{}_\lambda\Omega^{\nu\rangle\lambda} + \lambda_3\Omega^{\langle\mu}{}_\lambda\Omega^{\nu\rangle\lambda},\end{aligned} \tag{85}$$

where $\sigma^{\mu\nu}$ is the first order shear tensor defined above,

$$A^{\langle\mu\nu\rangle} = \tfrac{1}{2}\Delta^{\mu\alpha}\Delta^{\nu\beta}\left(A_{\alpha\beta} + A_{\beta\alpha} - \tfrac{2}{3}\Delta^{\mu\nu}\Delta^{\alpha\beta}A_{\alpha\beta}\right) \tag{86}$$

denotes the transverse traceless part of $A^{\alpha\beta}$ and

$$\Omega^{\mu\nu} = \tfrac{1}{2}\Delta^{\mu\alpha}\Delta^{\nu\beta}\left(\partial_\alpha u_\beta - \partial_\beta u_\alpha\right) \tag{87}$$

is the vorticity. Equation (85) defines four new second order transport coefficients, $\tau_{\rm II}$ and $\lambda_{1,2,3}$. These coefficients can be determined using kinetic theory [76] or the AdS/CFT correspondence [75, 77].

Equation (85) is a constitutive relation that determines the stress tensor in terms of thermodynamic variables. Formally, we may replace time derivatives by spatial derivatives using the lower order equations of motion. Another option, inspired by the approach of Israel and Stewart [78], is to promote $\pi^{\mu\nu} = \delta T^{\mu\nu}$ to a hydrodynamic variable. The equation of motion for $\pi^{\mu\nu}$ is

$$\begin{aligned}\pi^{\mu\nu} = {}&-\eta\sigma^{\mu\nu} - \tau_{\rm II}\left[{}^{\langle}D\pi^{\mu\nu\rangle} + \frac{4}{3}\pi^{\mu\nu}(\partial\cdot u)\right]\\ &+\frac{\lambda_1}{\eta^2}\pi^{\langle\mu}_\lambda\pi^{\nu\rangle\lambda} - \frac{\lambda_2}{\eta}\pi^{\langle\mu}_\lambda\Omega^{\nu\rangle\lambda} + \lambda_3\Omega^{\langle\mu}_\lambda\Omega^{\nu\rangle\lambda}.\end{aligned} \tag{88}$$

This equation describes the relaxation of $\pi^{\mu\nu}$ to the Navier–Stokes form $-\eta\sigma^{\mu\nu}$. There are also a number of more phenomenological approaches that include some subset of higher order terms, for example the already mentioned Israel–Stewart formalism [78] or the equations of Lindblom and Geroch [79], see [31] for a review. We note that whatever formalism is used, a necessary condition for the applicability of second order hydrodynamics is that higher order corrections are small, $\delta^{(2)}T^{\mu\nu} \ll \delta^{(1)}T^{\mu\nu} \ll T^{\mu\nu}$.

Remarks. The second order formalism was initially developed for non-relativistic fluids by Burnett [80, 81], see [82] for a review. Higher order hydrodynamic equations can be derived from kinetic theory by computing moments of the Boltzmann equation. This procedure is known as Grad's moment method [83]. It is not easy to find systems

in which the second order theory provides a quantitative improvement over the Navier–Stokes equation. An example is the work of Uhlenbeck, Foch and Ford on sound propagation in gases [84, 85]. Finally, we note that relativistic superfluid hydrodynamics was formulated by Carter, Khalatnikov and Lebedev [86, 87], see [88–90] for more recent studies that emphasize the connection to effective field theory.

3.2. Diffusion

An important diagnostic of the properties of a fluid is the diffusion of a dilute gas of impurities suspended in the fluid. We will see, in particular, that if the fluid is composed of quasi-particles then the diffusion of impurities and the shear viscosity, which is related to momentum diffusion, are closely linked. The two transport coefficients have the same dependence on the coupling constant, and their temperature dependence is the same up to kinematic factors. In a perfect fluid, however, this link may be broken: the diffusion constant goes to zero while the shear viscosity remains finite.

We will assume that the number of impurity particles is conserved. The number density satisfies the continuity equation

$$\frac{\partial n}{\partial t} + \boldsymbol{\nabla}\cdot \jmath = 0. \tag{89}$$

If the number density varies smoothly then the current $\jmath$ can be expressed in terms of the thermodynamic variables. At leading order in derivatives of the density we can write $\vec{j} = -D\boldsymbol{\nabla} n$, where D is the diffusion constant. Inserting this expression into the continuity equation gives the diffusion equation

$$\frac{\partial n}{\partial t} = D\boldsymbol{\nabla}^2 n. \tag{90}$$

A more microscopic view of diffusion is provided by studying the Brownian motion of an individual suspended particle. The motion is described by a stochastic (Langevin) equation

$$\frac{\mathrm{d}\boldsymbol{p}}{\mathrm{d}t} = -\eta_{\mathrm{D}}\boldsymbol{p} + \boldsymbol{\xi}(t), \quad \langle \xi_i(t)\xi_j(t')\rangle = \kappa\delta_{ij}\delta(t-t'). \tag{91}$$

Here, $\boldsymbol{p}$ is the momentum of the particle, η_{D} is the drag coefficient and $\boldsymbol{\xi}(t)$ is a stochastic force. The coefficient κ is related to the mean square momentum change per unit time, $3\kappa = \langle(\Delta \boldsymbol{p})^2\rangle/(\Delta t)$. The Langevin equation can be integrated to determine the mean squared momentum. In the long time limit ($t \gg \eta_{\mathrm{D}}^{-1}$) the particle thermalizes and we expect that $\langle \boldsymbol{p}^2\rangle = 3mT$. This requirement leads to the Einstein relation

$$\eta_{\mathrm{D}} = \frac{\kappa}{2mT}. \tag{92}$$

The relation between η_{D} and the diffusion constant can be determined from the mean square displacement. At late times $\langle[\Delta \boldsymbol{x}(t)]^2\rangle = 6D|t|$ and

$$D = \frac{T}{m\eta_{\mathrm{D}}} = \frac{2T^2}{\kappa}. \tag{93}$$

A special case is the diffusion of large spherical particles suspended in a simple fluid. In this case the drag coefficient can be computed using the Navier–Stokes equation and the drag is related to the shear viscosity of the fluid, $\eta_{\mathrm{D}} = 6\pi\eta a/m$, where a is the radius of the particles. This leads to a relation between the diffusion constant and the shear viscosity, $D = T/(6\pi\eta a)$.

3.3. Dynamic universality

In the vicinity of a second order phase transition fluctuations of the order parameter relax slowly. This implies that order parameter fluctuations have to be included in the hydrodynamic description. The resulting hydrodynamic models describe universal features of transport phenomena near a continuous phase transition [91]. Dynamic universality classes, like the well-known static ones, depend on the symmetries of the order parameter and the number of dimensions. Universal aspects of transport also depend on the nature of the order parameter, whether it is conserved or not, and on the presence of couplings (non-vanishing Poisson brackets) between the order parameter and the conserved fields. In this section we will briefly review the hydrodynamic description of a simple fluid near the liquid–gas endpoint. This theory is known as model H in the classification of Hohenberg and Halperin [91]. We will see that critical fluctuations lead to a divergent shear and bulk viscosity at the liquid–gas endpoint. The hydrodynamic description of the superfluid–normal transition in liquid helium and dilute atomic gases is called model F. This model describes the divergence of the heat conductivity at the superfluid transition.

Near the critical point sound modes ($\omega \sim k$) are higher in energy than diffusive modes ($\omega \sim k^2$), and the longitudinal components of the momentum density $\boldsymbol{g}$ can be neglected. A minimal model that describes the coupling of the order parameter ϕ to the transverse momentum density $\boldsymbol{g}_{\mathrm{T}}$ is [91]

$$\frac{\partial \phi}{\partial t} = \lambda_0 \boldsymbol{\nabla}^2 \frac{\delta \mathcal{F}_{\mathrm{T}}}{\delta \phi} - g_0 \boldsymbol{\nabla}\phi \cdot \frac{\delta \mathcal{F}_{\mathrm{T}}}{\delta \boldsymbol{g}} + \zeta_\phi, \tag{94}$$

$$\frac{\partial g_i}{\partial t} = P^{\mathrm{T}}_{ij}\left[\eta_0 \boldsymbol{\nabla}^2 \frac{\delta \mathcal{F}_{\mathrm{T}}}{\delta g_j} + g_0(\nabla_j \phi)\frac{\delta \mathcal{F}_{\mathrm{T}}}{\delta \phi} + \zeta_{g_j}\right], \tag{95}$$

where $P^{\mathrm{T}}_{ij} = (\delta_{ij} + \nabla_i\nabla_j/\boldsymbol{\nabla}^2)$ is a transverse projector, ζ_ϕ and ζ_{g_j} are random forces, and the free energy $\mathcal{F}_{\mathrm{T}} = \mathcal{F} - \mathcal{F}_h$ is given by

$$\mathcal{F} = \int \mathrm{d}^d x \left[\frac{1}{2}(\boldsymbol{\nabla}\phi)^2 + \frac{r_0}{2}\phi^2 + u_0\phi^4 + \frac{1}{2}\boldsymbol{g}^2\right], \tag{96}$$

$$\mathcal{F}_h = \int \mathrm{d}^d x \ [h\phi + \boldsymbol{A}\cdot\boldsymbol{g}], \tag{97}$$

where h and $\boldsymbol{A}$ are external fields. The coefficients λ_0 and η_0 are the bare values of the thermal conductivity and shear viscosity. Fluctuations cause the physical value of the zero frequency transport coefficients to diverge near the critical point. In order to study the critical behavior of the bulk viscosity the longitudinal component of $\boldsymbol{g}$ has to be included [92].

In a normal fluid the only conserved charges are the particle density, the energy density and the momentum density. The order parameter is a suitable linear combination of the energy density and the particle density. In QCD the hydrodynamic variables include the chiral condensate, and the conserved energy density, baryon density and isospin density. The QCD phase diagram is expected to have two critical points, one that corresponds to the endpoint of the nuclear liquid–gas phase transition and another one that is related to the

endpoint of the first order chiral phase transition [93]. QCD hydrodynamics in the vicinity of the chiral critical point was analyzed by Son and Stephanov [94] who argue that the chiral endpoint, like the nuclear liquid–gas endpoint, is correctly described by model H. The values of the critical exponents can be determined using the epsilon expansion. The shear and bulk viscosity diverge with the correlation length ξ as [91, 92]

$$\eta \sim \xi^{x_\eta}\ (x_\eta \simeq 0.06), \qquad \zeta \sim \xi^{x_\zeta}\ (x_\eta \simeq 2.8). \tag{98}$$

The critical endpoint is in the same static universality class as the Ising model and $\xi \sim t^{-0.63}$, where $t = (T - T_c)/T$. We note that the divergence in the bulk viscosity is much stronger than the divergence in the shear viscosity. These results demonstrate that, while there is empirical evidence for the suggestion that the viscosity minimum is located at the endpoint of the liquid–gas phase transition (see table 1), this idea cannot be rigorously correct. Indeed, both η/s and ζ/s diverge near the critical endpoint.

3.4. Kubo relations and spectral functions

Hydrodynamics is an effective description of the low energy, long wavelength response of a fluid. The transport coefficients appear as unknown constants in the hydrodynamic equations. These constants can be extracted from experiment, or computed from a more microscopic theory. The relationship between transport coefficients and correlation functions in a microscopic quantum field theory is provided by Kubo relations. We have seen that hydrodynamics fixes the low energy and low momentum behavior of the correlation functions of conserved charges, see equations (62–65). In the field theory these correlation functions can be computed using linear response theory. The response is governed by the retarded correlation function. In the case of shear viscosity the relevant correlation function is

$$G_{\rm R}^{xy,xy}(\omega,\boldsymbol{k}) = -\mathrm{i}\int \mathrm{d}t \int \mathrm{d}^3x\, \mathrm{e}^{\mathrm{i}(\omega t - \boldsymbol{k}\cdot\boldsymbol{x})}\Theta(t) \times \left\langle \left[T^{xy}(\boldsymbol{x},t), T^{xy}(0,0)\right]\right\rangle, \tag{99}$$

where $T^{\mu\nu}$ is the energy momentum tensor. The spectral function is defined by $\rho(\omega,\boldsymbol{k}) = -2\,\mathrm{Im}\,G_{\rm R}(\omega,\boldsymbol{k})$. The imaginary part of the retarded correlator is a measure of dissipation, while the correlation function $S(\omega,\boldsymbol{k})$ (see section 3.1.1) is related to fluctuations. The relation between these two functions is called the fluctuation–dissipation theorem [95]. In the low frequency limit $\rho(\omega,\boldsymbol{k}) = (\omega/T)S(\omega,\boldsymbol{k})$. Matching the correlation function from linear response theory to the hydrodynamic correlator gives the Kubo relation

$$\eta = \lim_{\omega\to 0}\lim_{k\to 0}\frac{\rho^{xy,xy}(\omega,\boldsymbol{k})}{2\omega}. \tag{100}$$

The formula for the bulk viscosity involves the trace of the energy momentum tensor

$$\zeta = \frac{1}{9}\lim_{\omega\to 0}\lim_{k\to 0}\frac{\rho^{ii,jj}(\omega,\boldsymbol{k})}{2\omega}, \tag{101}$$

and analogous results can be derived for the thermal conductivity and diffusion constants.

Table 2. Lattice QCD results for the ratio of shear and bulk viscosity to entropy density in a pure gluon plasma. The calculations were performed for three different temperatures, given in units of the critical temperature T_c. Data from [97, 103].

T	$1.02T_c$	$1.24T_c$	$1.65T_c$
η/s		0.102(56)	0.134(33)
ζ/s	0.73(3)	0.065(17)	0.008(7)

The spectral function contains information about the physical excitations that carry the response. We will discuss this issue in more detail when we compare the strong coupling (AdS/CFT) and weak coupling spectral functions in section 4. Dispersion relations connect the spectral function to correlation functions with different analyticity properties. The Matsubara (imaginary energy) correlation function is

$$G_E(\mathrm{i}\omega_n) = \int \frac{\mathrm{d}\omega}{2\pi}\frac{\rho(\omega)}{\omega - \mathrm{i}\omega_n}, \tag{102}$$

where $\omega_n = 2\pi nT$ is the Matsubara frequency. The imaginary time correlation function is given by

$$G_E(\tau) = \int \frac{\mathrm{d}\omega}{2\pi}K(\omega,\tau)\rho(\omega), \tag{103}$$

where the kernel $K(\omega,\tau)$ is defined by

$$K(\omega,\tau) = \frac{\cosh[\omega(\tau - 1/(2T))]}{\sinh[\omega/(2T)]} = [1 + n_{\rm B}(\omega)]\,\mathrm{e}^{-\omega\tau} + n_{\rm B}(\omega)\mathrm{e}^{\omega\tau}, \tag{104}$$

and $n_{\rm B}(\omega)$ is the Bose distribution function. Equation (103) is the basis of attempts to compute transport coefficients using imaginary time QMC data [96–99]. The idea is to compute $G_E(\tau)$ numerically, invert the integral transform in equation (103) to obtain $\rho(\omega)$ and then extract transport coefficients from $\rho'(0)$. The difficulty is that $G_E(\tau)$ is typically only computed on a small number of points, and that the imaginary time correlator is not very sensitive to the slope of the spectral function at low energy. Many recent calculations make use of the maximum entropy method to obtain numerically stable spectral functions and reliable error estimates [100, 101]. It was also observed that one can minimize the contribution from continuum states to the imaginary time Green function by studying the correlators of conserved charges, energy and momentum density, at non-zero spatial momentum [102, 103]. In more physical terms this means that one is extracting the viscosity from the sound pole rather than the shear pole. In table 2 we summarize some recent lattice QCD results on the shear and bulk viscosity in the high temperature phase of pure gauge QCD. We observe that the shear viscosity to entropy density ratio is close to the conjectured bound $1/(4\pi)$. The bulk viscosity is large in the vicinity of the phase transition but decreases quickly and becomes extremely small at $T = 1.64T_c$.

3.5. Kinetic theory: shear viscosity

If the fluid can be described in terms of weakly interacting quasi-particles then the hydrodynamic variables can be written

in terms of quasi-particle distribution functions $f_{\rm p}(\boldsymbol{x},t)$. In the case of a non-relativistic fluid the energy current, momentum current and stress tensor are given by

$$j_i^{\epsilon}(\boldsymbol{x},t) = \int \frac{{\rm d}^3p}{(2\pi)^3} E_{\rm p} v_{{\rm p},i} f_{\rm p}(\boldsymbol{x},t), \tag{105}$$

$$g_i(\boldsymbol{x},t) = \int \frac{{\rm d}^3p}{(2\pi)^3} m v_{{\rm p},i} f_{\rm p}(\boldsymbol{x},t), \tag{106}$$

$$\Pi_{ij}(\boldsymbol{x},t) = \int \frac{{\rm d}^3p}{(2\pi)^3} m v_{{\rm p},i} v_{{\rm p},j} f_{\rm p}(\boldsymbol{x},t), \tag{107}$$

where $E_{\rm p}$ is the quasi-particle energy and $v_{{\rm p},i} = (\partial E_{\rm p})/(\partial p_i)$ is the quasi-particle velocity. The equation of motion for $f_{\rm p}(\boldsymbol{x},t)$ is the Boltzmann equation

$$\frac{\partial f_{\rm p}}{\partial t} + \boldsymbol{v}\cdot\boldsymbol{\nabla} f_{\rm p} + \boldsymbol{F}\cdot\boldsymbol{\nabla}_p f_{\rm p} = C[f_{\rm p}], \tag{108}$$

where $\boldsymbol{F}$ is an external force and $C[f_{\rm p}]$ is the collision term. In local thermal equilibrium the distribution function is determined by the local temperature, chemical potential and flow velocity. We have

$$f_{\rm p}^0(\boldsymbol{x},t) = \frac{1}{\exp((E_{\rm p} - \boldsymbol{v}\cdot\boldsymbol{p} - \mu)/T) \mp 1}, \tag{109}$$

where the $\mp$ sign corresponds to bosons/fermions. Transport coefficients characterize how the distribution function relaxes to its equilibrium value if it is perturbed slightly away from it. We can write

$$f_{\rm p}(\boldsymbol{x},t) = f_{\rm p}^0(\boldsymbol{x},t) + \delta f_{\rm p}(\boldsymbol{x},t) \tag{110}$$

and linearize the Boltzmann equation in $\delta f_{\rm p}$. In order to determine transport coefficients we also use a gradient expansion of the local velocity, temperature and chemical potential and linearize the Boltzmann equation in the 'driving terms' $\nabla_i v_j$, $\nabla_i T$ and $\nabla_i \mu$. This procedure is known as the Chapman–Enskog method. In the next section we will describe the method in the case of phonon mediated transport in a superfluid, and then discuss some of the modifications that appear when studying high temperature Fermi and Bose gases as well as gauge theories.

3.5.1. Phonons in dilute Fermi gases. In the following we will concentrate on the shear viscosity of the low temperature, superfluid, phase of the dilute Fermi gas at unitarity. The calculation is similar to the computation of the shear viscosity of superfluid helium, but as explained in section 2.3 the low energy effective theory of the dilute Fermi gas is more tightly constrained. We discuss the shear viscosity of liquid helium, as well as the viscosity of the low temperature (chiral symmetry broken) phase of QCD in section 3.5.2. The stress tensor of a phonon gas is

$$\Pi_{ij}(\boldsymbol{x},t) = c_{\rm s}^2 \int \frac{{\rm d}^3p}{(2\pi)^3} \frac{p_i p_j}{E_{\rm p}} f_{\rm p}(\boldsymbol{x},t). \tag{111}$$

In order to study the shear viscosity we write $\delta f_{\rm p} = -\chi(p) f_{\rm p}^0(1+f_{\rm p}^0)/T$ with

$$\chi(p) = g(p)\left(p_i p_j - \tfrac{1}{3}\delta_{ij}\boldsymbol{p}^2\right)\left(\nabla_i v_j + \nabla_j v_i - \tfrac{2}{3}\delta_{ij}\boldsymbol{\nabla}\cdot\boldsymbol{v}\right). \tag{112}$$

Inserting this ansatz into the energy momentum tensor gives

$$\eta = \frac{4c_{\rm s}^2}{15T}\int \frac{{\rm d}^3p}{(2\pi)^3}\frac{p^4}{2E_{\rm p}} f_{\rm p}^0(1+f_{\rm p}^0) g(p). \tag{113}$$

The function $g(p)$ is determined by the linearized Boltzmann equation. Linearizing the lhs of the Boltzmann equation in derivatives of $\boldsymbol{v}$, μ, T gives

$$\frac{{\rm d}f_{\rm p}}{{\rm d}t} \simeq c_{\rm s}^2 \frac{f_{\rm p}^0(1+f_{\rm p}^0)}{2E_{\rm p}T} p_{ij} v_{ij}, \tag{114}$$

where we have defined

$$p_{ij} = p_i p_j - \tfrac{1}{3}\delta_{ij}\boldsymbol{p}^2, \qquad v_{ij} = \nabla_i v_j + \nabla_j v_i - \tfrac{2}{3}\delta_{ij}\boldsymbol{\nabla}\cdot\boldsymbol{v}. \tag{115}$$

The rhs of the Boltzmann equation contains the collision term $C[f_{\rm p}]$. In the present case the dominant contribution arises from binary $2 \leftrightarrow 2$ collisions. The linearized collision term is

$$\begin{aligned} C_{2\leftrightarrow 2}[f_{\rm p}] &\simeq \frac{1+f_{\rm p}^0}{2E_{\rm p}T}\int {\rm d}\Gamma(k;k',p')(1+f_k^0) f_{k'}^0 f_{p'}^0 |\mathcal{M}|^2 \\ &\quad\times\left[g(p)p_{ij} + g(k)k_{ij} - g(k')k'_{ij} - g(p')p'_{ij}\right] v_{ij} \\ &\equiv \frac{f_{\rm p}^0(1+f_{\rm p}^0)}{2E_{\rm p}T} C_{ij}[g(p)] v_{ij}, \end{aligned} \tag{116}$$

where $\mathcal{M}$ is the scattering matrix element,

$$\begin{aligned} {\rm d}\Gamma(k;k',p') &= \left(\prod_{q=k,k',p'}\frac{{\rm d}^3q}{(2\pi)^3 2E_{\rm q}}\right) \\ &\quad\times(2\pi)^4\delta^{(4)}(p+k-k'-p') \end{aligned} \tag{117}$$

is the phase space, and we have defined the linearized collision operator $C_{ij}[g(p)]$. The linearized Boltzmann equation can now be written as

$$C_{ij}[g(p)] = \frac{c_{\rm s}^2}{T} p_{ij}. \tag{118}$$

This result can be used to rewrite the relation for the viscosity in equation (113) as

$$\eta = \frac{2}{5}\int \frac{{\rm d}^3p}{(2\pi)^3}\frac{f_{\rm p}^0(1+f_{\rm p}^0)}{2E_{\rm p}T} p_{ij} g(p) C_{ij}[g(p)]. \tag{119}$$

The two relations equations (113) and (119) can be used to derive a variational estimate of the shear viscosity. We can view equation (113) as an inner product with measure $f^0(1+f^0)/(2E_{\rm p})$ and write

$$\eta = \tfrac{2}{5}\,\langle X|g\rangle\,, \tag{120}$$

where $X = (c_{\rm s}^2/T)p_{ij}$ and $g = g(p)p_{ij}$. The linearized Boltzmann equation is $C|g\rangle = |X\rangle$ and equation (119) can be written as $\eta = \frac{2}{5}\langle g|C|g\rangle$. The linearized collision

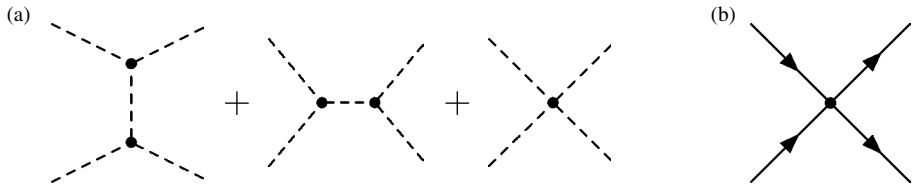

Figure 2. Leading order processes that contribute to the shear viscosity of the Fermi gas in the unitarity limit at low temperatures (a) and high temperatures (b). Dashed lines are phonon propagators and solid lines are fermion propagators.

operator C is a Hermitian, negative semi-definite operator. The zero eigenvalues of C correspond to the conservation laws for energy, momentum and particle number. Consider a variational ansatz $|g_{\rm var}\rangle$ for the exact solution $|g\rangle$ of the linearized Boltzmann equation. The triangle equality implies

$$\langle g_{\rm var}|C|g_{\rm var}\rangle\langle g|C|g\rangle \geqslant \langle g_{\rm var}|C|g\rangle^2 = \langle g_{\rm var}|X\rangle^2. \qquad (121)$$

Using $\eta = \frac{2}{5}\langle g|C|g\rangle$ we get

$$\eta \geqslant \frac{2}{5}\,\frac{\langle g_{\rm var}|X\rangle^2}{\langle g_{\rm var}|C|g_{\rm var}\rangle^2}. \qquad (122)$$

This result is, of course, not a lower bound on the exact value of η, but it is a bound within the approximation that is used to compute the collision term. A popular choice for $g_{\rm var}$ is the driving term X. This ansatz provides a good estimate in the case of non-relativistic particles interacting via short range interactions, as well as for gauge boson exchanges in QCD, but not in the case of phonon scattering[6].

A systematic method for improving the variational estimate is based on orthogonal polynomials. We can construct a complete set of polynomials that are orthogonal with respect to the inner product defined in equation (120). In non-relativistic physics these polynomials are known as Sonine polynomials [107] and suitable generalizations can be constructed for Bose and Fermi gases [108]. We now fix an integer N and expand the solution of the linearized Boltzmann equation in the first N polynomials. At finite N solving the Boltzmann equation reduces to the problem of inverting an $N \times N$ matrix. The solution provides a variational estimate for η which becomes exact as $N \to \infty$. Convergence is usually quite fast.

To complete the calculation of the shear viscosity we need to compute the scattering amplitude $\mathcal{M}$. The collision operator at leading order in T/μ is determined by the scattering amplitude at leading order in q/μ, where $q = p, p', k, k'$. The amplitude is given by the diagrams in figure 2(a) with vertices and propagators determined by the effective lagrangian given in equation (28). The expression for $\mathcal{M}$ is not very instructive and can be found in [108]. The best estimate for η is obtained by using $g(p) \sim p^{-1}$. We find

$$\eta = 9.3 \times 10^{-6}\frac{\xi^5}{c_{\rm s}^3}\frac{T_{\rm F}^8}{T^5}, \qquad (123)$$

[6] A detailed discussion of upper and lower bounds on transport coefficients can be found in [104, 105]. We also refer the reader to comparisons of the variational results with exact solutions of the Boltzmann equation [106].

where $\xi \simeq 0.4$ is the universal parameter we introduced in equation (23). In the low temperature limit the entropy density is dominated by the phonon contribution

$$s = \frac{2\pi^2}{45}\frac{T^3}{c_{\rm s}^3}. \qquad (124)$$

The ratio η/s drops sharply with temperature. Extrapolating to $T = T_{\rm c} \simeq 0.15T_{\rm F}$ gives $\eta/s \sim 0.8$, with very large uncertainties.

3.5.2. Phonons and rotons in liquid helium, pions in QCD. The calculations of shear viscosity of liquid ^{4}He below the λ point are similar to the computation of η in the superfluid Fermi gas. The main difference is that close to $T_{\rm c}$ it is important to include the roton contribution. Rotons form a dilute gas, and unlike phonons, their cross section is approximately constant. As a consequence the roton viscosity is independent of the roton density, see the discussion below equation (2). The typical roton momentum is determined by the roton minimum of the dispersion relation and depends only weakly on temperature. This implies that the roton viscosity is almost temperature independent. The value of the roton viscosity depends on the poorly known roton–roton interaction. A fit to experimental data for the shear viscosity below the lambda point gives $\eta_{\rm r} \simeq 1.2 \times 10^{-5}$ P. The leading correction to the roton term comes from phonon–roton scattering. Landau and Khalatnikov find [25]

$$\eta = \eta_{\rm r} + \frac{A}{T^{1/2}}\exp\left(\frac{\Delta}{T}\right)\frac{10 + 8\bar{\Theta}/\Theta_{\rm ph}}{1 + 8\bar{\Theta}/\Theta_{\rm ph}}, \qquad (125)$$

where Δ is the roton energy defined in equation (16), A is a constant and Θ/Θ_{ph} is the ratio of the roton–roton and roton–phonon relaxation rates. This ratio scales as $T^{4.5}\exp(\Delta/T)$. For $T < 0.9$ K we can use $\bar{\Theta} \gg \Theta_{\rm ph}$ and the temperature dependence of the phonon–roton term is governed by the $T^{-0.5}\exp(\Delta/T)$ term. For $T < 0.7$ K phonon–phonon scattering dominates and the viscosity scales as T^{-5}, as in the previous section. At even smaller temperatures, $T < 0.5$ K, phonon splitting, also known as Beliaev damping, becomes important and the temperature dependence changes to $\eta \sim T^{-1}$ [109]. The roton contribution to the entropy density is

$$s_{\rm r} = \frac{2(m^*)^{1/2}p_0^2\Delta}{(2\pi)^{3/2}T^{1/2}}\left(1 + \frac{3T}{2\Delta}\right)\exp\left(-\frac{\Delta}{T}\right), \qquad (126)$$

where m^* and p_0 are given in equation (16). The phonon contribution is given by equation (124) with $c_{\rm s} = 238\,{\rm m\,s^{-1}}$.

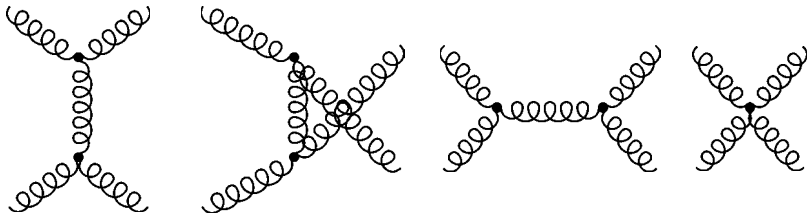

Figure 3. Leading order processes that contribute to the shear viscosity of a pure gluon plasma. The coefficient k defined in equation (133) is determined by the t-channel diagram. The full leading order result, including the coefficient μ^*, requires the remaining diagrams, as well as gluon bremsstrahlung from the external legs (not shown).

If we push equations (125) and (126) to the limit of their applicability, $T \sim 2\,\mathrm{K}$, we find $\eta/s \sim 2$.

The computation of the shear viscosity in low temperature QCD also proceeds along similar lines. The analog of the phonon in QCD is the pion, and pion interactions are governed by the effective lagrangian given in equation (46). The pion is not massless, $m_\pi = 139\,\mathrm{MeV}$. At very low temperatures, $T \ll m_\pi$, the pion scattering amplitude is approximately constant and the viscosity is only weakly temperature dependent. At higher temperatures we can set $m_\pi \simeq 0$ and the scattering amplitude is energy dependent. The main difference as compared with phonon scattering is that the four-pion interaction is of the form $(\phi\partial\phi)^2$ instead of $(\partial\phi)^4$, and that there is no three-pion interaction. As a consequence the $\pi\pi$ scattering matrix element scales as the second power of the external momenta. The pion entropy is given by equation (124) with $c_s = c/\sqrt{3}$ and an isospin degeneracy factor 3. An approximate calculation of the ratio η/s gives [110, 111]

$$\frac{\eta}{s} = \frac{15}{16\pi}\frac{f_\pi^4}{T^4}. \tag{127}$$

Variational solutions of the Boltzmann equation reported in [112] give η/s ratios that are about five times larger. The first study of the shear viscosity of a pion gas can be found in [113]. More detailed investigations of the viscosity of hadronic mixtures were published in [110, 114].

3.5.3. Non-relativistic atoms: dilute Fermi gases and ^{4}He. The shear viscosity of the dilute Fermi gas at high temperatures is determined by binary scattering between the atoms. The s-wave scattering matrix is

$$\mathcal{M} = \frac{4\pi}{m}\frac{1}{1/a + \mathrm{i}q}, \tag{128}$$

where q is the relative momentum. In the unitarity limit $a \to \infty$ the scattering amplitude diverges as $1/q$ in the limit of small momenta. For $T \gg T_\mathrm{F}$ the infrared divergence is effectively cut off by the thermal momentum $(mT)^{1/2}$. The viscosity in the high temperature limit is [115, 116]

$$\eta = \frac{15}{32\sqrt{\pi}}(mT)^{3/2}. \tag{129}$$

This result is based on the variational function $g(p) \sim 1$. Corrections due to more complicated distribution functions are small, $\Delta\eta/\eta < 2\%$ [117]. The scaling of η with temperature can be understood as a combination of the $T^{1/2}$ scaling of a dilute hard sphere gas (see section 1) with an extra factor (mT) from the $1/q^2$ behavior of $|\mathcal{M}|^2$. The high temperature limit of the entropy density is that of a classical gas

$$s = \frac{2\sqrt{2}}{3\pi^2}(mT_\mathrm{F})^{3/2}\left[\log\left(\frac{3\sqrt{\pi}}{4}\frac{T^{3/2}}{T_\mathrm{F}^{3/2}}\right) + \frac{5}{2}\right]. \tag{130}$$

Combining equations (129) and (130) gives $\eta/s \sim x^{3/2}/\log(x)$ with $x = T/T_\mathrm{F}$. The classical expression for the entropy becomes unphysical (negative) for $T \simeq T_\mathrm{c}$. Extrapolating to $T \simeq 2T_\mathrm{c}$ gives $\eta/s \simeq 0.5$.

The shear viscosity of helium is governed by scattering in the potential given in equation (15). In the high temperature limit the dominant contribution does not come from the Van der Waals tail, but from the repulsive short range contribution. For a potential of the form $V \sim r^{-\nu}$ the viscosity scales as T^s with $s = \frac{1}{2} + \frac{2}{\nu-1}$ [118]. In the case of a Lennard-Jones (6–12) potential this implies $\eta \sim T^{0.68}$. A somewhat better fit to the data is provided by

$$\eta = \eta_0\left(\frac{T}{T_0}\right)^{0.647} \tag{131}$$

with $\eta_0 = 1.88 \times 10^{-5}\,\mathrm{Pa\,s}$ and $T_0 = 273.15\,\mathrm{K}$. The entropy density is given by the classical result, equation (130). For $T = 10\,\mathrm{K}$ we get $\eta/s \simeq 4$, and extrapolating to $T = 4\,\mathrm{K}$ gives $\eta/s \simeq 1.5$. Very accurate calculations that are based on realistic potentials and include higher order terms in the density can be found in [119]. These calculations are reliable down to about 10 K.

3.5.4. Gauge fields in QCD. The shear viscosity of a QGP is determined by binary quark and gluon scattering. We first consider a pure gluon plasma. The leading order gluon–gluon scattering diagrams are shown in figure 3. The squared tree level amplitude is

$$|\mathcal{M}|^2 = \frac{9g^4}{2}\left(3 - \frac{ut}{s^2} - \frac{us}{t^2} - \frac{ts}{u^2}\right), \tag{132}$$

where g is the gauge coupling and s, t, u are the Mandelstam variables. The differential cross section diverges for small momentum transfer q as $1/q^4$. This is the standard Rutherford behavior, which arises from t-channel gluon exchange. In the calculation of the shear viscosity the

differential cross section is weighted by an extra factor of $(1-\cos\theta)$, where θ is the scattering angle. The quantity $\sigma_{\rm T} = \int {\rm d}\cos\theta\,({\rm d}\sigma)/({\rm d}\cos\theta)(1-\cos\theta)$ is known as the transport cross section. The transport cross section diverges logarithmically at small θ. This divergence is regulated by medium corrections to the gluon propagator, see equations (39) and (40). Electric gluon exchanges are screened at a distance $r_{\rm D} \sim m_{\rm D}^{-1}$, and the electric contribution to $\sigma_{\rm T}$ is proportional to $g^4\log(m_{\rm D})$. There is no static magnetic screening, but gluons with energy ω are dynamically screened at a distance $r \sim (\omega m_{\rm D}^2)^{-1/3}$. After integrating over energy the magnetic contribution also scales as $g^4\log(m_{\rm D})$. Combining electric and magnetic t-channel exchanges gives [16, 17]

$$\eta = k\frac{T^3}{g^4\log(\mu^*/m_{\rm D})}, \tag{133}$$

where $k = 27.13$. We will specify the coefficient μ^* below. This result corresponds to an optimized trial function $\chi(p) = A(p)p_{ij}v_{ij}$, but the simple approximation $A(p) \sim$ const agrees with the exact result to better than 1%. In order to compute the shear viscosity of a QGP we have to include t-channel diagrams for quark–quark and quark–gluon scattering. The result is of the same form as equation (133) with [17]

$$k(N_{\rm f}) = (27.13, 60.81, 86.47, 106.67), \qquad (N_{\rm f} = 0, 1, 2, 3). \tag{134}$$

Note that k increases with $N_{\rm f}$ faster than the total number of degrees of freedom. This is related to the fact that quarks have smaller color charges than gluons, which implies that quark–gluon scattering amplitudes are suppressed relative to gluon–gluon amplitudes.

In order to make an absolute prediction for the shear viscosity we need to determine the constant μ^* in equation (133). This coefficient receives contributions from s and u-channel gluon exchanges. These contributions are straightforward to include. A more difficult problem arises from the fact that μ^* is sensitive to soft ($q \sim m_{\rm D}$) binary $2 \to 2$ scattering followed by collinear $1 \to 2$ splitting. The inverse mean free time for this process is given by $\tau^{-1} \sim g^4T^3/m_{\rm D}^2 \times g^2 \sim g^4T$, comparable to the transport mean free time $\tau_{\rm tr}^{-1} \sim T^4/\eta \sim g^4T$. Since the scattering angle is zero collinear splitting does not directly contribute to shear viscosity, but it degrades the momentum and assists in randomizing the momentum distribution in subsequent binary collisions.

The difficulty with collinear splitting is that the formation time of the emitted gluon is of order $1/(g^2T)$. This is the same order of magnitude as the quasi-particle lifetime given in equation (43), which implies that kinetic theory is breaking down. Arnold *et al* showed that if interference between subsequent gluon emission processes, the Landau–Pomeranchuk effect, is taken into account an effective Boltzmann equation with $2 \to 2$ and $1 \to 2$ collision terms can be derived [120]. Arnold *et al* find [18]

$$\mu^*(N_{\rm f} = 0) = 2.765\,T. \tag{135}$$

They also show that μ^* is only weakly dependent on the number of flavors, $\mu^*(N_{\rm f} = 3) = 2.957\,T$, and compute additional terms in an expansion in inverse logarithms of $\mu^*/m_{\rm D}$.

The entropy density of the QGP is given by

$$s = \frac{2\pi^2}{45}\left(2(N_{\rm c}^2-1) + \frac{7}{8}4N_{\rm f}\right)T^3. \tag{136}$$

Higher order corrections to the entropy density are large, but the situation in the regime $T \geqslant 2T_{\rm c}$ can be improved using resummation schemes, see figure 1. The resummed entropy differs from the free gas result by no more than 15% for $T > 2T_{\rm c}$. The magnitude of higher order corrections to the viscosity is not known, but next-to-leading order results for the heavy quark diffusion constant suggest that higher corrections to transport coefficients are large [121].

The leading order QCD result is shown in figure 4. Clearly, η/s is strongly dependent on the coupling, and without performing higher order calculations it is not clear what value of $\alpha_{\rm s}$ one should use at a given temperature. An interesting perspective is provided by exact results for η/s in the strong coupling limit of $\mathcal{N} = 4$ SUSY Yang–Mills theory, see section 4. These results can be compared to weak coupling calculations based on kinetic theory [123]. The weak coupling result for η/s in the $\mathcal{N} = 4$ theory is smaller than the corresponding ratio in QCD by a factor $\sim 1/7$. This is related to the fact that in the $\mathcal{N} = 4$ theory all states are in the adjoint representation, and that the theory contains extra scalars. Both of these differences lead to larger cross sections.

Weak and strong coupling results for η/s as a function of the 't Hooft coupling $\lambda = g^2N_{\rm c}$ in SUSY Yang–Mills theory are shown in the right panel of figure 4. We observe that η/s in the $\mathcal{N} = 4$ theory reaches the strong coupling limit when extrapolated to a 't Hooft coupling $\lambda = g^2N_{\rm c} \simeq 12$. As discussed in section 2.5 this is a large $N_{\rm c}$ result. Naively extrapolating to $N_{\rm c} = 3$ the value $\lambda \simeq 12$ corresponds to $\alpha_{\rm s} = g^2/(4\pi) \simeq 0.3$. We also note that the value of 't Hooft coupling at which the weak coupling result for η/s reaches the strong coupling limit is larger than the coupling $\lambda \sim 5$ at which the corresponding expression for the entropy reaches the strong coupling limit $s/s_0 = 0.75$, see figure 1. If we consider $s/s_0 = 0.8$ to be the 'QCD-like' point, then we should restrict ourselves to $\lambda < 5$. In this case η/s does not drop below 0.5.

3.6. Kinetic theory: Other transport properties

3.6.1. Bulk viscosity. Bulk viscosity measures the amount of energy dissipated as a fluid is slowly expanded or compressed. In a conformally invariant system changing all the momenta and positions by a constant scale factor connects equilibrium states and the bulk viscosity must vanish. In kinetic theory bulk viscosity is typically sensitive to processes that change the particle number or the composition of the system. The kinetic theory prediction for bulk viscosity is proportional to the corresponding relaxation time, and to deviations from conformality in the equation of state. Depending on the interplay between these two effects, the temperature dependence of the bulk viscosity can differ dramatically between different fluids, and between shear and bulk viscosity.

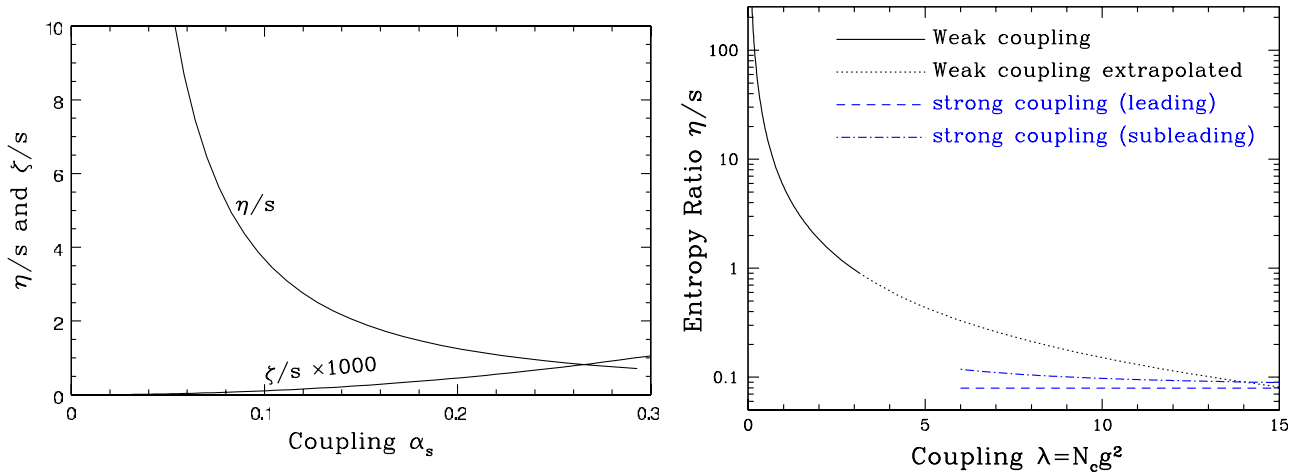

Figure 4. Shear and bulk viscosity to entropy density ratio in QCD (left panel) and $\mathcal{N} = 4$ supersymmetric Yang–Mills theory (right panel). The left panel shows the shear and bulk viscosity to entropy density ratio in QCD with $N_f = 3$ flavors as a function of the strong coupling constant α_s, from [122]. The right panel shows the ratio η/s in $\mathcal{N} = 4$ SUSY Yang–Mills theory as a function of the 't Hooft coupling $\lambda = g^2 N_c$. The solid line shows the weak coupling result, the dotted line is an extrapolation of the weak coupling result to the strong coupling regime, the dashed line is $\lambda \to \infty$ result from the AdS/CFT correspondence and the dashed–dotted line is the leading correction to the strong coupling result, from [123].

There are many fluids for which bulk viscosity is not an important source of dissipation, either because they are approximately incompressible, like water, or because the fluid is compressible but approximately scale invariant, like the QGP. On the other, we have seen that bulk viscosity is the dominant source of dissipation near a second order phase transition, see equation (98).

The Fermi gas at unitarity is exactly conformal and the bulk viscosity in the normal phase vanishes. In the low temperature phase conformal invariance requires $\zeta_1 = \zeta_2 = 0$, but ζ_3 can be non-zero [124]. This coefficient was recently computed in [125]. The result is sensitive to non-linearities in the phonon dispersion relation. If $1 \to 2$ phonon splitting is kinematically allowed then $\zeta_3 \sim T^3$, where the constant of proportionality depends on the curvature of the dispersion relation. The bulk viscosity of liquid helium was calculated by Khalatnikov [25]. As in the case of shear viscosity the main contribution comes from phonons and rotons. Khalatnikov finds that ζ_2, the bulk viscosity of the normal component, is about an order of magnitude bigger than η. The other two bulk viscosities, ζ_1 and ζ_3, involve motion of the normal fluid relative to the superfluid. They have different physical units, and cannot be directly compared with ζ_2. The linear combination that appears in the damping of second sound is $\alpha_\zeta = \zeta_2 + \rho^2\zeta_3 - 2\rho\zeta_1$. At normal density there are significant cancellations between these terms and $\zeta_2 \sim (\rho^2\zeta_3 - 2\rho\zeta_1)$. The bulk viscosity of helium vapor is small. Note that the bulk viscosity of most gases is dominated by internal excitations, such as rotational and vibrational modes.

The bulk viscosity of a pion gas at low temperature was computed by Chen and Wang [126]. They find that the bulk viscosity scales as $\zeta \sim T^7/f_\pi^4$ (up to logarithms). The bulk viscosity of the high temperature QGP phase was calculated by Arnold *et al* [122]. The result is

$$\zeta = \frac{A\alpha_s^2 T^3}{\log(\mu^*/m_D)}, \qquad (137)$$

where $A = 0.443$ and $\mu^* = 7.14\,T$ in pure gauge QCD. In full QCD with $N_f = 3$ quark flavors $A = 0.657$ and $\mu^* = 7.77\,T$. We observe that ζ scales as $\alpha_s^4 \times \eta$. The trace anomaly $\epsilon - 3P$ is proportional to α_s^2, so bulk viscosity scales like the shear viscosity times the second power of the deviation from conformality. This is in agreement with a simple formula proposed by Weinberg [127], $\zeta \sim (c_s^2 - \frac{1}{3})^2\eta$. However, Weinberg's relation is known to be violated in some theories, see [128] for an example.

3.6.2. Diffusion. The diffusion of impurities in liquid helium has been studied in some detail. Of particular interest is the behavior of dilute solutions of ^{3}He in ^{4}He. At low temperatures the diffusion constant is determined by scattering of phonons and $D \sim 1/T^7$ [25, 129]. At high temperatures diffusion is governed by scattering between atoms and $D \sim T^{1+s}$ with $s = \frac{1}{2} + \frac{2}{\nu-1}$ for a $1/r^\nu$ potential [118]. We conclude that the temperature dependence of the diffusion constant is identical to that of the shear viscosity. In the case of the unitary Fermi gas one can make use of the fact that the number of spin up and spin down fermions is separately conserved, and study the diffusion of minority spin down particles in a background of majority spin up fermions [130]. This process contains important information about the interaction between the different spin states, but it is not directly related to the viscosity of the spin balanced gas.

The diffusion constant for heavy quarks in a QGP can be determined by computing the mean square momentum transfer per unit time, see section 3.2. For approximately thermal heavy quarks the diffusion constant is dominated by heavy quark scattering on light quarks and gluons, $qQ \to qQ$ and $gQ \to gQ$. As in the case of shear viscosity the most important Feynman diagrams involve t-channel gluon exchanges. Since the heavy quark is slow the dominant interaction is electric gluon exchange and the cross section is regularized by Debye

screening. The leading order result is [131, 132]

$$D = \frac{36\pi}{C_F g^4 T}\left[N_c\left(\log\left(\frac{2T}{m_D}\right)+c\right)+\frac{N_f}{2}\left(\log\left(\frac{4T}{m_D}\right)+c\right)\right]^{-1}, \tag{138}$$

where $C_F = (N_c^2-1)/(2N_c)$ and $c = 0.5 - \gamma_E + \zeta'(2)/\zeta(2)$. We note that the diffusion constant has the same parametric dependence on the coupling as the shear viscosity. The relaxation time η_D^{-1} scales as $M_Q/(T^2 g^4 \log(g)$, which is larger by a factor M_Q/T compared with the hydrodynamic relaxation time $\eta/(sT) \sim 1/(Tg^4\log(g))$. This is confirmed by numerical estimates, which give $\eta_D^{-1} \simeq 6.7/T \simeq 7\,\text{fm}$ for charm quarks at $T = 200\,\text{MeV}$ [132]. For comparison, the hydrodynamic relaxation time is $\eta/(sT) \simeq 1\,\text{fm}$ (for $\eta/s \simeq 1$).

3.6.3. Thermal conductivity. Thermal transport in superfluid helium is a complicated process. In a superfluid heat transport can take place by a process similar to internal convection where the superfluid moves relative to the normal fluid. Only the normal fluid carries entropy and as a result heat is carried along with the normal component. The convective contribution to heat flow is controlled by the shear viscosity of the normal fluid. Within the normal fluid heat is carried by phonons and rotons. Khalatnikov showed that there is no heat transport in a gas of phonons with exactly linear dispersion relation [25]. The thermal conductivity of the normal fluid is dominated by rotons and phonon–roton scattering. This situation is somewhat similar to heat transport in a solid. At very low temperatures, heat transport is ballistic and the entropy is carried by a net flow of phonons along the temperature gradient. At higher temperatures non-linearities in the phonon dispersion relation and the 'umklapp' process play a role.

The situation at high temperatures is much simpler. Heat flow is a diffusive process, and the thermal conductivity is determined by scattering between atoms. A simple mean free path estimate analogous to equation (2) is

$$\kappa = \tfrac{1}{3} n c_p p l_{\text{mfp}}, \tag{139}$$

where c_p is the specific heat at constant pressure. This estimate suggests that the ratio of the shear and thermal diffusion constants, the Prandtl number

$$Pr = \frac{\eta c_p}{\kappa}, \tag{140}$$

is close to one. At large T the thermal conductivity of helium scales as T^s with $s = \frac{1}{2} + \frac{2}{\nu-1}$, as in the case of shear viscosity. The Prandtl number is approximately constant, $Pr \simeq 2.5$.

Most studies of the thermal conductivity of a QGP have focused on the regime of very high baryon density. In the limit $\mu \gg T$, where μ is the quark chemical potential, the thermal conductivity scales as $\kappa \sim \mu^2/\alpha_s^2$ [133]. In the opposite limit $T \gg \mu$ there is an old relaxation time estimate $\kappa \sim T^4/(\alpha_s^2\mu^2)$ [9]. Note that while κ diverges as $\mu \to 0$, the dissipative contribution to the baryon current, equation (81), is finite.

4. Holography

In kinetic theory conserved charges are carried by well-defined quasi-particles. The time between collisions is long compared with the quantum mechanical scale, $\hbar/T$, and quantum mechanical interference between scattering events is not important. In the strong coupling limit quantum mechanical effects are large and quasi-particles lose their identity. A powerful new tool to study transport phenomena in this regime is the AdS/CFT correspondence [20, 134, 135].

The AdS/CFT correspondence is referred to as a holographic duality—it relates string theory on a certain higher dimensional manifold to four-dimensional gauge theory on the boundary of this space. The correspondence is simplest if the field theory is strongly coupled. In this limit the string theory reduces to a classical gravitational theory. The holographic correspondence then implies that a four-dimensional field theory is capable of encoding gravity in five dimensions. The idea of a correspondence between field theories and higher dimensional gravity originated from developments within string theory, but there are precursors to the correspondence that come from the physics of black holes. It has been known for some time that black holes carry entropy, and that the entropy is proportional to the area, and not the volume of the black hole. It was also known that the evolution of black holes respects the second law of thermodynamics, and that it can be described by treating the event horizon as a physical membrane with well-defined transport properties like electric conductivity and shear viscosity [136].

The best studied example of the AdS/CFT correspondence is the equivalence between $\mathcal{N} = 4$ Super Yang–Mills theory (see section 2.5) and string theory on $AdS_5 \times S_5$. For our purposes the dynamics only involves AdS_5. This is a five-dimensional space, which in AdS/CFT terminology is called the *bulk*. The dual field theory exists on the *boundary* of this space, which is a 3+1-dimensional Minkowski space. The gauge gravity duality works as follows: classical gravity equations of motion are solved in the 4+1-dimensional curved geometry of AdS_5. Fluctuations of gravitational fields in the bulk induce charges on the 3 + 1-dimensional boundary. The dynamics of 3+1-dimensional boundary theory *is* the strongly coupled CFT which we wish to study. Transport properties of the boundary theory can be determined by perturbing the boundary charges with an external field which then propagates into the bulk. The response of the induced charges to the applied field determines the transport coefficients. For each conserved charge of the field theory there is a corresponding field in the gravitational theory. The field corresponding to the stress tensor $T^{\mu\nu}$ is the graviton $h^{\mu\nu}$, and the field corresponding to the conserved R charge current J_R^μ is the five-dimensional Maxwell field A^μ.

The AdS/CFT setup is analogous to a parallel plate capacitor. Electromagnetic fields in the bulk, the space between the plates, induce surface charges on the boundary. Fluctuations of the bulk field create fluctuations of the surface charges, and correlation functions of the surface charges can be related to normal modes of the bulk field. What is remarkable about the AdS/CFT correspondence is that the gravitational

theory in the bulk defines a local field theory on the boundary, and that there are classical gravitational field configurations that correspond to field theories at a finite temperature. These configurations can be used to study dissipative phenomena in the boundary field theory.

The gravitational field configuration relevant to field theories at a finite temperature is an AdS_5 black hole. In the black hole geometry the gravitational field is non-zero as we approach the boundary of the 4 + 1-dimensional space. This gravitational field is balanced by a non-zero stress tensor in the boundary field theory—the gravitational setup corresponds to the dynamics of a field theory with a non-zero density matrix. The event horizon of the back hole spans three spatial dimensions in the bulk and radiates at the Hawking temperature T_H. The black hole fills AdS_5 with a bath of gravitational radiation, and the temperature of the heat bath is identified with the temperature of the boundary field theory. The dynamics of graviton propagation in the black hole background determines stress tensor correlators at a finite temperature in the boundary field theory. These correlators determine the shear viscosity according to Kubo formulae.

There is a vast amount of literature on the AdS/CFT correspondence. A detailed review with extensive references is [137], and more pedagogical reviews can be found in [138–140]. Reviews with an emphasis on transport phenomena are [28, 29]. Here we will concentrate on a few selected issues that are relevant to this review. First, we will explain the calculation of the shear viscosity and the spectral weights of strongly coupled fluids. Then we will comment on the conjectured viscosity bound and the calculation of other transport properties. Finally, we will review the derivation of higher order fluid dynamics using holography, and summarize some recent attempts to extend the correspondence to non-relativistic theories.

4.1. The equation of state from holography

$AdS_5 \times S_5$ is the product of five-dimensional Anti-deSitter Space (AdS) and a five-sphere. Anti-deSitter space is a simple solution of the source free Einstein equation with a negative cosmological constant. Note that, on large scales, our universe is approximately a four-dimensional deSitter space. The geometry of $AdS_5 \times S_5$ is described by the metric

$$ds^2 = \frac{r^2}{L^2}\left(-dt^2 + d\boldsymbol{x}^2\right) + \frac{L^2}{r^2}\,dr^2 + L^2 d\Omega_5^2. \qquad (141)$$

Here, $d\Omega_5^2$ is the metric of the five-sphere and $(t, \boldsymbol{x}, r)$ are the coordinates on AdS_5. The coordinate r is referred to as the 'radial' AdS_5 coordinate. The limiting value $r \to \infty$ is the 'boundary' of AdS_5. A fixed r slice of AdS_5 is a 3 + 1-dimensional flat Minkowski space, but the five-dimensional space is curved, with a constant negative curvature. L is the corresponding curvature radius. We require that L is large compared with the string length ℓ_s which guarantees the validity of the classical approximation. In the AdS/CFT correspondence L is related to the coupling constant of the $\mathcal{N} = 4$ gauge theory, $\lambda \equiv g_{YM}^2 N_c$, through the relation $(L/\ell_s)^4 = \lambda$. The classical approximation to the gravitational theory is reliable if the field theory is strongly coupled. The classical fields can be expanded in S_5 spherical harmonics. At strong coupling higher harmonics are separated by a large gap, and we will ignore S_5 from now on.

The metric of an AdS_5 black hole is

$$ds^2 = \frac{r^2}{L^2}\left(-f(r)\,dt^2 + d\boldsymbol{x}^2\right) + \frac{L^2}{f(r)r^2}\,dr^2, \qquad (142)$$

where $f(r) = 1 - (r_0/r)^4$. The black hole horizon is a 3 + 1-dimensional surface at $r = r_0$. The horizon radius is related to the Hawking temperature of the black hole by $r_0\hbar/L^2 = \pi T_H$. This formula is an example of a general radius–energy relation in the AdS/CFT correspondence. A modification of the AdS geometry at radius r corresponds to a modification of the field theory at an energy scale $r\hbar/L^2$. It is convenient to perform a change in variables $u \equiv (r_0/r)^2$ and write the metric as

$$ds^2 = \frac{(\pi T L)^2}{u}\left(-f(u)\,dt^2 + d\boldsymbol{x}^2\right) + \frac{L^2}{4u^2 f(u)}\,du^2, \qquad (143)$$

where $f(u) = 1 - u^2$. Now the horizon is at $u = 1$. The boundary limit is found by evaluating all quantities at $u = \epsilon$ and then taking the boundary limit $\epsilon \to 0$.

As discussed in the introduction to this section, the modified metric implies that there is an induced stress tensor at the boundary, $u = \epsilon$. This is an important point, and we will compute the induced stress tensor in two different ways. First, we will determine it by varying the action with respect to the boundary metric. This is the standard method by means of which one can determine the source of a given gravitational field. The only unusual ingredient is the fact that the induced stress tensor is located on the boundary. We will provide an alternative derivation based on the analogy with the induced surface charge in electrodynamics below.

The boundary metric $g_{\mu\nu}$ is related to the metric of the five-dimensional theory $G_{\mu\nu}$ by the AdS scale factor

$$g_{\mu\nu} \equiv \frac{u}{(\pi T L)^2}\,G_{\mu\nu}. \qquad (144)$$

Here and below Greek letters denote four-dimensional indices $(x^\mu) = (t, x, y, z)$ while Roman letters denote five-dimensional indices $(x^M) = (x^\mu, u)$. Near the boundary the metric can be written as

$$g_{\mu\nu} = g^o_{\mu\nu} + u^2 \mathcal{B}_{\mu\nu} + O(u^4), \qquad (145)$$

where $g^o_{\mu\nu}$ is interpreted as the metric of $\mathcal{N} = 4$ gauge theory. Usually $g^o_{\mu\nu}$ is simply $\eta_{\mu\nu}$. We will see that the coefficient of u^2 determines the induced stress tensor on the boundary.

The induced stress tensor is

$$\langle T_{\mu\nu}\rangle = \lim_{\epsilon\to 0}\frac{-2}{\sqrt{-g}}\frac{\delta S}{\delta g^{\mu\nu}}\bigg|_{u=\epsilon}, \qquad (146)$$

where $\sqrt{-g} = (-\det g_{\mu\nu})^{1/2}$. The action is a sum of the Einstein–Hilbert action, the Gibbons–Hawking–York boundary term and counter terms which are needed to render the action finite in the limit $u \to 0$,

$$S \equiv S_{EH} + S_{GH} + S_{CT}. \qquad (147)$$

The Einstein–Hilbert action is

$$S_{\rm EH} = \frac{1}{2\kappa_5^2}\int_{\mathcal{M}} {\rm d}^5x\,\sqrt{-g}\,(\mathcal{R}+2\Lambda)\,, \tag{148}$$

where $\mathcal{R}$ is the Ricci scalar and $\Lambda = 6/L^2$ is the cosmological constant. The five-dimensional Newton constant $1/\kappa_5^2$ is related to the number of colors in the field theory, $1/\kappa_5^2 = N_{\rm c}^2/(4\pi^2L^3)$. The Gibbons–Hawking–York [141, 142] boundary action is

$$S_{\rm GH} = \frac{1}{2\kappa_5^2}\int_{\partial\mathcal{M}} {\rm d}^4x\sqrt{-\gamma}\,2K, \tag{149}$$

where we have defined the boundary metric

$$\gamma_{\mu\nu} = G_{\mu\nu}\big|_{u=\epsilon}\,, \tag{150}$$

and K is the trace of the extrinsic curvature[7]. The boundary term guarantees that the variation of the action with respect to the five-dimensional metric gives the Einstein equations in the bulk provided the variation vanishes on the boundary. Without the boundary action one also has to require that derivatives of the variation vanish on the boundary, see [143]. Finally, the counter term

$$S_{\rm CT} = -\frac{6}{L}\int_{\partial\mathcal{M}} {\rm d}^4x\sqrt{\gamma}, \tag{151}$$

is needed to render the action finite in the limit $u\to 0$. Note that the counter term is independent of temperature. With these definitions, the variation relates the stress tensor to the extrinsic curvature:

$$\langle T_{\mu\nu}\rangle = -\frac{1}{\kappa_5^2}\lim_{u\to 0}\frac{(\pi TL)^2}{u}\left[K_{\mu\nu}-K\gamma_{\mu\nu}+\frac{3}{L}\gamma_{\mu\nu}\right]. \tag{152}$$

Substituting the black hole metric equation (143) and using the definition of the extrinsic curvature we have

$$\langle T_{\mu\nu}\rangle = {\rm diag}(\epsilon,\,p,\,p,\,p), \qquad \frac{\epsilon}{3} = p = \frac{N_{\rm c}^2}{8\pi^2}(\pi T)^4. \tag{153}$$

We find that $\epsilon = 3P$, as expected for a scale invariant theory. We can compare the coefficient of T^4 with its value in the non-interacting theory. $\mathcal{N}=4$ SUSY QCD has $8(N_{\rm c}^2-1)\simeq 8N_{\rm c}^2$ bosonic and fermionic degrees of freedom. The contribution of a massless fermion to the pressure is 7/8 of that of a massless boson, see equation (35). Equation (153) shows that the pressure in strongly coupled $\mathcal{N}=4$ SUSY QCD is three quarters of the Stefan–Boltzmann value.

We can also obtain equation (152) in analogy with the induced surface charge on a capacitor plate. Consider a plate that spans the x–y plane. The surface charge density is related to the jump of electric field across the plate

$$\sigma = \Big[E^z\Big], \tag{154}$$

where $[E^z] = E^z_+ - E^z_-$ notates the jump. The analogous formulae in the gravitational theory are known as junction conditions [144]. Integrating the Einstein equations across a Gaussian pill box relates the surface stress $\tau^\mu{}_\nu$ to the jump in the extrinsic curvature

$$\tau^\mu{}_\nu = -\frac{1}{\kappa_5^2}\Big[K^\mu{}_\nu - K\delta^\mu{}_\nu\Big]. \tag{155}$$

Thus the particular combination of extrinsic curvature plays an analogous role in the normal electric field, i.e. a combination of $-K_{\mu\nu} = n_u\Gamma^u_{\mu\nu}$ is the analog of $\boldsymbol{n}\cdot\boldsymbol{E}$. If we have a semi-infinite metal block with surface charge density σ, then the outgoing electric field is related to the surface charge $E^z = \sigma$. By analogy, we associate the outgoing flux of extrinsic curvature at $u=\epsilon$ with the stress tensor in the gauge theory:

$$\sqrt{-g}T^\mu{}_\nu = -\frac{1}{\kappa_5^2}\sqrt{\gamma}\left(K^\mu{}_\nu - K\delta^\mu{}_\nu\right). \tag{156}$$

Then taking the boundary limit $u\to 0$, we tentatively define the stress:

$$T^\mu{}_\nu = -\frac{1}{\kappa_5^2}\lim_{u\to 0}\frac{(\pi TL)^4}{u^2}\left(K^\mu{}_\nu - K\delta^\mu{}_\nu\right). \tag{157}$$

Substituting the black hole AdS metric into this expression gives a divergent result. Nevertheless, the difference between this stress and the stress determined with the vacuum AdS metric equation (141) is finite:

$$\langle T^\mu{}_\nu\rangle - \langle T^\mu{}_\nu\rangle_{\rm vacuum} = -\frac{1}{\kappa_5^2}\lim_{u\to 0}\frac{(\pi TL)^4}{u^2} \times\left(K^\mu{}_\nu - K\delta^\mu{}_\nu + \frac{3}{L}\delta^\mu{}_\nu\right). \tag{158}$$

After lowering the indices of $K^\mu{}_\nu$ with $\gamma_{\mu\nu} = [(\pi TL)^2/u]\,\eta_{\mu\nu}$, this equation is the same as derived previously in equation (152).

4.2. Shear viscosity from holography

In the previous section we computed the average stress tensor on the boundary, $\langle T^{\mu\nu}(\boldsymbol{x},t)\rangle$, which is a one-point function of the CFT. By Kubo's formula, equation (100), the shear viscosity can be related to a retarded two-point function. We will determine this function using linear response theory. Momentarily ignore the fifth dimension and consider turning on a time varying gravitational field $h^o_{xy}(\omega)$ in the usual four-dimensional field theory. This time varying gravitational field induces a deviation from the equilibrium stress tensor in the same way that a time varying electric field induces a net current. According to linear response theory, the expectation value of the stress energy tensor is

$$\langle T_{xy}(\omega)\rangle_{h^o_{xy}} = T^{\rm eq}_{xy}(\omega) + G_{\rm R}(\omega)\,h^o_{xy}(\omega), \tag{159}$$

where $T^{\rm eq}_{xy} = (\epsilon+p)u_xu_y + pg_{xy} = ph^o_{xy}(\omega)$ is the equilibrium stress tensor and $G_{\rm R}(\omega)$ is the equilibrium retarded correlator defined in equation (99). Kubo's formula dictates the functional form of this correlator in the small frequency

[7] More explicitly, $K = G^{\mu\nu}\nabla_\mu n_\nu$ with n^M an outward directed normal to the boundary of the AdS space, $n^M = -\sqrt{G^{55}}\delta^{5M}$. Note that $K_{\mu\nu} = \nabla_\mu n_\nu = -n_u\Gamma^u_{\mu\nu} = n^u\partial_u G_{\mu\nu}$.

limit, $G_{\rm R}(\omega) = -{\rm i}\omega\eta$. Thus the average stress tensor in the presence of a time varying gravitational field is

$$\left\langle T_{xy}(\omega)\right\rangle_{h^o_{xy}} = p h^o_{xy} - {\rm i}\omega\eta\, h^o_{xy}(\omega). \tag{160}$$

Now consider the small fluctuations of the metric field $H_{xy}(\omega, u)$ around the black hole metric equation (143) of the five-dimensional theory. The equation of motion for the gravitational fluctuation is found by linearizing the Einstein equations

$$\mathcal{R}_{\rm MN} - \tfrac{1}{2} G_{\rm MN}\,(\mathcal{R} + 2\Lambda) = 0. \tag{161}$$

After a modest amount of algebra, the $\mathcal{R}_{xy}$ equation becomes an equation for $h_{xy} \equiv u H_{xy}(\omega, u)/(\pi T L)^2$:

$$h''_{xy}(\omega, u) - \frac{1+u^2}{uf} h'_{xy}(\omega, u) + \frac{\omega^2}{(2\pi T)^2 u f^2} h_{xy}(\omega, u) = 0, \tag{162}$$

where the primes denote derivatives with respect to u. This is a second order linear differential equation with regular singular points in the physical domain at the horizon $u = 1$ and the boundary $u = 0$. Solving equation (162) near the black hole horizon $u = 1$, we determine that the fluctuation of the metric is a linear combination of two solutions, $h_{xy}(\omega, u) \sim (1-u)^{\mp {\rm i}\omega/4\pi T}$. These solutions describe the gravitational wave propagating into $(-)$ and out of $(+)$ the black hole, respectively. The infalling solution is the physically relevant retarded solution. Near the boundary $u \to 0$ (or $r \to \infty$) the gravitational field is also a linear combination of two solutions:

$$h_{xy}(\omega, u) = h^o_{xy}(\omega)\,(1 + \cdots) + \mathcal{B}(\omega)\, u^2\,(1 + \cdots), \tag{163}$$

where $\cdots$ denotes the terms that vanish as $u \to 0$. The two modes are called the non-normalizable mode and the normalizable mode. The non-normalizable mode is constant as $r \to \infty$ while the normalizable mode falls as $1/r^4$. Inserting the metric perturbation equation (163) into equation (152) the average stress tensor is

$$\left\langle T_{xy}(\omega)\right\rangle = p\, h^o_{xy}(\omega) + (\epsilon + p)\, \mathcal{B}(\omega), \tag{164}$$

with the previously defined energy density and pressure, equation (153). We observe that the coefficient of the non-normalizable mode, h^o_{xy}, can be interpreted as the external gravitational field applied to the gauge theory, while the coefficient of the normalizable mode, $\mathcal{B}(\omega)$, is proportional to the induced stress tensor in the boundary theory.

For an arbitrary value of $\mathcal{B}(\omega)$ the general linear combination of solutions near the boundary would approach a linear combination of the infalling and outgoing solutions near the horizon. Thus the coefficient $\mathcal{B}(\omega)$ should be adjusted so that only the infalling solution $(1-u^2)^{-{\rm i}\omega/4\pi T}$ is present near $u = 1$. In general, the required $\mathcal{B}(\omega)$ has to be determined numerically. For small ω however, a straightforward calculation shows that to linear order in ω the solution which is infalling at the horizon is

$$h_{xy} = h^o_{xy}(\omega)(1-u)^{-{\rm i}\omega/4\pi T}\left[1 - \frac{{\rm i}\omega}{4\pi T}\log(1+u) + O(\omega^2)\right]. \tag{165}$$

Expanding this functional form near the boundary we find $\mathcal{B}(\omega) = -{\rm i}\omega/(4\pi T)$. Then using $\epsilon + p = sT$ and comparing the functional forms in equations (160) and (164) we conclude that $\left\langle T_{xy}(\omega)\right\rangle = p h^o_{xy} - {\rm i}\omega\eta h^o_{xy}$ with

$$\frac{\eta}{s} = \frac{1}{4\pi}. \tag{166}$$

Remarkably, the strong coupling limit of the shear viscosity is small and independent of the coupling. The difference as compared with the weak coupling result becomes even clearer if one considers the spectral function. As described in section 3.4 the Kubo formula relates the shear viscosity to the zero energy limit of the stress-energy spectral function. In weak coupling QCD the spectral function has a narrow peak near zero energy which reflects the fact that momentum transport is due to quasi-particles that are almost on-shell. The height of the transport peak is governed by the kinetic theory result for the shear viscosity. Kubo's formula implies that $\rho(\omega)/\omega \sim T^3/g^4$ as $\omega \to 0$. The width can be reconstructed from the f-sum rule

$$T\int_0^\Lambda \frac{{\rm d}\omega}{\omega}\rho^{xyxy}(\omega) = \frac{T(\epsilon + P)}{5}, \tag{167}$$

where $g^4 T \ll \Lambda \ll g^2 T$. Since the height of the transport peak is T^3/g^4, the width must be $g^4 T$. The high energy part of the spectral density can be computed from the one-loop correlation function. The result is $\rho(\omega) \sim \omega^4$. A schematic picture of the spectral function is shown in figure 5(*a*).

In the strong coupling limit the width of the transport peak becomes bigger and the height becomes smaller. In $\mathcal{N} = 4$ SUSY Yang–Mills the infinite coupling limit can be determined as outlined above [147, 148]. Specifically, the spectral function may be found by determining $G_{\rm R}(\omega)$ from the numerical coefficient $\mathcal{B}(\omega)$. The result is shown in figure 5(*b*). Clearly, the transport peak has completely disappeared, and there is no possibility of a quasi-particle interpretation of momentum transport. Whether the spectral function of the QGP near $T_{\rm c}$ looks more like figure 5(*a*) or (*b*) will have to be settled by numerical calculations on the lattice, see section 3.4. It is interesting to note that numerical calculations of the shear viscosity, which require the determination of the zero energy limit of $\rho(\omega)/\omega$, are easier in the case of strong coupling than they are for weak coupling.

4.3. The KSS bound

The calculation of the shear viscosity has been extended to other strongly coupled field theories with gravitational duals. It was discovered that within a large class of theories the strong coupling limit of η depends on the theory, but the ratio η/s does not. This observation can be understood using Kubo's formula and the optical theorem. The optical theorem implies that the imaginary part of a correlation function can be related to the total cross section. As a consequence, the shear viscosity can be expressed in terms of the total graviton absorption cross section [19],

$$\eta = \frac{\sigma_{\rm abs}(0)}{2\kappa_5^2}. \tag{168}$$

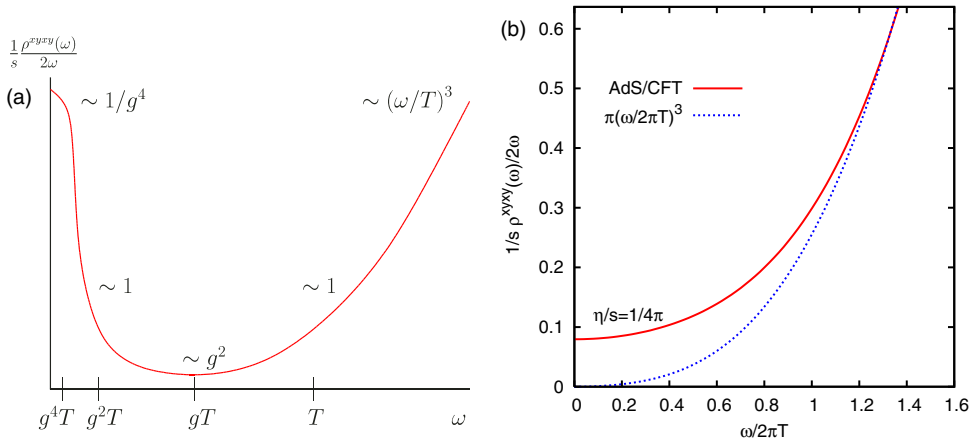

Figure 5. Spectral function $\rho^{xyxy}(\omega, \boldsymbol{k} = 0)$ associated with the correlation function of the xy component of the energy momentum tensor. The spectral function is normalized to entropy density s. (*a*) Schematic picture of the spectral density in weak coupling QCD or SUSY Yang–Mills theory [145, 146]. (*b*) Spectral density in strong coupling SUSY Yang–Mills theory calculated using the AdS/CFT correspondence, from [147].

The low energy limit of $\sigma_{\rm abs}$ is equal to the area A of the event horizon, and the entropy density is given by the Hawking–Bekenstein formula, $s = A/(4G)$ where $G = \kappa_5^2/(8\pi)$. The ratio η/s is independent of A and κ_5. More formal arguments for the universality of η/s in the strong coupling limit of field theories with holographic duals were given in [28, 149, 150]. Corrections to the infinite coupling limit of $\mathcal{N} = 4$ SUSY Yang–Mills theory were studied in [21, 151–153]. The result is

$$\frac{\eta}{s} = \frac{1}{4\pi}\left\{1 + \frac{15\zeta(3)}{\lambda^{3/2}} + \cdots\right\}. \tag{169}$$

The first correction is positive, as one would expect from the fact that $\eta/s \to \infty$ as $\lambda \to 0$. Based on these observations, Kovtun, Son and Starinets (KSS) conjectured that

$$\frac{\eta}{s} \geqslant \frac{1}{4\pi} \tag{170}$$

is a universal bound that applies to all fluids [10]. There is no proof of this conjecture, and a number of authors have attempted to construct counter examples. One possibility is a weakly interacting non-relativistic fluid with an exponentially large number of species or internal degrees of freedom, and therefore a very large entropy [10, 154, 155]. These systems are unusual because the timescale for thermal equilibration vastly exceeds the timescale for momentum equilibration, and because the fluid is not stable on very long timescales [156]. More recently, it was realized that theories with holographic duals described by higher derivative gravity may violate the KSS bound [157–160]. An explicit example was constructed by Kats and Petrov [159]. They showed that in $\mathcal{N} = 2$ SUSY $Sp(N_{\rm c})$ gauge theory with a certain combination of matter fields

$$\frac{\eta}{s} = \frac{1}{4\pi}\left(1 - \frac{1}{2N_{\rm c}}\right), \tag{171}$$

up to corrections of $O(\lambda^{-3/2})$. For $\lambda^{3/2} \gg N_{\rm c} \gg \lambda \gg 1$ we find a violation of the KSS bound in a controlled calculation. However, there are bounds on the coefficients of higher derivative terms, and a modified bound on η/s may yet exist [160].

4.4. Other transport properties

There has been a large amount of work on applications of the AdS/CFT correspondence to transport properties other than the shear viscosity. Here we briefly summarize some results relevant to this review. $\mathcal{N} = 4$ SUSY Yang–Mills theory has a conserved R-charge (see section 2.5), and we can study transport in the presence of a finite R-charge density. Son and Starinets find that the shear viscosity and entropy density depend on the density, but the ratio η/s does not [161]. They also determine the thermal conductivity

$$\kappa = \frac{8\pi^2 T}{\mu^2}\,\eta, \tag{172}$$

as well as the R-charge diffusion constant. The heavy quark diffusion constant was calculated in [162–164]. The result is

$$D = \frac{2}{\pi T}\frac{1}{\sqrt{\lambda}}, \tag{173}$$

which depends on the value of the coupling λ, and goes to zero in the strong coupling limit. The functional dependence on λ is unusual from the point of view of perturbation theory, but typical of other AdS/CFT results. We also note that in the strong coupling limit the ratio of the heavy quark diffusion coefficient to the kinematic viscosity $\eta/(sT)$ goes to zero, whereas this ratio is independent of the coupling in the perturbative limit.

The bulk viscosity of $\mathcal{N} = 4$ SUSY Yang–Mills theory vanishes, but non-conformal deformations of the original AdS/CFT correspondence have been studied. Buchel proposed that in holographic models there is a lower bound on the bulk viscosity, $\zeta \geqslant 2(\frac{1}{3} - c_{\rm s}^2)\eta$, where $c_{\rm s}$ is the speed of sound [165]. Note that the weak coupling formula involves the square of $(\frac{1}{3} - c_{\rm s}^2)$. Gubser *et al* considered a number of model geometries tuned to reproduce the QCD equation of state, and find that ζ/s has a maximum near the critical temperature where $\zeta/s \simeq 0.05$ [166]. Larger values of ζ/s near $T_{\rm c}$ have been suggested based on lattice data for the QCD trace anomaly [167].

4.5. Hydrodynamics and holography

Up to this point we have used the AdS/CFT correspondence to calculate the transport coefficients that appear in first order hydrodynamics. However, AdS/CFT can be used to compute the full correlation function, and not just the hydrodynamic limit. An example is the spectral function shown in figure 5, and similar calculations have been performed in other channels as well. In this section we wish to discuss how the stress tensor of the fluid relaxes to the Navier–Stokes form. This process can be described by the second order terms introduced in section 3.1.3. We will follow the method outlined in [77].

A static fluid at temperature T corresponds to a black hole with a Hawking temperature $T_{\rm H} = r_0/(\pi L^2)$. First we switch to Eddington–Finkelstein coordinates, defining a new time coordinate $v = t + \int^r {\rm d}r\, L^2/fr^2$. Then the metric is regular at the event horizon of the black hole,

$$ {\rm d}s^2 = 2\,{\rm d}v\,{\rm d}r + \frac{r^2}{L^2}\left[-f(r)\,{\rm d}v^2 + r^2\,{\rm d}\boldsymbol{x}^2\right]. \tag{174} $$

Introducing four-dimensional coordinates $x^\mu = (x^0, x^1, x^2, x^3) = (v, \boldsymbol{x})$, a vector $u^\mu = (1, \mathbf{0})$ characterizing the local rest frame and a scale parameter b characterizing the temperature the metric becomes

$$ \begin{aligned} {\rm d}s^2 &= -2u_\mu\,{\rm d}x^\mu\,{\rm d}r + \frac{r^2}{L^2}[-f(br)u_\mu u_\nu\,{\rm d}x^\mu\,{\rm d}x^\nu \\ &\quad + r^2 P_{\mu\nu}\,{\rm d}x^\mu\,{\rm d}x^\nu], \end{aligned} \tag{175} $$

where $P_{\mu\nu} = u_\mu u_\nu + \eta_{\mu\nu}$. The basic idea is to promote the variables u^μ and b to slowly varying functions of x^μ. The metric is then

$$ \begin{aligned} {\rm d}s^2 &= -2u_\mu(x)\,{\rm d}x^\mu\,{\rm d}r \\ &\quad + \frac{r^2}{L^2}\left[-f(b(x)r)u_\mu(x)u_\nu(x)\,{\rm d}x^\mu\,{\rm d}x^\nu + r^2 P_{\mu\nu}(x)\,{\rm d}x^\mu\,{\rm d}x^\nu\right] \\ &\quad + \text{corrections due to gradients.} \end{aligned} \tag{176} $$

Variations in u_μ and b correspond to fluctuations in the local fluid velocity and temperature. Substituting this form into the Einstein equations, the corrections to the metric are determined order by order in the gradients of $u^\mu(x)$ and $b(x)$. These metric corrections lead to deviations of the boundary stress tensor from an ideal fluid of precisely the form required by hydrodynamics. Up to second order we can write

$$ T^{\mu\nu} = T_0^{\mu\nu} + \delta^{(1)}T^{\mu\nu} + \delta^{(2)}T^{\mu\nu} + \cdots, \tag{177} $$

and each term has physical significance. At zeroth order

$$ T_0^{\mu\nu} = \frac{N_{\rm c}^2}{8\pi^2}(\pi T)^4\left(\eta^{\mu\nu} + 4u^\mu u^\nu\right), \tag{178} $$

which shows that $\epsilon = 3P$ and that the pressure is 3/4 of the Stefan–Boltzmann value. At first order

$$ \delta^{(1)}T^{\mu\nu} = -\frac{N_{\rm c}^2}{8\pi^2}(\pi T)^3\sigma^{\mu\nu}, \tag{179} $$

where $\sigma^{\mu\nu}$ is defined as in equation (80). This result shows that $\eta = N_{\rm c}^2\pi T^3/8$. Combined with the zeroth order stress tensor we find $\eta/s = 1/4\pi$, in agreement with previous results. Finally, at second order

$$ \begin{aligned} \delta^{(2)}T^{\mu\nu} &= \eta\tau_\Pi\left[\langle D\sigma^{\mu\nu\rangle} + \tfrac{1}{3}\sigma^{\mu\nu}(\partial\cdot u)\right] \\ &\quad + \lambda_1\sigma_\lambda^{\langle\mu}\sigma^{\nu\rangle\lambda} + \lambda_2\sigma_\lambda^{\langle\mu}\Omega^{\nu\rangle\lambda} + \lambda_3\Omega_\lambda^{\langle\mu}\Omega^{\nu\rangle\lambda}, \end{aligned} \tag{180} $$

where $D = u\cdot\partial$, and the vorticity $\Omega_{\mu\nu}$ as well as the transverse traceless tensor $A^{\langle\mu\nu\rangle}$ are defined in section 3.1.3. The form of $T^{\mu\nu}_{(2)}$ agrees with the general second order result for a conformal relativistic fluid derived in [75]. The second order coefficients are

$$ \tau_\Pi = \frac{2-\ln 2}{\pi T}, \quad \lambda_1 = \frac{2\eta}{\pi T}, \quad \lambda_2 = \frac{2\eta\ln 2}{\pi T}, \quad \lambda_3 = 0. \tag{181} $$

We observe that the relaxation times are of order $(\pi T)^{-1}$, the shortest timescale characterizing the plasma.

4.6. Non-relativistic AdS/CFT correspondence

Given the role that the AdS/CFT correspondence has played in improving our understanding of conformal relativistic fluids it is natural to ask whether the correspondence can be extended to non-relativistic scale invariant fluids like the dilute Fermi gas at unitarity. There has recently been significant progress in constructing holographic duals for non-relativistic field theories [168–171].

The basic idea proposed in [168, 169] can be explained by looking at the metric of $d+2$-dimensional flat space:

$$ {\rm d}s^2 = \eta_{\mu\nu}\,{\rm d}x^\mu\,{\rm d}x^\nu = -2\,{\rm d}x^+\,{\rm d}x^- + {\rm d}x^i\,{\rm d}x^i, \tag{182} $$

where we have introduced light cone coordinates (x^+, x^-, x^i) with $X^\pm = (x^0 \pm x^{d+1})/\sqrt{2}$ and $i = 1, \ldots, d$. Consider the massless Klein–Gordon equation in this space. In light cone coordinates

$$ \left(-2\frac{\partial}{\partial x^-}\frac{\partial}{\partial x^+} + \sum_{i=1}^{d}\frac{\partial^2}{\partial x_i^2}\right)\phi(x) = 0. \tag{183} $$

If the x^--direction is compactified, then the corresponding momenta become discrete. We may write the lowest mode as $\phi(x) \sim {\rm e}^{-{\rm i}mx^-}\psi(x^+, x_i)$ and the equation for ψ becomes the non-relativistic Schrödinger equation:

$$ \left(2{\rm i}m\frac{\partial}{\partial x^+} + \boldsymbol{\nabla}^2\right)\psi(x^+, x_i) = 0, \tag{184} $$

where x^+ plays the role of time. The symmetry group of this equation is known as the Schrödinger group Schr(d). The generators of the Schrödinger algebra include temporal and spatial translations, rotations, Galilean boosts, non-relativistic dilatations (which scale space and time by different factors, $\boldsymbol{x} \to s\boldsymbol{x}$ and $t \to s^2 t$), a special conformal transformation (which scales $t \to t/(1+\lambda t)$ and $\boldsymbol{x} \to \boldsymbol{x}/(1+\lambda t)$) and the mass operator [172].

The goal is to extend this construction to spaces that are asymptotically Anti-deSitter. The specific proposal in [168, 169] is that the Schr(d) symmetry of a non-relativistic

$d+1$-dimensional CFT can be mapped onto the isometries of the $d+3$-dimensional metric

$$ds^2 = r^2\left(-2\,dx^+\,dx^- - \beta^2 r^2 (dx^+)^2 + (dx^i)^2\right) + \frac{dr^2}{r^2}, \quad (185)$$

which reduces to the metric of AdS_{d+3} for $\beta \to 0$. This metric can be realized in string theory by starting from $AdS_5 \times \mathcal{X}_5$, where $\mathcal{X}_5$ is a generalized sphere called an Einstein–Sasaki manifold, and by applying a certain series of transformations that preserve solutions of the Einstein equations [170, 171, 173]. The resulting field theory is a $2+1$-dimensional field theory with infinitely many bosonic and fermionic fields, and an unusual equation of state $P \sim T^4/\mu^2$ [173]. This is still quite far from the $3+1$ unitary Fermi gas, but the theory provides an explicit realization of a non-relativistic fluid which satisfies $\eta/s = 1/(4\pi)$.

The hydrodynamics of a holographic fluid with Schrödinger symmetry was studied in more detail in [174]. An interesting observation that was made in this paper is that the light cone reduction of a viscous relativistic stress tensor automatically leads to a $\vec{\nabla}T$ term in the non-relativistic energy current. The thermal conductivity is completely fixed by the shear viscosity and the equation of state,

$$\kappa = 2\eta \frac{\epsilon + P}{\rho T}. \quad (186)$$

This result can be expressed in terms of the Prandtl number $Pr = c_p\eta/\kappa$, see equation (140). Using the equation of state of a non-relativistic conformal fluid we find $Pr = 1$. The Prandtl number of many gases is indeed close to one, see section 3.6.3, but at strong coupling there is no obvious reason for the relation $Pr = 1$ to hold.

5. Experimental determination of transport properties

In this section we will review experimental determinations of transport properties of liquid helium, cold atomic gases and the QGP. We will focus on shear viscosity, since it is the main focus of this review, and since it is the only transport property for which good data are available for all three systems.

Liquid helium can be produced in bulk, and transport properties can be measured using methods that were developed for classical fluids. Cold atomic gases are produced in optical or magneto-optical traps. These traps typically contain 10^5–10^6 atoms. Hydrodynamic behavior is observed when the trapping potential is modified, or if the local density or energy density is modified using laser beams. The QGP can only be created for brief periods in collisions of ultra-relativistic heavy ions. The system typically contains on the order of 10^3–10^4 quarks and gluons, and lasts for about 10 fm/c (3×10^{-23} s). Hydrodynamic behavior may take place during the expansion of the system and is reflected in the momentum spectra of particles in the final state.

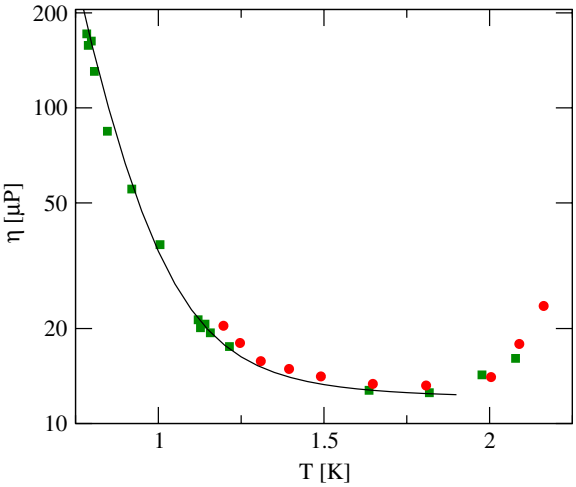

Figure 6. Viscosity of ^{4}He at atmospheric pressure as a function of temperature. Data taken from Woods and Hollis-Hallett (green squares) [175] and Heikkila and Hollis-Hallett (red circles) [176]. This figure was adapted from [8]. The solid line shows the theory of Landau and Khalatnikov, see equation (125). The viscosity minimum corresponds to $\eta/n \simeq 0.5$ and $\eta/s \simeq 1.9$.

5.1. Liquid helium

There are a number of techniques for measuring the viscosity of fluids. Three popular instruments are the following:

(i) Capillary viscometers are based on Poiseuille flow. Poiseuille's formula states that the flow through a pipe is inversely proportional to the shear viscosity, and proportional to the pressure drop as well as the fourth power of the diameter.

(ii) Rotation viscometers measure the torque on a rotating cylinder or disk. The torque per unit length exerted by a pair of coaxial infinitely long cylinders is proportional to the shear viscosity and the difference between the angular velocities, and proportional to the ratio $R_1R_2/(R_1^2 - R_2^2)$, where $R_{1,2}$ are the two radii.

(iii) Vibration viscometers determine the damping of an oscillating sphere or plate. These devices have many advantages but the data are more difficult to interpret, because the damping depends not only on the viscosity, but also on the density of the fluid.

Initial measurements of the viscosity of superfluid liquid helium lead to an apparent contradiction between the results obtained using different methods. Capillary flow viscometers indicated vanishing viscosity below T_c [177], oscillatory viscometers showed a drop in the shear viscosity [178] and experiments with rotation viscometers yielded a rise in viscosity below T_c [175]. The contradictions can be resolved using superfluid hydrodynamics. The flow through a narrow capillary is entirely a superflow, and not sensitive to viscosity. Oscillation viscometers measure the product of viscosity and normal density, which drops with temperature. Modern measurements confirm the rise of viscosity below T_c which is predicted by the phonon–roton theory, see figure 6. The minimum viscosity of helium at normal pressure occurs just below the λ point where $\eta \simeq 1.2 \times 10^{-5}$ P. The minimum

of η/s occurs at higher temperatures, close to the liquid–gas phase transition. Recent measurements confirm the (weak) divergence of the shear viscosity at the critical endpoint of the liquid–gas phase transition predicted by dynamical universality [179]. Experiments also find the expected (much stronger) divergence of the heat conductivity near the lambda point [44].

Once the shear viscosity and the heat conductivity are determined sound attenuation experiments can be used to measure the bulk viscosity (ζ_2 in the superfluid phase) [180]. Below the λ point $\zeta_2 \simeq 10^{-4}$ P. Damping of second sound determines a linear combination of ζ_1 and ζ_3 in the superfluid phase [181], but the remaining linear combination is poorly constrained.

5.2. Cold atomic gases

Dilute Bose or Fermi gases are studied using optical traps that provide an approximately harmonic confinement potential

$$V(x) = \frac{m}{2}\sum_i \omega_i^2 x_i^2. \tag{187}$$

The equilibrium density n_0 can be determined from the equation of hydrostatic equilibrium, $\boldsymbol{\nabla} P_0 = -n_0 \boldsymbol{\nabla} V$. Using the Gibbs–Duhem relation $\mathrm{d}P = n\mathrm{d}\mu + s\,\mathrm{d}T$ we can see that this equation is solved by $n_0(x) = n(\mu(x))$, where $n(\mu)$ is the equilibrium density as a function of the chemical potential and $\mu(x) = \mu - V(x)$. This result is known as the local density (or Thomas–Fermi) approximation, introduced by Thomas and Fermi in connection with the structure of heavy atoms. For dilute fermions at unitarity the equation of state at zero temperature is given by equation (27) and

$$n_0(\boldsymbol{r}) = n_0(0)\left(1 - \sum_i \frac{x_i^2}{R_i^2}\right)^{1/\gamma}, \qquad R_i^2 = \frac{2\mu}{m\omega_i^2}, \tag{188}$$

where μ is the chemical potential and $\gamma = 2/3$. The chemical potential is related to the Fermi energy by the universal parameter ξ introduced in equation (23). Transport properties of strongly interacting dilute Fermi gases can be extracted from a variety of experiments such as free expansion from a deformed trap (elliptic flow) [182], damping of collective oscillations [50, 183–186], sound propagation [187] and expansion out of rotating traps [188]. In the following we shall concentrate on damping of collective oscillations, as these experiments have been most carefully analyzed [189–192].

We consider small oscillations around the equilibrium density, $n = n_0 + \delta n$. Since the damping is small, the motion is approximately described by ideal hydrodynamics. The compressibility at constant entropy is

$$\left(\frac{\partial P}{\partial n}\right)_S = (\gamma+1)\frac{P}{n}. \tag{189}$$

From the linearized continuity and Euler equation we get [193]

$$m\frac{\partial^2 \boldsymbol{v}}{\partial t^2} = -\gamma\,(\boldsymbol{\nabla}\cdot\boldsymbol{v})\,(\boldsymbol{\nabla} V) - \boldsymbol{\nabla}\,(\boldsymbol{v}\cdot\boldsymbol{\nabla} V), \tag{190}$$

where we have dropped terms of the form $\nabla_i\nabla_j v$ that involve higher derivatives of the velocity. This equation has simple scaling solutions of the form $v_i = a_i x_i \exp(\mathrm{i}\omega t)$ (no sum over i). Inserting this ansatz into equation (190), we get an equation that determines the eigenfrequencies ω. The experiments are performed using a trapping potential with axial symmetry, $\omega_1 = \omega_2 = \omega_0$, $\omega_3 = \lambda\omega_0$. In this case we find one solution with $\omega^2 = 2\omega_0^2$ and two solutions with [193–195]

$$\omega^2 = \omega_0^2\left\{\gamma + 1 + \frac{\gamma+2}{2}\lambda^2 \pm\sqrt{\frac{(\gamma+2)^2}{4}\lambda^4 + (\gamma^2 - 3\gamma - 2)\lambda^2 + (\gamma+1)^2}\right\}. \tag{191}$$

In the limit of a very asymmetric trap ($\lambda \to 0$) the eigenfrequencies are $\omega^2 = 2\omega_0^2$ and $\omega^2 = (10/3)\omega_0^2$. The mode $\omega^2 = (10/3)\omega_0^2$ is a radial breathing mode with $\boldsymbol{a} = (a, a, 0)$ and the mode $\omega^2 = 2\omega_0^2$ corresponds to a radial quadrupole $\boldsymbol{a} = (a, -a, 0)$.

The prediction of ideal hydrodynamics for the frequency of the radial breathing mode agrees very well with experimental results [183]. Damping of collective modes is due to viscous effects. The dissipated energy is given by

$$\dot{E} = -\int \mathrm{d}^3x \left\{\frac{\eta(x)}{2}\left(\nabla_i v_j + \nabla_j v_i - \frac{2}{3}\delta_{ij}\boldsymbol{\nabla}\cdot\boldsymbol{v}\right)^2 + \zeta(x)\left(\boldsymbol{\nabla}\cdot\boldsymbol{v}\right)^2 + \frac{\kappa(x)}{T}(\boldsymbol{\nabla}T)^2\right\}, \tag{192}$$

where $\eta(x)$, $\zeta(x)$ and $\kappa(x)$ are the local shear viscosity, bulk viscosity and thermal conductivity. In the unitarity limit the system is scale invariant and the bulk viscosity in the normal phase vanishes. In the superfluid phase there are three bulk viscosities, $\zeta_1, \zeta_2, \zeta_3$, see equations (71) and (72). Scale invariance implies $\zeta_1 = \zeta_2 = 0$, see section 3.6.1, and the contribution of ζ_3 vanishes if $\boldsymbol{v}_s = \boldsymbol{v}_n$. For isentropic oscillations $\delta T \sim (\delta n/n)T$. The solutions of equation (190) satisfy $\delta n(x) \sim n_0(x)$. This implies that there are no temperature gradients, and that thermal conductivity does not contribute to dissipation.

We conclude that damping is dominated by shear viscosity. The energy dissipated by the radial scaling solutions is

$$\overline{\dot{E}} = -\tfrac{2}{3}\left(a_x^2 + a_y^2 - a_x a_y\right)\int \mathrm{d}^3x\,\eta(x), \tag{193}$$

where $\overline{E}$ is a time average. The damping rate is given by the ratio of the energy dissipated to the total energy of the collective mode. The kinetic energy is

$$E_{\mathrm{kin}} = \frac{m}{2}\int \mathrm{d}^3x\, n(x)\boldsymbol{v}^2 = \frac{mN}{2}\left(a_x^2 + a_y^2\right)\langle x^2\rangle. \tag{194}$$

In the case of a harmonic trapping potential the average $\langle x^2\rangle$ can be extracted using a virial theorem, $E = 2N\langle V\rangle$ [196]. The damping rate is

$$-\frac{1}{2}\frac{\overline{\dot{E}}}{E} = \frac{2}{3}\frac{a_x^2 + a_y^2 - a_x a_y}{a_x^2 + a_y^2}\frac{\int \mathrm{d}^3x\,\eta(x)}{mN\langle x^2\rangle}, \tag{195}$$

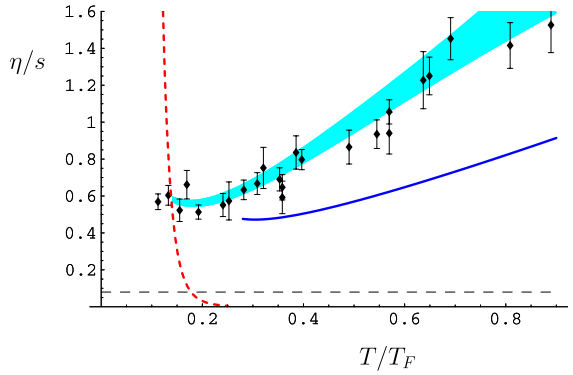

Figure 7. Viscosity to entropy density ratio of a cold atomic gas in the unitarity limit, from [191]. These data points are based on the damping data published in [185] and the thermodynamic data in [198, 199]. The light blue band is an estimate of the systematic uncertainty due to the breakdown of hydrodynamics near the surface of the cloud. The dashed red and solid blue lines show the low and high temperature limits of η/s, see equations (123) and (129). The dashed line shows the conjectured viscosity bound $\eta/s = 1/(4\pi)$.

where the factor 1/2 takes into account that the experiments measure an amplitude, not energy, damping rate. We note that the second factor on the rhs is $1/2$ for the radial breathing mode and $3/2$ for the radial quadrupole mode. This dependence provides an important check for the assumption that damping is dominated by shear viscosity. Also note that if the shear viscosity is proportional to the density or the entropy density then $\dot{E}/E$ scales as $N^{-1/3}$. Near the surface the density is small and $\eta(x)$ will approach the Boltzmann limit, which is independent of density, see equation (129). This is a problem, because the total volume of the system is infinite (at non-zero temperature the density has an infinite range tail). This difficulty is related to the breakdown of hydrodynamics near the surface of the cloud. An elegant solution to the problem is to include a finite relaxation time $\tau_\eta(r) = \eta/(n(r)k_{\rm B}T)$ which diverges in the low density limit [197].

In order to compare with the proposed viscosity bound we will assume that the shear viscosity is proportional to the entropy density, $\eta(x) = \alpha s(x)$. Note that in general α is a function of $T/T_{\rm F}$ and varies across the trap ($T_{\rm F}$ depends on density). This means that we will extract an average value of $\alpha = \eta/s$. We can write

$$\frac{\eta}{s} = \frac{3}{4}\xi^{1/2}(3N)^{1/3}\left(\frac{\bar{\omega}\Gamma}{\omega_\perp^2}\right)\left(\frac{E}{E_{T=0}}\right)\left(\frac{N}{S}\right), \qquad (196)$$

where $\Gamma/\omega_\perp$ is the dimensionless damping rate, $\bar{\omega} = \omega_\perp^{2/3}\omega_z^{1/3}$ is the mean trap frequency, (S/N) is the entropy per particle and $E/E_{T=0}$ is the equilibrium energy of the cloud in units of the zero temperature value. Figure 7 shows η/s extracted from the experimental results of the Duke group [185]. The entropy per particle was also taken from experiment [199]. Similar results are obtained if the entropy is extracted from QMC data. We observe that η/s in the vicinity of the transition temperature is about 1/2. We also note that the extracted shear viscosity roughly agrees with the high temperature, fermion quasi-particle, kinetic theory result. The low temperature, phonon dominated, result is not seen in the data, presumably because the phonon mean free path is bigger than the system size.

There are many caveats that one should keep in mind regarding this analysis. First, we assume that shear viscosity is the only source of dissipation. There is some evidence for this assumption from comparisons of the damping rate of different collective modes [200]. On the other hand, the dependence of the damping rate on particle number predicted by viscous hydrodynamics has never been demonstrated. Second, hydrodynamics can only be applied in a relatively narrow temperature regime $T < (2-3)T_{\rm c}$. For higher temperatures the observed frequencies cross over from hydrodynamic behavior to a weakly collisional Boltzmann gas. This means that the kinetic theory prediction for the shear viscosity, equation (129), is reliable but the frequency of the collective mode is too large for hydrodynamics to be applicable. Finally, there is an issue that is specific to the scaling flows ($v_i \sim a_{ij}x_j$) considered here. Since the velocity field is linear in the coordinates, the second derivative of the velocity vanishes. This means that the viscous term in the Navier–Stokes equation, $\rho\dot{v}_i \sim \nabla_j[\eta(\nabla_i v_j + \cdots)]$, is only sensitive to the density dependent part of the viscosity. But for a dilute gas the viscosity is expected to be density independent, see equation (129), so the dilute limit cannot be verified using experiments that involve scaling flows.

There is clearly a need for additional experimental constraints. The first indication of almost ideal hydrodynamic behavior was the observation of elliptic flow by O'Hara *et al* [182]. The experiment showed that if the trapping potential is removed the gas expands rapidly in the transverse direction while remaining nearly stationary in the axial. This is a consequence of the much larger pressure gradient in the short direction. The ideal hydrodynamics of this experiment was worked out in [201] but the effects of viscosity have not been carefully studied, in part because the data were taken at a single temperature. More recently Clancy *et al* studied the expansion of a gas cloud with an initial velocity field corresponding to a scissors mode [188]. This is an interesting system, because the initial velocity field is irrotational ($\nabla \times \boldsymbol{v} = 0$) but carries angular momentum. If the trapping potential is removed then the transverse size will grow initially, but if the gas remains irrotational then angular momentum conservation will force the transverse expansion to slow down (and the rotation to speed up) before the transverse and axial radii become equal [202]. This phenomenon was observed in the experiment, and an initial analysis leads to values of η/s close to $1/(4\pi)$ [203, 204]. This result is very important, but some of the caveats mentioned above still apply.

5.3. The QGP at RHIC

Cold quantum fluids can be studied in conditions that are very close to equilibrium. The QGP, on the other hand, can only be created in relativistic heavy ion collisions. In these collisions the initial state is very far from equilibrium, and the system size is limited by the size of the heaviest stable nuclei. The applicability of hydrodynamics is not clear *a priori*. In this section we will summarize some of the evidence that has been

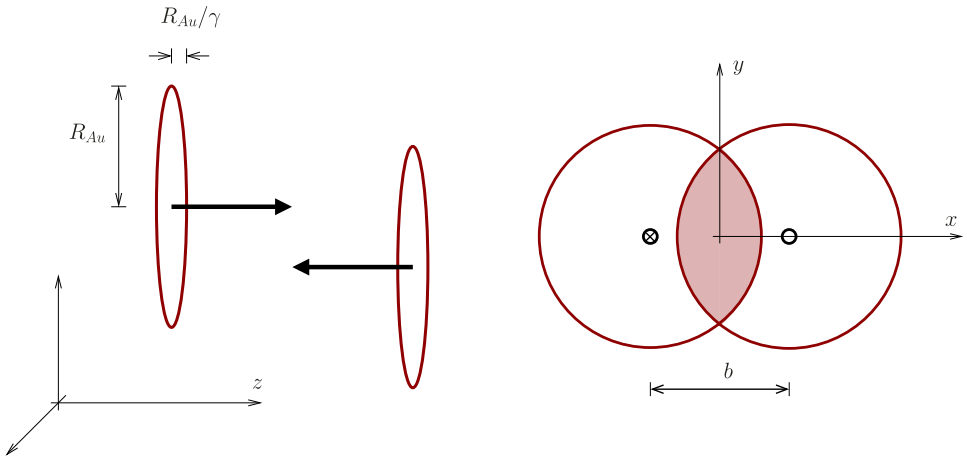

Figure 8. Geometry of a high energy heavy ion collision. The left panel shows the collision of two Lorentz contracted gold nuclei. The beam direction is the z-axis. The right panel shows the same collision in the transverse plane. The impact parameter is along the x-axis, and the remaining transverse direction is the y-axis.

obtained from experiments at the RHIC. These experiments indicate that local equilibration takes place, that nearly ideal fluid dynamics is applicable and that the shear viscosity to entropy density ratio near T_c is within a factor of a few of the KSS bound.

The collision energy in Au+Au collisions at RHIC is 100 GeV per nucleon, and the nuclei are Lorentz contracted by a factor of $\gamma \simeq 100$. The transverse radius of a Au nucleus is approximately 6 fm/c and on the order of 7000 particles are produced overall. The motion of the particles is relativistic, and the duration of a heavy ion event is $\tau \sim 6$ fm. In order for hydrodynamics to be applicable this time has to be large compared with the equilibration time.

The main observables are the spectra $\mathrm{d}N/\mathrm{d}^3p$ of produced particles. For momenta less than 2 GeV the spectra roughly follow Boltzmann distributions with a characteristic temperature close to the QCD critical temperature. The first hint that the system is behaving collectively is the existence of radial flow. Heavy particle spectra have apparent temperatures that are larger than the temperatures extracted from light particles. This can be understood if there is a collective transverse expansion velocity $v_\perp$ which boosts the observed transverse momenta by an amount $p_\perp \sim m v_\perp$.

More dramatic evidence for hydrodynamics is provided by the observation of elliptic flow in non-central heavy ion collisions. The centrality of the collision is characterized by the impact parameter b, the transverse separation of the two nuclei. The magnitude of b can be determined experimentally by selecting events with a given multiplicity of produced particles. The uncertainty in the impact parameter determination is small except in very peripheral bins [205]. The direction of the impact parameter can be determined on an event by event basis using the azimuthal dependence of the spectra. Imagine that the impact parameter direction is already known. This defines a coordinate system where z is along the beam axis and x is along the impact parameter direction, see figure 8. We write $(p_x, p_y, p_z) = (p_\perp \cos(\phi), p_\perp \sin(\phi), p_z)$, and the particle distribution can be expanded in Fourier components of ϕ:

$$p_0 \frac{\mathrm{d}N}{\mathrm{d}^3p}\bigg|_{p_z=0} = v_0(p_\perp)(1 + 2v_2(p_\perp)\cos(2\phi) + 2v_4(p_\perp)\cos(4\phi) + \cdots). \quad (197)$$

For a typical mid-central collision with $b \simeq 6$ fm the v_2 harmonic, called the elliptic flow coefficient, is approximately 6%. In an actual event the reaction plane can be determined (in principle) by plotting the distribution in ϕ relative to an arbitrarily chosen axis, and then requiring that the distribution has a maximum at $\phi = 0$. This intuitive method to determine the reaction plane forms the basis of the event plane method. The result can be corrected for v_2 fluctuations and additional correlations among the produced particles. Current analyses are not based on the event plane method but use two, four and higher particle cumulants—see [206] and references therein for a complete review. The scaling of these cumulants with multiplicity demonstrates that one can reliably extract collective flow down to small system sizes. These measurements provide a unique opportunity to study the approach to hydrodynamic behavior in a controlled fashion [207].

Elliptic flow represents the collective response of the system to pressure gradients in the initial state. At finite impact parameter the initial state has the shape of an ellipse, with the short axis along the x-direction and the long axis along the y-direction. This implies that pressure gradients along the x-axis are larger than along the y-axis. Hydrodynamic evolution converts the initial pressure gradients to velocity gradients in the final state. Elliptic flow is a direct measure of collectivity. In particular, if the nucleus–nucleus event were a simple superposition of proton–proton collisions then the particle distribution would be azimuthally symmetric.

5.3.1. The Bjorken model. The application of hydrodynamics to relativistic heavy ion collisions goes back to the work of Landau [208] and Bjorken [209]. Bjorken discovered a simple scaling solution that provides a natural starting point for more

elaborate solutions in the ultra-relativistic domain. Consider two highly relativistic nuclei moving with equal but opposite momenta in the z-direction. In the relativistic regime the natural variable to describe the motion in the z-direction is the rapidity

$$y = \frac{1}{2}\log\left(\frac{E+p_z}{E-p_z}\right). \tag{198}$$

At RHIC the energy of the colliding nuclei is 100 + 100 GeV per nucleon, and the separation in rapidity is $\Delta y = 10.6$. Bjorken suggested that the two highly Lorentz contracted nuclei pass through each other and create a longitudinally expanding fireball in which particles are produced. In the original model the number of produced particles is independent of rapidity, and the subsequent evolution is invariant under boosts along the z-axis. The evolution in proper time is the same for all comoving observers. The flow velocity is

$$u_\mu = \gamma(1,0,0,v_z) = (t/\tau,0,0,z/\tau), \tag{199}$$

where γ is the boost factor and $\tau = \sqrt{t^2-z^2}$ is the proper time. The velocity field (199) solves the relativistic Euler equation (78). In particular, there is no longitudinal acceleration. The remaining hydrodynamic variables are determined by entropy conservation. Equation (77) gives

$$\frac{\mathrm{d}}{\mathrm{d}\tau}[\tau s(\tau)] = 0 \tag{200}$$

and $s(\tau) = s_o\tau_o/\tau$. For an ideal relativistic gas $s \sim T^3$ and $T \sim 1/\tau^{1/3}$. Typical parameters at RHIC are $\tau_o \simeq (0.6\text{–}1.6)$ fm and $T_o \simeq (300\text{–}425)$ MeV. The combination $\tau_o T_o^3$ is constrained by the final multiplicity, but individually τ_o and T_o are not well constrained. We note that the corresponding initial temperature is significantly larger than the critical temperature for the QCD phase transition.

The temperature drops as a function of τ and eventually the system becomes too dilute for the hydrodynamic evolution to make sense. At this point, the hydrodynamic description is matched with kinetic theory:

$$T^{\rm hydro}_{\mu\nu} \equiv T^{\rm kin}_{\mu\nu} = \int \mathrm{d}\Gamma\; p_\mu p_\nu f(\boldsymbol{x},\boldsymbol{p},t). \tag{201}$$

For an ideal fluid the distribution function is parametrized by the local temperature and flow velocity:

$$f(\boldsymbol{x},\boldsymbol{p},t) = \sum_i \frac{d_i}{\exp(p\cdot u/T)\pm 1}, \tag{202}$$

where i labels different particle species and d_i are the corresponding degeneracies. Finally, the observed particle spectra are given by

$$\left(p_0\frac{\mathrm{d}N}{\mathrm{d}^3p}\right)_i = \frac{1}{(2\pi)^3}\int \mathrm{d}\Sigma_\mu\; p^\mu f_i(\boldsymbol{x},\boldsymbol{p},t), \tag{203}$$

where Σ_μ is the normal vector on the 'freezeout' hypersurface, the surface on which the matching between the hydrodynamics and kinetic descriptions is performed.

In order to quantitatively describe the observed particle distributions several improvements of the simple Bjorken model are necessary. First, one has to include the transverse expansion of the system [210]. Transverse expansion becomes important at a proper time $\tau \sim R/c_{\rm s}$, where R is the (rms) size of the nucleus and $c_{\rm s}$ is the speed of sound. At very late times the expansion becomes three dimensional,

$$s(\tau) \sim \frac{1}{\tau^3}, \tag{204}$$

and $T \sim 1/\tau$. Transverse expansion is caused by transverse pressure gradients. These gradients are sensitive to the initial energy density of the system. One simple model for the initial energy density (or entropy density) in the transverse plane is the Glauber model. In the Glauber model the entropy density is

$$s(\boldsymbol{x}_\perp,b) \propto T_{\rm A}(\boldsymbol{x}_\perp+\boldsymbol{b}/2)\Big[1-\exp\left(-\sigma_{\rm NN}\,T_{\rm A}(\boldsymbol{x}_\perp-\boldsymbol{b}/2)\right)\Big] + T_{\rm A}(\boldsymbol{x}_\perp-\boldsymbol{b}/2)\Big[1-\exp\left(-\sigma_{\rm NN}\,T_{\rm A}(\boldsymbol{x}_\perp+\boldsymbol{b}/2)\right)\Big], \tag{205}$$

where $\boldsymbol{b}$ is the impact parameter,

$$T_{\rm A}(\boldsymbol{x}_\perp) = \int \mathrm{d}z\;\rho_{\rm A}(\boldsymbol{x}) \tag{206}$$

is the thickness function and $\sigma_{\rm NN}(\sqrt{s})$ is the nucleon–nucleon cross section. Here, $\rho_{\rm A}(\boldsymbol{x})$ is the nuclear density. The idea behind the Glauber model is that the initial entropy density is proportional to the number of nucleons per unit area which actually collide. Other variants exist. For instance, one can distribute the energy density according to the number of binary nucleon–nucleon collisions—see [211] for a comparison. A more sophisticated theory of the initial energy density is provided by the color glass condensate (CGC) [212, 213]. This model leads to somewhat steeper initial transverse energy density distributions.

Gradients in the transverse pressure lead to transverse acceleration and generate collective transverse flow. The collective expansion leads to a blue-shift of the transverse momentum spectra of produced particles. For an azimuthally symmetric source with temperature T and radial flow velocity $u^r(r)$ we get [214]

$$\left(p_0\frac{\mathrm{d}N}{\mathrm{d}^3p}\right)_i = \frac{2d_i}{(2\pi)^2}rm_\perp\int r\,\mathrm{d}r\;K_1\left(\frac{m_\perp u^\tau}{T}\right)I_1\left(\frac{p_\perp u^r}{T}\right), \tag{207}$$

where $m_\perp = \sqrt{p_\perp^2+m_i^2}$ is the transverse 'mass' and $K_1(z)$, $I_1(z)$ are generalized Bessel functions. Using the asymptotic form of the Bessel functions one can show that the spectrum has the form

$$\frac{\mathrm{d}N}{\mathrm{d}m_\perp^2} \sim \exp\left(-\frac{m_\perp}{T_{\rm eff}}\right), \qquad T_{\rm eff} = T\sqrt{\frac{1+v_r}{1-v_r}}. \tag{208}$$

This effect of transverse flow on the spectra is seen in the data. At RHIC, transverse velocities at freezeout reach $0.6c$. At finite impact parameter the initial energy density in the transverse plane is not azimuthally symmetric. The pressure gradient along the direction of the impact parameter is larger than the gradient in the orthogonal direction. The resulting anisotropy of the transverse flow can be characterized by the elliptic flow

parameter v_2 defined in equation (197). The observed elliptic flow is remarkable because v_2 is a very direct measure of transverse pressure. The observed radial flow is proportional to the radial pressure and the expansion time, but elliptic flow has to be generated early, when the system is still deformed.

5.3.2. Estimates of viscous corrections. We are now in a position to discuss the role of dissipative effects. We begin with the effect of shear and bulk viscosity on the Bjorken solution. The scaling flow given in equation (199) is a solution of the relativistic Navier–Stokes equation. Viscosity only modifies the entropy equation. We get

$$\frac{1}{s}\frac{\mathrm{d}s}{\mathrm{d}\tau} = -\frac{1}{\tau}\left(1 - \frac{\frac{4}{3}\eta + \zeta}{sT\tau}\right). \tag{209}$$

We observe that dissipation is governed by the sound attenuation length Γ_s, see equation (84). The applicability of the Navier–Stokes equation requires that the viscous correction is small [9]:

$$\frac{\eta}{s} + \frac{3}{4}\frac{\zeta}{s} \ll \frac{3}{4}(T\tau). \tag{210}$$

For the Bjorken solution $T\tau \sim \tau^{2/3}$ grows with time, and this condition is most restrictive during the initial phase. Using $\tau_o = 1$ fm and $T_o = 300$ MeV gives $\eta/s < 0.6$. For a three-dimensional expansion $T\tau$ is independent of time. At very late time the fluid is composed of hadrons, or pre-formed hadronic resonances. In that case $\eta \sim T/\sigma$, where σ is a hadronic cross section. Then, for a three-dimensional expansion, the viscous correction $\eta/(sT\tau)$ grows with proper time as τ^2. This shows that the system has to freeze out at late time.

It is instructive to study the viscous contribution to the stress tensor in more detail. At central rapidity we have (for $\zeta = 0$)

$$T_{zz} = P - \frac{4}{3}\frac{\eta}{\tau}, \qquad T_{xx} = T_{yy} = P + \frac{2}{3}\frac{\eta}{\tau}. \tag{211}$$

This means that the shear viscosity decreases the longitudinal pressure and increases the transverse one. In the Bjorken scenario there is no acceleration, but if pressure gradients are taken into account shear viscosity will tend to increase transverse flow. A similar effect will occur at finite impact parameter, see figure 8. The shear viscosity reduces the pressure along the x-direction and increases the pressure in the y-direction. As a consequence there is less acceleration in the x-direction, and elliptic flow is suppressed. This is the basic observation that motivates attempts to extract shear viscosity from the observed elliptic flow.

Viscosity modifies the stress tensor, and via the matching condition (201) this modification changes the distribution functions of produced particles. In [215] a simple quadratic ansatz for the leading correction δf to the distribution function was proposed:

$$\delta f = \frac{3}{8}\frac{\Gamma_s}{T^2} f_0(1+f_0)\, p_\alpha p_\beta \nabla^{\langle\alpha} u^{\beta\rangle}, \tag{212}$$

where $\nabla^{\langle\alpha} u^{\beta\rangle}$ is a symmetric traceless tensor, see equation (86). This form summarizes the results of more involved kinetic calculations [17]. The modified distribution function leads to a modification of the single particle spectrum. For a simple Bjorken expansion and at large $p_\perp$ we find

$$\frac{\delta(\mathrm{d}N)}{\mathrm{d}N_0} = \frac{\Gamma_s}{4\tau_f}\left(\frac{p_\perp}{T}\right)^2, \tag{213}$$

where τ_f is the freezeout time. We observe that the dissipative correction to the spectrum is controlled by the same parameter Γ_s/τ that appeared in equation (209). We also note that the viscous term grows with $p_\perp$. At RHIC transverse momentum spectra are in agreement with hydrodynamic predictions out to transverse momenta several times larger than the temperature. In equation (213) this is partially compensated by the fact that τ_f/τ_o is a large number, but typically the requirement $\delta(\mathrm{d}N)/(\mathrm{d}N_0) < 1$ provides a more stringent bound on η/s than equation (210). We can also include transverse expansion and study the leading dissipative correction to v_2 [215]. The viscous correction tends to reduce v_2 and grows with $p_\perp$. At $p_\perp = 1$ GeV an estimate similar to equation (213) gives $(\delta v_2)/v_2 \sim 1$ for $\Gamma_s/\tau_f \sim 0.2$. Using $\tau_f \sim 5$ fm and $T_f = 160$ MeV, this translates into $\eta/s \leqslant 0.6$.

5.3.3. Hydrodynamic simulations. There have been a number of recent numerical studies devoted to extracting the shear viscosity of the quark gluon plasma [216–220]. Here, we will follow the work of Dusling and Teaney [216], and refer the reader to the recent review by Heinz [30] for a more detailed comparison between different strategies for implementing relativistic viscous hydrodynamics for heavy ion collisions at RHIC. In order to respect causality in viscous hydrodynamics we have to use a second order formalism. This means that the strains $\delta T^{\mu\nu}$ are promoted to dynamical fields which relax on a collisional timescale to the Navier–Stokes form rather than being specified instantaneously by the constitutive relations. Such relaxation processes are second order in the hydrodynamic expansion, see section 3.1.3. Dusling and Teaney considered a 2+1-dimensional boost invariant flow and used a second order fluid model studied by Öttinger [221]. This model is formulated along the lines of equation (88), and the dynamical strains are parametrized by an additional field $\mathring{c}^{\mu\nu}$:

$$\delta T^{\mu\nu} = -P(\epsilon)\alpha\, \mathring{c}^{\mu\nu}. \tag{214}$$

The relaxation equation for $\mathring{c}^{\mu\nu}$ is written in terms of a tensor $c^{\mu\nu}$. This tensor satisfies the constraint

$$c_{\mu\nu}u^\nu = u_\mu, \tag{215}$$

and is decomposed as

$$c_{\mu\nu} = -u_\mu u_\nu + \mathring{c}_{\mu\nu} + \bar{c}_{\mu\nu}, \tag{216}$$

$$\bar{c}_{\mu\nu} = \tfrac{1}{3}\left(c_\lambda{}^\lambda - 1\right)\left(\eta_{\mu\nu} + u_\mu u_\nu\right). \tag{217}$$

The field $c_{\mu\nu}$ obeys the relaxation equation

$$u^\lambda(\partial_\lambda c_{\mu\nu} - \partial_\mu c_{\lambda\nu} - \partial_\nu c_{\mu\lambda}) = -\frac{1}{\tau_0}\bar{c}_{\mu\nu} - \frac{1}{\tau_2}\mathring{c}_{\mu\nu}. \tag{218}$$

The constraint equation (215) is preserved under time evolution. In the limit that the relaxation times τ_0 and τ_2 are

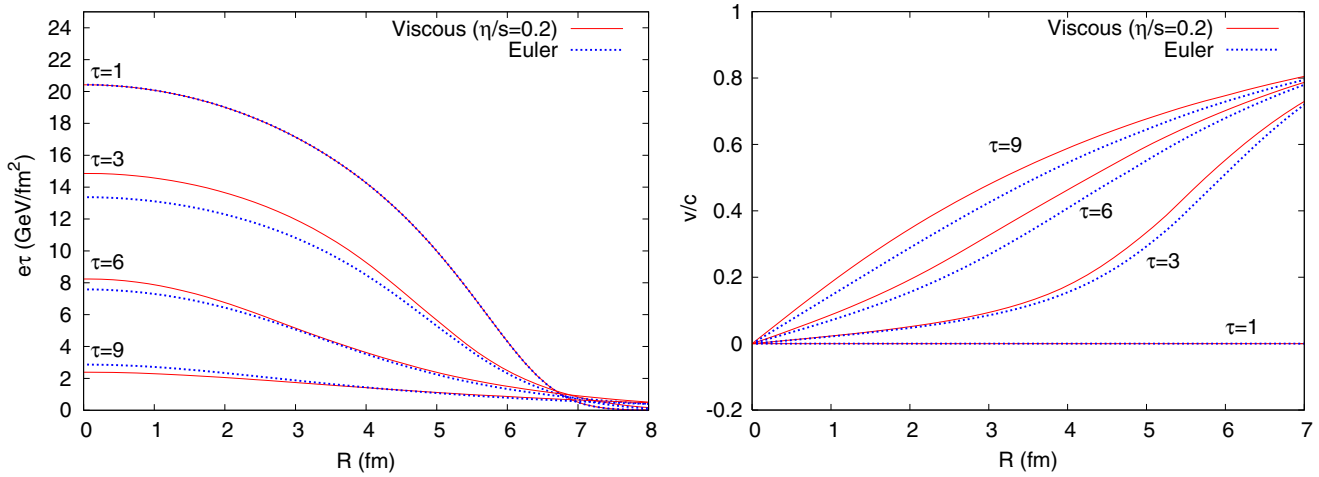

Figure 9. Plot of the energy density per unit rapidity $e\tau$ (left) and of the transverse velocity (right) at times of $\tau = 1, 3, 6, 9$ fm/c, for $\eta/s = 0.2$ (solid red line) and for ideal hydrodynamics (dotted blue line), from [216].

small the evolution equation leads to the following solution for $c^{\mu\nu}$ in the local rest frame:

$$c^{ij} = \tau_2 \left(\partial^i u^j + \partial^j u^i - \tfrac{2}{3}\delta^{ij}\partial_k u^k\right) + \tfrac{2}{3}\,\tau_0 \delta^{ij}\partial_k u^k. \qquad (219)$$

Comparing with the Navier–Stokes equation, we see that

$$\eta = \tau_2 P\alpha, \qquad \zeta = \tfrac{2}{3}\tau_0 P\alpha. \qquad (220)$$

Dusling and Teaney used these relations (with $\alpha = 0.7$) to fix (τ_0, τ_2) in terms of η and ζ, and studied the sensitivity to the parameter α. They considered a simple conformal equation of state $P = \epsilon/3$, and set $\zeta = 0$.

An advantage of Öttinger's approach is that equation (218) is relatively simple to solve. One just evolves the spatial components of c_{ij} and then uses the constraints (215) to solve for the time components c_{00} and c_{0i}. As hydrodynamics is universal, any fluid model can be recast in terms of the first and second order formalism described in section 3.1.3. For the Öttinger fluid model, expanding out the equations of motion to second order leads to the relation

$$\pi^{\mu\nu} = -\eta\sigma^{\mu\nu} - \tau_2\left[{}^{\langle}D\pi^{\mu\nu\rangle} + \frac{4}{3}\pi^{\mu\nu}(\partial\cdot u)\right] + \frac{\tau_2}{\eta}\pi_\lambda^{\langle\mu}\pi^{\nu\rangle\lambda} + \tau_2\pi_\lambda^{\langle\mu}\Omega^{\nu\rangle\lambda} - \frac{2}{3}\,\tau_2\pi_{\mu\nu}(\partial\cdot u). \qquad (221)$$

The last term in this expression differs from the general result in equation (221), which indicates that at second order in gradients this model contains terms that break conformal symmetry.

The hydrodynamic equations were solved for several fixed values of the shear viscosity to entropy density ratio η/s. At the initial time $\tau_o = 1$ fm the entropy per participant is adjusted and closely corresponds to the results of full hydrodynamic simulations [222–224]. The maximum initial temperature is $T_o = 420$ MeV at an impact parameter $b = 0$. The initial components of the stress tensor are set to the Navier–Stokes values.

Numerical results are shown in figure 9. The effect of viscosity is twofold. The longitudinal pressure is initially reduced and the viscous case does less longitudinal $P\,\mathrm{d}V$ work as in the simple Bjorken expansion. This means that at early times the energy per rapidity decreases more slowly in the viscous case. The reduction of longitudinal pressure is accompanied by a larger transverse pressure. This causes the transverse velocity to grow more rapidly. The larger transverse velocity causes the energy density to deplete faster at late times in the viscous case. The net result is that a finite viscosity, even as large as $\eta/s = 0.2$, does not integrate to give major deviations from the ideal equations of motion.

Freezeout occurs when the viscous terms become large compared with the ideal terms. Roughly, the system begins to break apart when

$$\frac{\eta}{P}\partial\cdot u \sim 1. \qquad (222)$$

This combination of parameters can be motivated from kinetic theory. The pressure is of order $P \sim \epsilon\langle v_{\rm th}^2\rangle$ where $\langle v_{\rm th}^2\rangle$ is the typical quasi particle velocity and ϵ is the energy density. The viscosity is of order $\eta \sim \epsilon\langle v_{\rm th}^2\rangle\tau_{\rm R}$ where $\tau_{\rm R}$ is the relaxation time. Thus the freezeout condition is $\frac{\eta}{P}(\partial\cdot u) \sim \tau_{\rm R}(\partial\cdot u) \sim 1$. Ideally there should be an overlap region where both viscous hydrodynamics and kinetic theory are valid. In this region hydrodynamics can be systematically coupled to a kinetic description in order to correctly model the breakup. In simulations of heavy ion collisions the size of the overlap region is small, and the breakdown of hydrodynamics is typically modeled via a freezeout surface. In practice the freezeout surface was chosen to satisfy $(\eta/P)\,\partial\cdot u = 0.5$, where the precise number on the right hand side is simply an educated guess based on examining the output of second order hydrodynamic simulations. Typical freezeout surfaces which satisfy this criterion are shown in figure 10. We note that hydrodynamics breaks down both at late and also at early times. The latter is most clearly seen from the $\eta/s = 0.4$ curve. If η/s is very small then freezeout will occur at very late proper time. In the following, we shall therefore use a simpler criterion $\chi \equiv \frac{1}{T}(\partial\cdot u) = \text{const}$ which is independent of η/s. Taking $\chi = 3$ roughly corresponds to the $\eta/s = 0.2$ freezeout surface in figure 10.

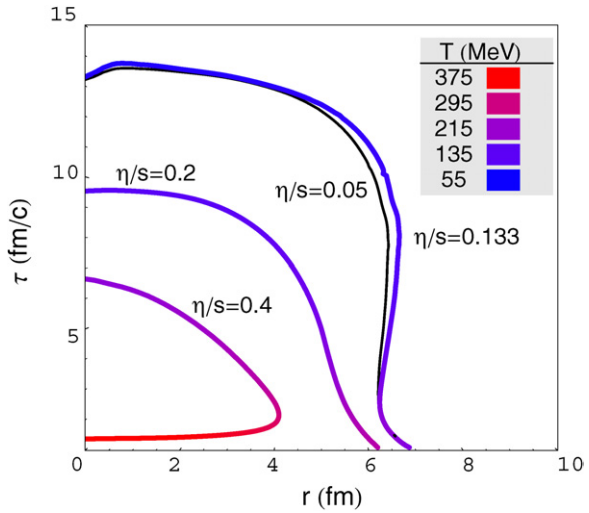

Figure 10. Location of freezeout surfaces for central Au–Au collisions. The surfaces are determined by the condition $\frac{\eta}{p}(\partial \cdot u) = 0.6$, slightly larger than the value 0.5 discussed in the text. Different surfaces correspond to different values of η/s. The shading corresponds to the freezeout temperature. The thin solid black curve shows the contour set by $\frac{\eta}{p}(\partial \cdot u) = 0.225$ for comparison.

Finally, we can compute the spectra of produced particles. We follow the procedure outlined above, see equation (212), and write the distribution function as $f = f_0 + \delta f$ with

$$\delta f = \frac{1}{2(\epsilon + P)T^2} f_0(1 + f_0)\, p^\mu p^\nu \delta T_{\mu\nu}. \qquad (223)$$

The spectrum is determined by integrating the distribution function over the freezeout surface as in equation (203), and the elliptic flow parameter v_2 is computed from the definition in equation (197). A comparison with the data obtained by the STAR collaboration is shown in figure 11. There are several curves here and we will go through them one by one:

- For the two different values of η/s, 0.05 and 0.2, there are three curves each. Our best estimates for the elliptic flow as a function of p_T are labeled $f_0 + \delta f_\pi$ and are shown by the blue ($\eta/s = 0.05$) and orange ($\eta/s = 0.2$) lines.
- To disentangle what part of the viscous modification is due to the distribution function δf and what part of it is due to changes in the flow, we also compute $v_2(p_T)$ with f_0 only. We see that the effect on v_2 from viscous modifications of the flow is relatively minor. This may be the largest obstacle to reliably extracting the shear viscosity from the heavy ion data. However, it is important to realize that the modification to the distribution function reflects the viscous correction to the stress tensor itself. In hydrodynamic simulations the p_T integrated v_2 tracks the asymmetry of the stress tensor [226]. In the context of viscous hydrodynamics this is nicely illustrated in figure 8 of [219]. Nevertheless, in contrast to the atomic physics experiments discussed in section 5.2, the observed viscous corrections to the elliptic flow do not reflect a resummation of secular terms in the gradient expansion.
- Finally, instead of showing the spectrum computed with $\delta T^{\mu\nu}$, we show $v_2(p_T)$ computed with velocity gradients directly. For this purpose $\delta T^{\mu\nu}$ in equation (223) is replaced by $-\eta\sigma^{\mu\nu}$ where $\sigma^{\mu\nu}$ is computed from the flow velocities. $v_2(p_T)$ computed in this way is denoted by $f_0 + \delta f_G$ in the figure and corresponds to the magenta and black curves. To first order in gradients this is an identity and the difference between f_π and f_G is a measure of the magnitude of second order terms. For the smallest viscosity $\eta/s = 0.05$ the differences are quite small, but the effect is more noticeable for $\eta/s = 0.2$.

We conclude that for small values of $\eta/s \lesssim 0.2$ the gradient expansion is working. There are, however, a number of issues that have to be considered in order to extract reliable values for η/s:

- The constraints on η/s are sensitive to the initial values for the transverse energy density. In particular, using color glass initial conditions produces higher transverse pressure gradients, and allows for values of η/s about twice as large as Glauber model initial conditions [219].
- Near the edge of the nucleus the gradient expansion breaks down completely. It is important to quantify the extent to which the effects of the edge propagate into the interior and invalidate the hydrodynamic description. One way to do this is by comparing the results of hydrodynamic simulations with kinetic theory. For strongly coupled plasmas kinetic theory is not an appropriate description of the microscopic interactions. However, hydrodynamics is independent of the microscopic details. Thus extrapolating kinetic theory into the strongly coupled domain is a good way to construct a model which gracefully transitions from a hydrodynamic description in the interior to a kinetic description near the edge. There are several important developments in this direction [220, 227, 228].
- Viscous effects in the hadronic phase are very important [222, 213]. These effects can be taken into account by coupling the hydrodynamic evolution to a hadronic cascade.
- Effects due to bulk viscosity may reduce both radial and elliptic flow [229, 230]. Bulk viscosity is likely to be much smaller than shear viscosity in the plasma phase, but it is expected to grow near the phase transition. The magnitude of this growth is not clear.

Some of these effects are yet to be carefully studied. However, even if one conservatively assumes that all uncertainties tend to increase the bound on η/s, one still has to conclude that for a shear viscosity of $\eta/s > 0.4$ it will be impossible to reproduce the observed flow. The question now is whether it will be possible to describe the large set of available data on energy, impact parameter, rapidity, transverse momentum and species dependence of flow using viscous hydro, and whether it is possible to extract a reliable value, with controlled error bars, for η/s of the QGP.

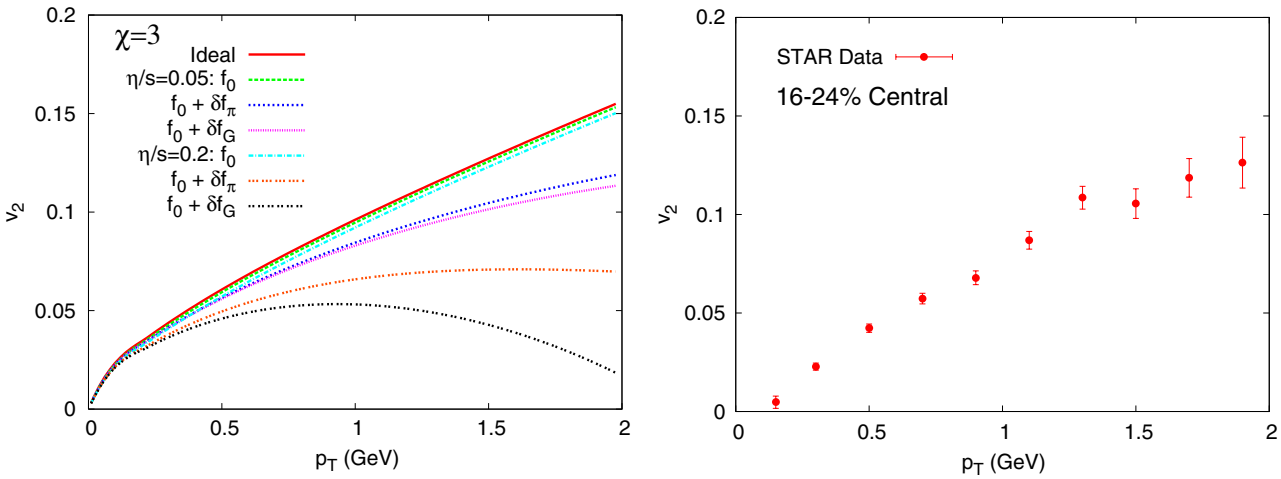

Figure 11. Left: $v_2(p_T)$ for massless Bose particles for simulations using $\eta/s = 0, 0.05, 0.2$ at an impact parameter of $b = 6.5$ fm. Right: four-particle cumulant data as measured in Au–Au collisions at $\sqrt{s} = 200$ GeV for a centrality selection of 16–24% [225].

6. Summary and outlook

6.1. Summary

In this review we summarized theoretical and experimental information on the behavior of nearly perfect fluids. We characterized the 'perfectness' in terms of the shear viscosity of the fluid. Shear viscosity is special because

- shear viscosity is the 'minimal' transport property of a fluid. Thermal transport, diffusion or conductivities require the presence of conserved charges, and bulk viscosity vanishes in the case of scale invariant fluids. The 'perfectness' of any fluid can be characterized by the dimensionless ratio η/s. If factors of $\hbar$ and k_B are reinstated, the dimensionless measure of fluidity is $[\eta/\hbar]/[s/k_B]$.
- a small shear viscosity is uniquely associated with strong interactions. Other transport coefficients may vanish even if the interaction strength remains weak. For example, bulk viscosity vanishes if the theory is conformal, and the diffusion constant goes to zero at the localization phase transition, but the shear viscosity of a weakly coupled fluid is always large.

Note that the reverse of the last statement is not true: the viscosity can be large, even if the interaction is strong. One possible scenario is that the interaction is so strong that it leads to the breakdown of a continuous symmetry, and the emergence of a new set of weakly coupled quasi-particles. Note that the $\mathcal{N} = 4$ super-conformal fluid is special in this regard: there is no symmetry breaking in the strong coupling limit. Another example is the liquid–gas phase transition. There are no weakly coupled quasi-particles, but the viscosity diverges because of critical fluctuations.

We summarized the main theoretical approaches to transport coefficients: kinetic theory, holography and non-perturbative approaches based on the Kubo formula.

- Kinetic theory applies whenever the fluid can be described in terms of quasi-particles. For many fluids this is the case in both the high and the low temperature limit. Typically, at high temperatures the quasi-particles are the 'fundamental' degrees of freedom (quarks, gluons, atoms) whereas the low temperature degrees of freedom are composite (phonons, rotons, pions). In the regime in which kinetic theory applies the ratio η/s is always parametrically large. This leads to a characteristic 'concave' temperature dependence of η/s. Kinetic theory is useful in constraining the location of the viscosity minimum (usually, near the crossover between the high and low temperature regimes). Also, despite the weak coupling restriction, kinetic theory is quantitatively accurate for many quantum fluids in the whole temperature range covered by experiment.
- Holography is a new method for studying the transport behavior of quantum fluids. It is most useful in the strong coupling limit of certain model field theories (like $\mathcal{N} = 4$ super-CFT), but the range of field theories that have known holographic duals has grown significantly over the years. More importantly, holographic dualities have led to important new insights into the transport properties of strongly coupled fluids. This includes the proposed universal bound on η/s, consistent higher order hydrodynamic theories, computations of the spectral function associated with the shear and other transport modes, etc. Holography has also been used to study specific solutions to the hydrodynamic equations, such as the wake of a moving heavy quark or the approach to equilibrium after the collision of two highly Lorentz contracted sources.
- The Kubo formula connects non-perturbative calculations of equilibrium correlation functions with non-equilibrium transport coefficients. Possible non-perturbative approaches include Euclidean lattice, large-N, exact renormalization group and Dyson–Schwinger calculations. Significant progress has been made in computing the shear viscosity of the QGP on the lattice. The results are close to the proposed bound. Future calculations will answer the question of whether transport phenomena in the QCD plasma can be understood in terms of quasi-particles.

Finally, we summarized the experimental situation for the three most strongly coupled fluids that can be prepared in the laboratory.

- Liquid helium has been studied for many years and its shear viscosity is well determined. The minimum value of η/s is about 0.8 and is attained near the endpoint of the liquid–gas phase transition. The ratio η/n has a minimum closer to the lambda transition. Even though $\eta/s < 1$ the transport properties of liquid helium can be quantitatively understood using kinetic theory.
- Strongly interacting cold atomic Fermi gases were first created in the laboratory in 1999. These systems are interesting because the interaction between the atoms can be controlled, and a large set of hydrodynamic flows (collective oscillations, elliptic flow, rotating systems) can be studied. Current experiments involve 10^5–10^6 atoms, and the range of temperatures and interaction strengths over which hydrodynamic behavior can be observed is not large. There are also some difficulties in extracting the viscosity that are related to the nature of the flow profiles that have been studied. A conservative estimate is $\eta/s < 0.5$.
- The QGP has been studied in heavy ion collisions at a number of facilities: AGS (Brookhaven), SPS (CERN), RHIC (Brookhaven). Almost ideal hydrodynamic behavior was observed for the first time in 200 GeV per nucleon (in the center of mass) Au on Au collisions at RHIC. These experiments are difficult to analyze—the initial state is very far from equilibrium and not completely understood, final state interactions are important and the size and lifetime of the system are not very large. Important progress has nevertheless been made in extracting constraints on the transport properties of the QGP. A conservative bound is $\eta/s < 0.4$, but the value of η/s that provides the best fit to the data is smaller, $\eta/s \sim 0.1$.

6.2. *Outlook*

Much work remains to be done in order to advance theoretical methods for predicting the transport properties of strongly coupled quantum fluids, to improve the determination of transport coefficients of these fluids and to discover new nearly perfect fluids.

However, in addition to that, we also want to understand what nearly perfect fluids are like, in particular whether they can be understood using quasi-particles and the tools of kinetic theory. There are several avenues for addressing this question:

- QMC calculations can be used to determine the spectral function of the energy momentum tensor. If energy and momentum are carried by quasi-particles then the spectral function has a peak at low energy. If, on the other hand, the fluid is AdS/CFT-like then there are no quasi-particles and no peak in the spectral functions. Current calculations in lattice QCD seem to prefer the AdS/CFT picture [97, 103], but the issue is far from settled.
- Detailed simulations of kinetic equations can be used to study the crossover from kinetic behavior (the Knudsen limit) to hydrodynamic behavior, see [220, 227, 231, 228] for work in the context of QCD and [115, 197] for studies of the dilute Fermi gas at unitarity. The main question is whether it is possible to extend a self-consistent kinetic theory into the domain $\eta/s < 1$, and whether one can describe not only flow properties but also all other transport properties like diffusion and energy loss. Self-consistency requires that the lifetime of the quasi-particles is long compared with the characteristic thermal time, $\tau \sim 1/T$. A simultaneous description of momentum diffusion, charge diffusion and energy loss is important because in kinetic theory there is a close connection between these observables. In AdS/CFT-like fluids the relation between different transport processes is non-trivial. For example, at infinite coupling shear viscosity is finite while the heavy quark diffusion coefficient is zero. The current experimental situation in QCD is not entirely clear, with both AdS/CFT based [232] and kinetic approaches [233] demonstrating some success.
- Phenomenological studies address the quasi-particle structure of nearly perfect fluids by studying fluctuations and correlations of conserved charges other than energy and momentum. In liquid helium quasi-particles were studied using neutron scattering, and in the dilute Fermi gas one can study the quasi-particle structure using radio-frequency spectra, see [234, 235]. In the QGP there is some evidence for quasi-particles from charge fluctuations [236] and from the success of the recombination model in reproducing the flow of identified particles at intermediate momenta [237].

Acknowledgments

This work was supported in parts by the US Department of Energy grant DE-FG02-03ER41260 (TS) and DE-FG02-08ER41540 (DT). DT is also supported by the Alfred P Sloan foundation. The authors would like to thank Gordon Baym for providing the impetus to write this review. They would like to acknowledge useful discussions with Dam Son, Edward Shuryak and John Thomas. In preparing a revised version the authors benefited from the remarks of an anonymous referee, and from communications by G Aarts, C Greiner, A Sinha and F Zwerger.

References

[1] Darrigol O 2005 *Worlds of Flow* (Oxford: Oxford University Press)
[2] Brush S G 1986 *The Kind of Motion We Call Heat* (Amsterdam: North-Holland)
[3] Frenkel J 1955 *Kinetic Theory of Liquids* (New York: Dover)
[4] Eyring H 1936 *J. Chem. Phys.* **4** 283
[5] Tabor D 1979 *Gases, Liquids and Solids* 2nd edn (Cambridge: Cambridge University Press)
[6] Linstrom P J and Mallard W G (ed) *NIST Chemistry WebBook, NIST Standard Reference Database* Number 69, National Institute of Standards and Technology http://webbook.nist.gov

[7] Cox J D, Wagman D D and Medvedev V A 1989 *CODATA Key Values for Thermodynamics* (New York: Hemisphere Publishing) http://www.codata.org

[8] Wilks J 1966 *The Properties of Liquid and Solid Helium* (Oxford: Clarendon)

[9] Danielewicz P and Gyulassy M 1985 *Phys. Rev.* D **31** 53

[10] Kovtun P, Son D T and Starinets A O 2005 *Phys. Rev. Lett.* **94** 111601 (arXiv:hep-th/0405231)

[11] DeMarco B and Jin D S 1999 *Science* **285.5434** 1703

[12] O'Hara K M, Granade S R, Gehm M E, Savard T A, Bali S, Freed C and Thomas J E 1999 *Phys. Rev. Lett.* **82** 4204

[13] Adler S S *et al* 2003 (PHENIX Collaboration) *Phys. Rev. Lett.* **91** 182301 (arXiv:nucl-ex/0305013)

[14] Back B B *et al* 2005 (PHOBOS Collaboration) *Phys. Rev.* C **72** 051901 (arXiv:nucl-ex/0407012)

[15] Adams J *et al* 2005 (STAR Collaboration) *Phys. Rev.* C **72** 014904 (arXiv:nucl-ex/0409033)

[16] Baym G, Monien H, Pethick C J and Ravenhall D G 1990 *Phys. Rev. Lett.* **64** 1867

[17] Arnold P, Moore G D and Yaffe L G 2000 *J. High Energy Phys.* 0011(2000) 001 (arXiv:hep-ph/0010177)

[18] Arnold P, Moore G D and Yaffe L G 2003 *J. High Energy Phys.* 0305(2003) 051 (arXiv:hep-ph/0302165)

[19] Policastro G, Son D T and Starinets A O 2001 *Phys. Rev. Lett.* **87** 081601 (arXiv:hep-th/0104066)

[20] Maldacena J M 1998 *Adv. Theor. Math. Phys.* **2** 231
Maldacena J M 1999 *Int. J. Theor. Phys.* **38** 1113 (arXiv:hep-th/9711200)

[21] Buchel A, Liu J T and Starinets A O 2005 *Nucl. Phys.* B **707** 56 (arXiv:hep-th/0406264)

[22] Bloch I, Dalibard J and Zwerger W 2008 *Rev. Mod. Phys.* **80** 885 (arXiv:0704.3011)

[23] Giorgini S, Pitaevskii L P and Stringari S 2008 *Rev. Mod. Phys.* **80** 1215 (arXiv:0706.3360)

[24] Shuryak E 2009 *Prog. Part. Nucl. Phys.* **62** 48 (arXiv:0807.3033 [hep-ph])

[25] Khalatnikov I M 1965 *Introduction to the Theory of Superfluidity* (New York: Benjamin)

[26] Baym G and Pethick C 1991 *Landau Fermi Liquid Theory* (New York: Wiley)

[27] Arnold P 2007 *Int. J. Mod. Phys.* E **16** 2555 (arXiv:0708.0812 [hep-ph])

[28] Son D T and Starinets A O 2007 *Ann. Rev. Nucl. Part. Sci.* **57** 95 (arXiv:0704.0240 [hep-th])

[29] Rangamani M 2009 arXiv:0905.4352 [hep-th]

[30] Heinz U W 2009 arXiv:0901.4355 [nucl-th]

[31] Romatschke P 2009 arXiv:0902.3663 [hep-ph]

[32] Teaney D A 2009 arXiv:0905.2433 [nucl-th]

[33] Huang K 1987 *Statistical Mechanics* 2nd edn (New York: Wiley)

[34] Baym G, Blaizot J-P, Holzmann M, Laloe F and Vautherin D 1999 *Phys. Rev. Lett.* **83** 1703

[35] Arnold P and Moore G D 2001 *Phys. Rev. Lett.* **87** 120401 (arXiv:cond-mat/0103228)

[36] Kalos M H, Levesque D and Verlet L 1974 *Phys. Rev.* A **9** 2178

[37] Aziz R A and Slaman M J 1991 *J. Chem. Phys.* **94** 8047

[38] Tang K T, Toennies J P and Yiu C L 1995 *Phys. Rev. Lett.* **74** 1546

[39] Braaten E and Hammer H W 2007 *Ann. Phys.* **322** 120 (arXiv:cond-mat/0612123)

[40] Ceperley D M 1995 *Rev. Mod. Phys.* **67** 279

[41] Grüter P, Ceperley D and Laloe F 1997 *Phys. Rev. Lett.* **79** 3549

[42] Glyde H R, Azuah R T and Stirling W G 2000 *Phys. Rev.* B **62** 14337

[43] Campostrini M, Hasenbusch M, Pelissetto A and Vicari E 2006 *Phys. Rev.* B **74** 144506 (arXiv:cond-mat/0605083)

[44] Lipa J A, Swanson D R, Nissen J A, 'Chui T C P and Israelsson U E 1996 *Phys. Rev. Lett.* **76** 944

[45] Feynman R P 1954 *Phys. Rev.* **94** 262

[46] Regal C 2005 *PhD Thesis* University of Colorado (arXiv:cond-mat/0601054)

[47] Gorkov L P and Melik-Barkhudarov T K 1961 *Sov. Phys.—JETP* **13** 1018

[48] Nozieres P, Schmitt-Rink S 1984 *J. Low Temp. Phys.* **59** 195

[49] Chang S-Y, Pandharipande V R, Carlson J and Schmidt K E 2004 *Phys. Rev.* A **70** 043602

[50] Bartenstein M, Altmeyer A, Riedl S, Jochim S, Chin C, Hecker Denschlag J and Grimm R 2004 *Phys. Rev. Lett.* **92** 203201 (arXiv:cond-mat/0412712)

[51] Mehen T, Stewart I W and Wise M B 2000 *Phys. Lett.* B **474** 145 (arXiv:hep-th/9910025)

[52] Son D T and Wingate M 2006 *Ann. Phys.* **321** 197 (arXiv:cond-mat/0509786)

[53] Burovski E, Prokof'ev N, Svistunov B and Troyer M 2006 *Phys. Rev. Lett.* **96** 160402 (arXiv:cond-mat/0602224)

[54] Carlson J and Reddy S 2005 *Phys. Rev. Lett.* **95** 060401 (arXiv:cond-mat/0503256)

[55] Carlson J, Chang S-Y, Pandharipande V R and Schmidt K E 2003 *Phys. Rev. Lett.* **91** 050401 (arXiv:physics/0303094)

[56] Luo L and Thomas J E 2009 *J. Low Temp. Phys.* at press (arXiv:0811.1159 [cond-mat.other])

[57] Rupak G and Schäfer T 2009 *Nucl. Phys.* A **816** 52 (arXiv:0804.2678 [nucl-th])

[58] Astrakharchik G E, Boronat J, Casulleras J and Giorgini S 2004 *Phys. Rev. Lett.* **93** 200404 (arXiv:cond-mat/0406113)

[59] Alford M G, Schmitt A, Rajagopal K and Schäfer T 2008 *Rev. Mod. Phys.* **80** 1455 (arXiv:0709.4635 [hep-ph])

[60] Shuryak E V 1978 *Sov. Phys.—JETP* **47** 212
Shuryak E V 1978 *Zh. Eksp. Teor. Fiz.* **74** 408

[61] LeBellac M 1996 *Thermal Field Theory* (Cambridge: Cambridge University Press)

[62] Braaten E and Pisarski R D 1990 *Phys. Rev.* D **42** 2156

[63] Blaizot J P, Iancu E and Rebhan A 2004 Thermodynamics of the high-temperature quark gluon plasma *Quark Gluon Plasma* 3 ed R Hwa and X-N Wang (Singapore: World Scientific)

[64] Braaten E and Nieto A 1995 *Phys. Rev.* D **51** 6990 (arXiv:hep-ph/9501375)

[65] Hietanen A, Kajantie K, Laine M, Rummukainen K and Schroder Y 2009 *Phys. Rev.* D **79** 045018 (arXiv:0811.4664 [hep-lat])

[66] Laermann E and Philipsen O 2003 *Ann. Rev. Nucl. Part. Sci.* **53** 163 (arXiv:hep-ph/0303042)

[67] Karsch F 2007 *J. Phys. G* **34** S627 (arXiv:hep-ph/0701210)

[68] Aoki Y, Fodor Z, Katz S D and Szabo K K 2006 *Phys. Lett.* B **643** 46 (arXiv:hep-lat/0609068)

[69] Terning J 2006 *Modern Supersymmetry: Dynamics and Duality* (Oxford: Clarendon)

[70] Gubser S S, Klebanov I R and Tseytlin A A 1998 *Nucl. Phys.* B **534** 202 (arXiv:hep-th/9805156)

[71] Fotopoulos A and Taylor T R 1999 *Phys. Rev.* D **59** 061701 (arXiv:hep-th/9811224)

[72] Nieto A and Tytgat M H G 1999 arXiv:hep-th/9906147

[73] Blaizot J P, Iancu E, Kraemmer U and Rebhan A 2007 *J. High Energy Phys.* 0706(2007) 035 (arXiv:hep-ph/0611393)

[74] Landau L D and Lifshitz E M 1959 *Fluid Dynamics* (*Course of Theoretical Physics* vol VI) (Oxford: Pergamon)

[75] Baier R, Romatschke P, Son D T, Starinets A O and Stephanov M A 2008 *J. High Energy Phys.* 0804(2008) 100 (arXiv:0712.2451 [hep-th])

[76] York M A and Moore G D 2008 arXiv:0811.0729 [hep-ph]

[77] Bhattacharyya S, Hubeny V E, Minwalla S and Rangamani M 2008 *J. High Energy Phys.* 0802(2008) 045 (arXiv:0712.2456 [hep-th])

[78] Israel W and Stewart J M 1979 *Ann. Phys.* **118** 341
[79] Geroch R P and Lindblom L 1990 *Phys. Rev.* D **41** 1855
[80] Burnett D 1935 *Proc. Lond. Math. Soc.* **39** 385
[81] Burnett D 1936 *Proc. Lond. Math. Soc.* **40** 382
[82] Garcia-Colina L S, Velascoa R M and Uribea F J 2008 *Phys. Rep.* **465** 149
[83] Grad H 1949 *Commun. Pure Appl. Math.* **2** 331
[84] Foch J and Uhlenbeck G E 1967 *Phys. Rev. Lett.* **19** 1025
[85] Foch J D and Ford G W 1970 ed J deBoer and G E Uhlenbeck *Studies in Statistical Mechanics* part B vol V (Amsterdam: North-Holland)
[86] Khalatnikov I M and Lebedev V V 1982 *Phys. Lett.* A **91** 70
[87] Carter B and Khalatnikov I M 1992 *Phys. Rev.* D **45** 4536
[88] Son D T 2001 *Int. J. Mod. Phys.* A **16S1C** 1284 (arXiv:hep-ph/0011246)
[89] Son D T arXiv:hep-ph/0204199
[90] Mannarelli M and Manuel C 2008 *Phys. Rev.* D **77** 103014 (arXiv:0802.0321 [hep-ph])
[91] Hohenberg P C and Halperin B I 1977 *Rev. Mod. Phys.* **49** 435
[92] Onuki A 1997 *Phys. Rev.* E **55** 403
[93] Stephanov M A 2004 *Prog. Theor. Phys. Suppl.* **153** 139 (arXiv:hep-ph/0402115)
[94] Son D T and Stephanov M A 2004 *Phys. Rev.* D **70** 056001 (arXiv:hep-ph/0401052)
[95] Forster D 1995 *Hydrodynamic Fluctuations, Broken Symmetry, and Correlation Functions* (Reading, MA: Addison-Wesley)
[96] Karsch F and Wyld H W 1987 *Phys. Rev.* D **35** 2518
[97] Meyer H B 2007 *Phys. Rev.* D **76** 101701 (arXiv:0704.1801 [hep-lat])
[98] Meyer H B 2008 *Phys. Rev. Lett.* **100** 162001 (arXiv:0710.3717 [hep-lat])
[99] Sakai S and Nakamura A 2007 *Proc. Sci.* **LAT2007** 221 (arXiv:0710.3625 [hep-lat])
[100] Aarts G, Allton C, Foley J, Hands S and Kim S 2007 *Phys. Rev. Lett.* **99** 022002 (arXiv:hep-lat/0703008)
[101] Aarts G 2007 *Proc. Sci.* **LAT2007** 001 (arXiv:0710.0739 [hep-lat])
[102] Aarts G, Allton C, Foley J, Hands S and Kim S 2007 *Nucl. Phys.* A **785** 202 (arXiv:hep-lat/0607012)
[103] Meyer H B 2008 *J. High Energy Phys.* 0808(2008) 031 (arXiv:0806.3914 [hep-lat])
[104] Jensen H, Smith H and Wilkins J W 1969 *Phys. Rev.* **185** 323
[105] Smith H and Hojgaard Jensen H 1989 *Transport Phenomena* (Oxford: Oxford University Press)
[106] Brooker G A and Sykes J 1968 *Phys. Rev. Lett.* **21** 279
[107] Landau L D and Lifshitz E M 1981 *Physical Kinetics* (*Course of Theoretical Physics* vol X) (Oxford: Pergamon)
[108] Rupak G and Schäfer T 2007 *Phys. Rev.* A **76** 053607 (arXiv:0707.1520 [cond-mat.other])
[109] Maris H J 1973 *Phys. Rev.* A **8** 1980
[110] Prakash M, Prakash M, Venugopalan R and Welke G 1993 *Phys. Rep.* **227** 321
[111] Csernai L P, Kapusta J I and McLerran L D 2006 *Phys. Rev. Lett.* **97** 152303 (arXiv:nucl-th/0604032)
[112] Chen J W and Nakano E 2007 *Phys. Lett.* B **647** 371 (arXiv:hep-ph/0604138)
[113] Gavin S 1985 *Nucl. Phys.* A **435** 826
[114] Itakura K, Morimatsu O and Otomo H 2008 *Phys. Rev.* D **77** 014014 (arXiv:0711.1034 [hep-ph])
[115] Massignan P, Bruun G M and Smith H 2005 *Phys. Rev.* A **71** 033607 (arXiv:cond-mat/0409660)
[116] Bruun G M and Smith H 2005 *Phys. Rev.* A **72** 043605 (arXiv:cond-mat/0504734)
[117] Bruun G M and Smith H 2007 *Phys. Rev.* A **75** 043612 (arXiv:cond-mat/0612460)
[118] Chapman S and Cowling T G 1970 *The Mathematical Theory of Non-Uniform Gases* 3rd edn (Cambridge: Cambridge University Press)
[119] Aziz R A, Janzen A R and Moldover M R 1995 *Phys. Rev. Lett.* **74** 1586
[120] Arnold P, Moore G D and Yaffe L G 2003 *J. High Energy Phys.* 0301(2003) 030 (arXiv:hep-ph/0209353)
[121] Caron-Huot S and Moore G D 2008 *J. High Energy Phys.* 0802(2008) 081 (arXiv:0801.2173 [hep-ph])
[122] Arnold P, Dogan C and Moore G D 2006 *Phys. Rev.* D **74** 085021 (arXiv:hep-ph/0608012)
[123] Huot S C, Jeon S and Moore G D 2007 *Phys. Rev. Lett.* **98** 172303 (arXiv:hep-ph/0608062)
[124] Son D T 2007 *Phys. Rev. Lett.* **98** 020604 (arXiv:cond-mat/0511721)
[125] Escobedo M A, Mannarelli M and Manuel C 2009 arXiv:0904.3023 [cond-mat]
[126] Chen J W and Wang J arXiv:0711.4824 [hep-ph]
[127] Weinberg S 1972 *Gravitation and Cosmology* (New York: Wiley)
[128] Jeon S 1995 *Phys. Rev.* D **52** 3591 (arXiv:hep-ph/9409250)
[129] Bowley R M 2002 *Europhys. Lett.* **58** 725
[130] Bruun G M, Recati A, Pethick C J, Smith H and Stringari S 2008 *Phys. Rev. Lett.* **100** 240406
[131] Svetitsky B 1988 *Phys. Rev.* D **37** 2484
[132] Moore G D and Teaney D 2005 *Phys. Rev.* C **71** 064904 (arXiv:hep-ph/0412346)
[133] Heiselberg H and Pethick C J 1993 *Phys. Rev.* D **48** 2916
[134] Witten E 1998 *Adv. Theor. Math. Phys.* **2** 253 (arXiv:hep-th/9802150)
[135] Gubser S S, Klebanov I R and Polyakov A M 1998 *Phys. Lett.* B **428** 105 (arXiv:hep-th/9802109)
[136] Thorne K S, Price R H and MacDonald D A 1986 *Black Holes: The Membrane Paradigm* (New Haven, CT: Yale University Press)
[137] Aharony O, Gubser S S, Maldacena J M, Ooguri H and Oz Y 2000 *Phys. Rep.* **323** 183 (arXiv:hep-th/9905111)
[138] Petersen J L 1999 *Int. J. Mod. Phys.* A **14** 3597 (arXiv:hep-th/9902131)
[139] D'Hoker E and Freedman D Z 2002 TASI 2001 Lectures on Supersymmetric gauge theories and the AdS/CFT correspondence arXiv:hep-th/0201253
[140] Maldacena J M *TASI 2003 Lectures on AdS/CFT* arXiv:hep-th/0309246
[141] Gibbons G W and Hawking S W 1977 *Phys. Rev.* D **15** 2752
[142] York J W 1972 *Phys. Rev. Lett.* **28** 1082
[143] Wald R M 1984 *General Relativity* (Chicago: University of Chicago Press)
[144] Misner C W, Thorne K S and Wheeler J A 1973 *Gravitation* (San Francisco: Freeman)
[145] Aarts G and Martinez Resco J M 2002 *J. High Energy Phys.* 0204(2002) 053 (arXiv:hep-ph/0203177)
[146] Moore G D and Saremi O 2008 *J. High Energy Phys.* 0809(2008) 015 (arXiv:0805.4201 [hep-ph])
[147] Teaney D 2006 *Phys. Rev.* D **74** 045025 (arXiv:hep-ph/0602044)
[148] Kovtun P and Starinets A 2006 *Phys. Rev. Lett.* **96** 131601 (arXiv:hep-th/0602059)
[149] Buchel A and Liu J T 2004 *Phys. Rev. Lett.* **93** 090602 (arXiv:hep-th/0311175)
[150] Iqbal N and Liu H 2009 *Phys. Rev.* D **79** 025023 (arXiv:0809.3808 [hep-th])
[151] Buchel A 2008 *Nucl. Phys.* B **802** 281 (arXiv:0801.4421 [hep-th])
[152] Buchel A 2008 *Nucl. Phys.* B **803** 166 (arXiv:0805.2683 [hep-th])
[153] Myers R C, Paulos M F and Sinha A 2009 *Phys. Rev.* D **79** 041901 (arXiv:0806.2156 [hep-th])
[154] Cohen T D 2007 *Phys. Rev. Lett.* **99** 021602 (arXiv:hep-th/0702136)
[155] Dobado A and Llanes-Estrada F J 2007 *Eur. Phys. J.* C **51** 913 (arXiv:hep-th/0703132)

[156] Son D T 2008 *Phys. Rev. Lett.* **100** 029101 (arXiv:0709.4651 [hep-th])
[157] Brigante M, Liu H, Myers R C, Shenker S and Yaida S 2008 *Phys. Rev.* D **77** 126006 (arXiv:0712.0805 [hep-th])
[158] Brigante M, Liu H, Myers R C, Shenker S and Yaida S 2008 *Phys. Rev. Lett.* **100** 191601 (arXiv:0802.3318 [hep-th])
[159] Kats Y and Petrov P 2009 *J. High Energy Phys.* 0901(2009) 044 (arXiv:0712.0743 [hep-th])
[160] Buchel A, Myers R C and Sinha A 2008 arXiv:0812.2521 [hep-th]
[161] Son D T and Starinets A O 2006 *J. High Energy Phys.* 0603(2006) 052 (arXiv:hep-th/0601157)
[162] Herzog C P, Karch A, Kovtun P, Kozcaz C and Yaffe L G 2006 *J. High Energy Phys.* 0607(2006) 013 (arXiv:hep-th/0605158)
[163] Casalderrey-Solana J and Teaney D 2006 *Phys. Rev.* D **74** 085012 (arXiv:hep-ph/0605199)
[164] Gubser S S 2006 *Phys. Rev.* D **74** 126005 (arXiv:hep-th/0605182)
[165] Buchel A 2008 *Phys. Lett.* B **663** 286 (arXiv:0708.3459 [hep-th])
[166] Gubser S S, Pufu S S and Rocha F D 2008 *J. High Energy Phys.* 0808(2008) 085 (arXiv:0806.0407 [hep-th])
[167] Karsch F, Kharzeev D and Tuchin K 2008 *Phys. Lett.* B **663** 217 (arXiv:0711.0914 [hep-ph])
[168] Son D T 2008 *Phys. Rev.* D **78** 046003 (arXiv:0804.3972 [hep-th])
[169] Balasubramanian K and McGreevy J 2008 *Phys. Rev. Lett.* **101** 061601 (arXiv:0804.4053 [hep-th])
[170] Herzog C P, Rangamani M and Ross S F 2008 *J. High Energy Phys.* 0811(2008) 080 (arXiv:0807.1099 [hep-th])
[171] Maldacena J, Martelli D and Tachikawa Y 2008 *J. High Energy Phys.* 0810(2008) 072 (arXiv:0807.1100 [hep-th])
[172] Hagen C R 1972 *Phys. Rev.* D **5** 377
[173] Adams A, Balasubramanian K and McGreevy J 2008 *J. High Energy Phys.* 0811(2008) 059 (arXiv:0807.1111 [hep-th])
[174] Rangamani M, Ross S F, Son D T and Thompson E G arXiv:0811.2049 [hep-th]
[175] Woods A D B and Hollis-Halet A C 1963 *Can. J. Phys.* **41** 596
[176] Heikkila W J and Hollis-Hallett A C 1955 *Can. J. Phys.* **33** 420
[177] Kapitza P L 1938 *Nature* **74** 141
[178] Keesom W H and Mac Wood G E 1938 *Physica* **5** 737
[179] Agosta C C, Wang S, Cohen L H and Meyer H 1987 *J. Low Temp. Phys.* **67** 237
[180] Putterman S J 1974 *Superfluid Hydrodynamics* (Amsterdam: North-Holland)
[181] Hanson W B and Pellam J R 1954 *Phys. Rev.* **95** 321
[182] O'Hara K M, Hemmer S L, Gehm M E, Granade S R and Thomas J E 2002 *Science* **298** 2179 (arXiv:cond-mat/0212463)
[183] Kinast J, Hemmer S L, Gehm M E, Turlapov A and Thomas J E 2004 *Phys. Rev. Lett.* **92** 150402
[184] Kinast J, Turlapov A and Thomas J E 2004 *Phys. Rev.* A **70** 051401(R)
[185] Kinast J, Turlapov A and Thomas J E 2005 *Phys. Rev. Lett.* **94** 170404 (arXiv:cond-mat/0502507)
[186] Altmeyer A, Riedl S, Kohstall C, Wright M, Geursen R, Bartenstein M, Chin C, Hecker Denschlag J and Grimm R arXiv:cond-mat/0609390
[187] Joseph J, Clancy B, Luo L, Kinast J, Turlapov A and Thomas J E 2007 *Phys. Rev. Lett.* **98** 170401 (arXiv:cond-mat/0612567)
[188] Clancy B, Luo L and Thomas J E 2007 *Phys. Rev. Lett.* **99** 140401 (arXiv:0705.2782 [cond-mat.other])
[189] Kavoulakis G M, Pethick C J and Smith H 1998 *Phys. Rev.* A **57** 2938 (arXiv:cond-mat/9710130)
[190] Gelman B A, Shuryak E V and Zahed I 2005 *Phys. Rev.* A **72** 043601 (arXiv:nucl-th/0410067)
[191] Schäfer T 2007 *Phys. Rev.* A **76** 063618 (arXiv:cond-mat/0701251)
[192] Turlapov A, Kinast J, Clancy B, Luo L, Joseph J and Thomas J E 2008 *J. Low Temp. Phys.* **150** 567 (arXiv:0707.2574)
[193] Heiselberg H 2004 *Phys. Rev. Lett.* **93** 040402 (arXiv:cond-mat/0403041)
[194] Stringari S 2004 *Europhys. Lett.* **65** 749 (arXiv:cond-mat/0312614)
[195] Bulgac A and Bertsch G F 2005 *Phys. Rev. Lett.* **94** 070401 (arXiv:cond-mat/0404687)
[196] Thomas J E, Kinast J and Turlapov A 2005 *Phys. Rev. Lett.* **95** 120402 (arXiv:cond-mat/0503620)
[197] Bruun G M and Smith H 2007 *Phys. Rev.* A **76** 045602 (arXiv:0709.1617)
[198] Kinast J, Turlapov A, Thomas J E, Chen Q, Stajic J and Levin K 2005 *Science* **307** 1296 (arXiv:cond-mat/0502087)
[199] Luo L, Clancy B, Joseph J, Kinast J and Thomas J E arXiv:cond-mat/0611566
[200] Riedl S, Sanchez Guajardo E R, Kohstall C, Altmeyer A, Wright M J, Hecker Denschlag J, Grimm R, Bruun G M and Smith H 2008 *Phys. Rev.* A **78** 053609 (arXiv:0809.1814 [cond-mat.other])
[201] Menotti C, Pedri P and Stringari S 2002 *Phys. Rev. Lett.* **89** 250402 (arXiv:cond-mat/0208150)
[202] Edwards M, Clark C W, Pedri P, Pitaevskii L and Stringari S 2002 *Phys. Rev. Lett.* **88** 070405
[203] Clancy B 2008 *PhD Thesis* Duke University
[204] Thomas J E 2009 arXiv:0907.0140
[205] Miller M L, Reygers K, Sanders S J and Steinberg P 2007 *Ann. Rev. Nucl. Part. Sci.* **57** 205 (arXiv:nucl-ex/0701025)
[206] Voloshin S A, Poskanzer A M and Snellings R 2008 arXiv:0809.2949 [nucl-ex]
[207] Gombeaud C and Ollitrault J Y 2008 *Phys. Rev.* C **77** 054904 (arXiv:nucl-th/0702075)
[208] Landau L D 1953 *Izv. Akad. Nauk Ser. Fiz.* **17** 51
[209] Bjorken J D 1983 *Phys. Rev.* D **27** 140
[210] Baym G, Friman B L, Blaizot J P, Soyeur M and Czyz W 1983 *Nucl. Phys.* A **407** 541
[211] Kolb P F, Heinz U W, Huovinen P, Eskola K J and Tuominen K 2001 *Nucl. Phys.* A **696** 197 (arXiv:hep-ph/0103234)
[212] McLerran L D and Venugopalan R 1994 *Phys. Rev.* D **49** 2233 (arXiv:hep-ph/9309289)
[213] Hirano T, Heinz U W, Kharzeev D, Lacey R and Nara Y 2006 *Phys. Lett.* B **636** 299 (arXiv:nucl-th/0511046)
[214] Schnedermann E, Sollfrank J and Heinz U W 1993 *Phys. Rev.* C **48** 2462 (arXiv:nucl-th/9307020)
[215] Teaney D 2003 *Phys. Rev.* C **68** 034913 (arXiv:nucl-th/0301099)
[216] Dusling K and Teaney D 2008 *Phys. Rev.* C **77** 034905 (arXiv:0710.5932 [nucl-th])
[217] Romatschke P and Romatschke U 2007 *Phys. Rev. Lett.* **99** 172301 (arXiv:0706.1522 [nucl-th])
[218] Song H and Heinz U W 2008 *Phys. Rev.* C **77** 064901 (arXiv:0712.3715 [nucl-th])
[219] Luzum M and Romatschke P 2008 *Phys. Rev.* C **78** 034915 (arXiv:0804.4015 [nucl-th])
[220] Huovinen P and Molnar D 2009 *Phys. Rev.* C **79** 014906 (arXiv:0808.0953 [nucl-th])
[221] Öttinger H C 1998 *Physica* A **254** 433
[222] Teaney D, Lauret J and Shuryak E V 2001 *Phys. Rev. Lett.* **86** 4783 (arXiv:nucl-th/0110037)
[223] Kolb P F, Huovinen P, Heinz U W and Heiselberg H 2001 *Phys. Lett.* B **500** 232 (arXiv:hep-ph/0012137)

[224] Huovinen P, Kolb P F, Heinz U W, Ruuskanen P V and Voloshin S A 2001 *Phys. Lett.* B **503** 58 (arXiv:hep-ph/0101136)
[225] Adler C *et al* (STAR Collaboration) 2002 *Phys. Rev.* C **66** 034904
[226] Kolb P F, Sollfrank J and Heinz U W 1999 *Phys. Lett.* B **459** 667 (arXiv:nucl-th/9906003)
[227] Xu Z and Greiner C 2009 *Phys. Rev.* C **79** 014904 (arXiv:0811.2940 [hep-ph])
[228] Bouras I, Molnar E, Niemi H, Xu Z, El A, Fochler O, Greiner C and Rischke D H 2009 arXiv:0902.1927 [hep-ph]
[229] Song H and Heinz U W arXiv:0812.4274 [nucl-th]
[230] Denicol G S, Kodama T, Koide T and Mota Ph 2009 arXiv:0903.3595 [hep-ph]
[231] El A, Muronga A, Xu Z and Greiner C 2008 arXiv:0812.2762 [hep-ph]
[232] Noronha J, Gyulassy M and Torrieri G 2009 arXiv:0906.4099 [hep-ph]
[233] Fochler O, Xu Z and Greiner C 2009 *Phys. Rev. Lett.* **102** 202301 (arXiv:0806.1169 [hep-ph])
[234] Baym G, Pethick C J, Yu Z and Zwierlein M W 2007 *Phys. Rev. Lett.* **99** 190407
[235] Haussmann R, Punk M and Zwerger W arXiv:0904.1333
[236] Koch V, Majumder A and Randrup J 2005 *Phys. Rev. Lett.* **95** 182301 (arXiv:nucl-th/0505052)
[237] Nonaka C, Fries R J and Bass S A 2004 *Phys. Lett.* B **583** 73 (arXiv:nucl-th/0308051)